
Human Liver Organoids as models for investigating Drug-Induced Liver Injury



Mewanthi Flaminia Kaluthantrige Don

Department of Physiology, Development and
Neuroscience

This thesis is submitted for the degree of
Doctor of Philosophy

Sidney Sussex College



April 2021

Declaration

This dissertation is the result of my own work and includes nothing which is the outcome of work done in collaboration except as specified in the text.

Also, it is not substantially the same as any that I have submitted or is being concurrently submitted for a degree or diploma or other qualification at the University of Cambridge or any other University or similar. I further state that no substantial part of my dissertation has already been submitted, or is being concurrently submitted for any such degree, diploma or other qualification at the University of Cambridge or any other university or similar institution.

This dissertation does not exceed the prescribed limit of 60.000 words.

April, 2021

Acknowledgments

I would first like to thank my supervisors for allowing me to undertake such a beautiful journey called PhD. Thank you to Meri for giving me the opportunity to work with you, for the guidance and for teaching me what it means to be a good scientist. You are a role model and such an inspiration for all the women in science. Thank you to Kevin for supporting me throughout my PhD as both my supervisor and friend despite I was across ocean. Thank you to Andy for letting me explore the cutting-edge technology and for the opportunity to connect to many wonderful people at GSK.

Research is exciting, but it also involves challenging days. In Cambridge I was lucky to work in a lab full of friends and to meet many more fellow students that made my PhD journey not so boring. Special thanks to Sohaib for being an amazing PhD buddy, for the Fourier transform sessions, for the coffees and college formals. To Gianmarco, thank you for making me laugh with your jokes and reminding me to be positive despite it can be difficult sometimes, for the adventure and trips, for the sneaky chocolate breaks. To Lucia (Regina), thank you for being the rock and for being the Regina of our mean girls group, Wednesdays will always be special to me. To Luigi, thank you for the constant mentorship and for being my number one fan. To Nicole, thank you for being always up for a party and taught to handle tough. To Gianmarco, Luigi, Lucia, Nikitas and Nicole all together, thank you for being the best lab one could ask for. To Sofia (Karen) and Olga, thank you for all the laughs and for the amazing Moroccan adventure. To Cristina, thank you for being the wise one, for the laughs and adventure in Frankfurt.

Moving to Dresden has been another incredible chapter of my PhD. Again, I would like to thank Meri for giving me the opportunity to experience another research environment. Despite the challenges due to the pandemic, the constant full support of my lab was extremely valuable. Thank you to Patricia, Anna and German for the constant support. To Patricia for the singing parties in the lab, for being there during my “drama” moments and for being such a good friend. To Javier, for the “MMs” moments, despite we met for such a short period of time I can be assured that you will carry on the Huch lab vibe. To Aleksandra for making the best ‘Burn Book’ someone could ask for. Thank you, Robert, for making my work easier and faster. The following

are a few other people who I have crossed during my time here at the MPI-CBG who I think of very fondly: Kira, Fabio, Deb, Suhrid and Marina. To Federica for being the missing F, thanks for being who you are, you made this place extra special to me.

And finally, I want to thank my family and loved ones for being my number one supporters. To my parents, Palitha and Anoma, for helping me grow into the person I am today. To my precious brothers, Serenella and Aurelio, thank you for being my special people on earth. Knowing how proud you are of me makes it all meaningful. This is all for you my loving family.

External contributions

The details about the external contribution to the work presented in this dissertation are as follows:

Dr. Carla Newmann (GlaxoSmithKline, Stevenage, UK) and Dr. Jean Luc (National Physical laboratory, London, UK) have performed the mass spectrometry imaging with the TOF-5 SIMS (Figures 4.4-4.6).

Abbreviations

2D	Two dimensions
2P	Two-photon excitation scanning microscope
3D	Three dimensions
ABC	ATP binding cassette
ABCB11	ATP Binding Cassette Subfamily B Member 11
ABCG2	ATP Binding Cassette Subfamily G Member 2
ADME	Absorption, distribution, metabolism, excretion
ADR	Adverse drug reactions
AdSCs	Adult stem cells
ALB	Albumin
APAP	Acetaminophen
BME	Basement Membrane Extract Type 2, Pathclear
BMP	Bone morphogenetic protein
BMP-7	Bone morphogenetic protein - 7
BSEP	Bile salt export pump
CA	Cholic acid
CDCA	Chenodeoxycholic acid
CFE	Organoid formation efficiency
CHIR	CHIR99201
Chol. Org	Ductal organoids
CMFDA	5-chloromethylfluorescein diacetate
CsA	Cyclosporine A
CYP2C8	Cytochrome P-450 2C8
CYP2C9	Cytochrome P-450 2C9
CYP3A4	Cytochrome P-450 3A4
DCA	Deoxycholic acid
DE	Definitive endoderm
DIC	Drug induced cholestasis
DILI	Drug induced liver injury
DIS	Drug induced steatosis
DIW	Deionised water
DM	Differentiation medium
DM Orgs	Hepatocyte organoids grown in DM
DM+ Orgs	Hepatocyte organoids grown in DM+
DM+(CHIR) Org	DM+ organoids without CHIR
DPPIV	Dipeptidyl peptidase IV
ECM	Extracellular matrix
EM	Expansion medium
ENT1	Nucleoside transporter 1
ESCs	Embryonic stem cells
FBS	Foetal bovine serum
FDA	Food and drug administration
FFA	Free fatty acid
FGF	Fibroblast growth factor
FGF19	Fibroblast growth factor 19
FGF4	Fibroblast growth factor 4

FXR	Farnesoid X receptor
FZD	Frizzled
GSK-3	Glycogen synthase kinase-3
Hep DM+VP Orgs	Hep-like Orgs with DM+VP
Hep Org	Hepatocyte organoids
Hep-like Orgs	Hep Orgs from hepatocytes isolated from human liver tissue resections
HGF	Hepatocyte growth factor
Hu Org	Hepatocyte organoids grown in Hu media
HUVECs	Human umbilication vein endothelial cells
HybHP	Hybrid hepatocytes
iPSCs	Induced pluripotent stem cells
LCA	Lithocholic acid
MMP	Matrix metalloproteinases
MSCs	Mesenchymal cells
NAFLD	Non-alcoholic fatty liver disease
NAPQI	N-acetyl-p-benzoquinone imine
NICD	Notch intracellular domain
NPL	National Physical laboratory
OSM	Oncostatin M
PBS	Phosphate buffer saline
PFA	Paraformaldehyde
PFIC2	Familial intrahepatic cholestasis type 2
PH	Partial hepatectomy
PHH	Primary human hepatocytes
PHPMMA	Polyhydroxylated methylmethacrylate
Porcn	Porcupine
ROS	Reactive oxygen species
RSPO-1	R-spondin 1
SEM	Standard error of the mean
STM	Septum transversum mesenchyme
TEM	Transmission electron microscopy
TOF	time-of-flight
UDPGT	Uridine diphosphate glucuronosyltransferase
VLDL	Very low-density lipoproteins
VP	Verteporfin
YAP1	Yes1-associated protein 1
ZO-1	Zonula occludens-1

List of Figures

Figure 1.1 The liver microenvironment.....	23
Figure 1.2 Liver plasticity.....	33
Figure 1.3 Overview of the Hippo signalling pathway.....	34
Figure 1.4 Hepatocyte polarisation.....	35
Figure 1.5 Metabolic zonation of the liver.....	37
Figure 1.6 The bile salt export pump.....	40
Figure 1.7 Overview of drug metabolism in hepatocytes.....	41
Figure 1.8 Overview of DILI process.....	43
Figure 1.9 Liver organoids as models to study drug toxicity.....	53
Figure 3.1 Schematics of the DM protocol.....	79
Figure 3.2 Targeting the canonical WNT signalling pathway.....	81
Figure 3.3 DM+ Orgs show an increase of hepatocyte-like morphology and a tendency for higher expression of hepatocyte markers.....	83
Figure 3.4 Assessment of mechanical dissociation in DM and DM+ Orgs.....	84
Figure 3.5 Organoid dissociation and WNT inhibition enhances ductal cells differentiation towards hepatocyte fate.....	86

Figure 3.6 DM+ Orgs recapitulate enhanced hepatocyte specification compared to DM Orgs.....	88
Figure 3.7 Enhanced organoid growth upon GSK-3 inhibition.....	90
Figure 3.8 GSK-3 inhibition favours hepatocyte fate specification.....	91
Figure 3.9 YAP is activated in Chol. Orgs following mechanical dissociation.....	93
Figure 3.10 YAP inhibition impairs Chol. Orgs maintenance.....	94
Figure 3.11 YAP is predominantly located in the cytoplasm in DM+ Orgs.....	95
Figure 3.12 Long term exposure to VP in DM+ Orgs leads to organoid toxicity.....	97
Figure 3.13 YAP activity inhibition following VP treatment in DM+ Orgs.....	97
Figure 3.14 VP supplementation to DM+ results in increased expression of hepatocyte markers.....	99
Figure 3.15 KRT19 protein expression in DM Orgs but not in DM+ and DM+VP Orgs.....	100
Figure 3.16 Establishment of human Hep Org using PHH.....	102
Figure 3.17 mRNA expression analysis of hepatocyte markers in cholangiocyte and hepatocyte derived Hep Orgs.....	103
Figure 3.18 Formation of Chol. Orgs from PHH cultures in Hu media.....	104
Figure 3.19 Differentiation of Hep-like Orgs following DM+VP treatment.....	106
Figure 4.1 DM+VP Orgs are viable for two weeks.....	110
Figure 4.2 Post-differentiated DM+VP Orgs cannot be maintained overtime in culture.....	111

Figure 4.3 Amiodarone is not detected inside the organoids.....	113
Figure 4.4 Treated organoids uptake amiodarone.....	114
Figure 4.5 Amiodarone is predominantly detected in the outer layer of organoids.....	115
Figure 4.6 Validation of BSEP expression in human liver tissue.....	117
Figure 4.7 BSEP is expressed in DM+VP Orgs.....	118
Figure 4.8 ZO-1 and β -Catenin expression in DM+VP Orgs.....	119
Figure 4.9 DM+VP Orgs present formation of bile canalicular like structures.....	120
Figure 4.10 DPPIV expression in human liver tissue.....	121
Figure 4.11 DPPIV is expressed in DM+VP Orgs.....	122
Figure 4.12 Active secretion of CMFDA into the bile canaliculi.....	123
Figure 4.13 Higher efficiency of DM+VP Orgs secretory system compared to HepG2 cells and DM Orgs.....	124
Figure 5.1 Chol. Orgs treated with CsA exhibit cell death above 1uM.....	127
Figure 5.2 CMFDA intracellular accumulation in DM+VP Orgs following CsA treatment.....	128
Figure 5.3 CsA treated DM+VP Orgs exhibited lower hepatocyte secretory activity.....	129
Figure 5.4 Differentiated Hep-like Orgs presented featured of CsA induced cholestasis.....	130
Figure 5.5 CsA specifically induce cholestasis in the organoid system.....	132
Figure 5.6 Intracellular accumulation of biliary pigments and lipid droplets following CsA treatment.....	133

Figure 5.7 Formation of lamellar bodies in amiodarone treated organoids.....	134
Figure 5.8 Titration of amiodarone, bosentan and acetaminophen in DM+VP Orgs.....	136
Figure 5.9 DM+VP Orgs show a toxic response to DILI compounds.....	137
Figure 6.1 Cellular degradation is observed after 3 days of live imaging.....	141
Figure 6.2 Establishment of an inverted imaging system to study organoid proliferation.....	143
Figure 6.3 Organoid formation efficiency is higher at low cellular concentration.....	145
Figure 6.4 Single cells derived liver organoids shows approximately 40h cell cycle duration before forming organoids.....	147
Figure 7.1 Working model for the differentiation of Chol. Org into DM+VP.....	156

List of tables

Table 2.1 Wnt3a and Rspo1 conditioned medium recipe and protocol.....	60
Table 2.2 List of differentiation media.....	64
Table 2.3 List of primary antibodies.....	67
Table 2.4 List of qPCR primers.....	71
Table 2.5 List of mouse lines.....	75
Table 2.6 List of compounds used.....	75
Table 5.1 Acetaminophen, amiodarone and bosentan DILI classification.....	135
Table 5.2 DM+VP Orgs can predict the risk of a compound to cause DILI.....	139

Abstract

The liver is the primary organ involved in drug detoxification, hence being highly exposed to the risk of drug induced liver injury (DILI). DILI is the main cause for acute liver failure in western countries and post-marketing withdrawal of drugs. This is highly due to the poor identification of potential human hepatotoxins during the preclinical phase of drug discovery. It is not surprising that interspecies difference between animal models could generate diverse biological responses compared to the human liver. Similarly, the current-state-of-the-art human *in vitro* hepatic systems lack the cellular spatial arrangement and hepatocyte functionality observed *in vivo*. Identification of an *in vitro* hepatic system capable to reproduce the essential features of the human liver *in vivo* is thus beneficial to better understand DILI and how it is triggered. Historically, maintenance of primary hepatocyte *in vitro* has been challenging due the intrinsic finite proliferative capacity of these cells, the shortage of donor livers, and the inability to maintain their *in vivo* structural and functional identity *in vitro*. All of the above hurdles have been addressed with the advent of 3D epithelial structures called organoids, yet its use in the liver safety field is currently unexplored. Liver organoids have the great advantage to be highly proliferative, to maintain the identity of the tissue of origin, and to retain the bipotential ability to differentiate into hepatocyte organoids. In this Thesis, we generated an enhanced hepatocyte organoid system through the directed stepwise differentiation *in vitro* of progenitor liver organoids using chemically defined culture conditions. Validation of these organoids in the context of DILI, showed structural and functional formation of tubular like structures called bile canaliculi which are essential morphological structures for the hepatocytes to secrete drugs/metabolites and bile from the intracellular compartment. Drug distribution mapping analysis revealed the ability of these organoids to uptake exogenous compounds. Therefore, we examined the potentiality of the hepatocyte organoids to detect known human hepatotoxins, which resulted in the obstruction of hepatic bile clearance and downregulation of transmembrane proteins in a process called cholestasis. Furthermore, formation of typical features of drug-induced steatosis were observed upon treatment with steatotic drugs. In summary, our findings highlight how this novel differentiated

organoid system could be a relevant human in vitro system with the potential to be incorporated into an initial drug safety screening, either as a replacement or complementary hepatic system.

Chapter 1

Introduction

1.1 Liver biology and anatomy

The liver is the largest internal organ in the human body located in the upper right portion of the abdominal cavity, above the stomach and beneath the diaphragm. Exhibiting a dark red colouration, the liver is morphologically divided in four uneven size lobes. The entire mass of each segment can be further anatomically subdivided into 1,000 hexagon shaped units identified as lobules (Matsumoto *et al.*, 1979). Each lobule is navigated by an intricate network of vessels to allow nutrients and oxygen exchange; at the centre there is the hepatic vein that radially branches into sinusoids towards the portal triad that surrounds each corner of the lobule. Portal triads are formed by the bile duct, hepatic artery and portal vein. Parenchymal cell cords surround vascular sinusoids and spread towards the portal triad; these are constituted by the fundamental type of liver epithelial cells, known as hepatocytes. Non-parenchymal cells include biliary epithelial cells or cholangiocytes, stellate cells, Kupffer cells and sinusoidal endothelial cells (Figure 1.1).

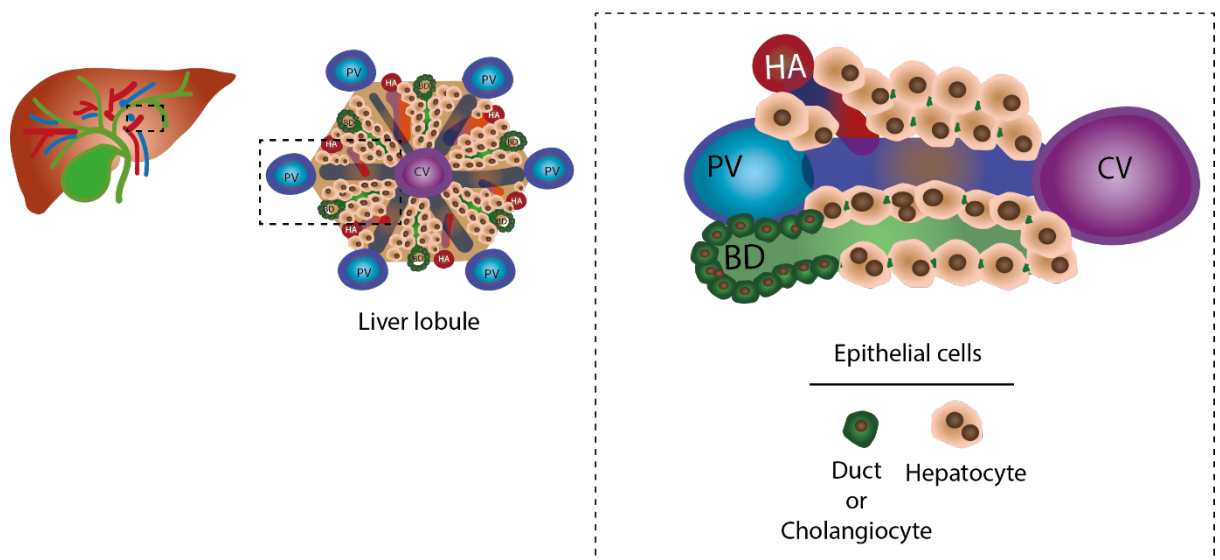


Figure 1.1 **The liver microenvironment.** The fundamental unit of the liver histoarchitecture is the liver lobule formed by the portal triads. Two types of epithelial cells navigate the liver tissue: cholangiocytes or ductal cells and hepatocytes. Hepatocytes secrete bile into the bile duct, lined by cholangiocytes which collect and modify the bile. Abbreviations: PV, portal triad; CV, central vein; BD, bile duct; HA, hepatic artery.

The liver covers an essential role to preserve homeostasis in the body. This is accomplished by the numerous functions that this organ provides to the organism including metabolism of nutrients, detoxification of xenobiotics, storage of glycogen; synthesis and secretion of bile and metabolites as well as serum proteins such as albumin (Matsumoto *et al.*, 1979; Gebhardt, 1992).

1.2 Liver epithelium formation and maturation during development, homeostasis and regeneration

1.2.1 Development

Originated as an endodermal organ, liver development is orchestrated by a tight regulation of morphogenetic signals that directs cell fate specification and maturation. During gastrulation, spatial and temporal gradients of signals arriving from the cardiogenic mesoderm and septum transversum mesenchyme (STM) initiate the patterning of the foregut endoderm into a proliferative structure called liver bud (Zorn, 2008; Zorn and Wells, 2009); this occurs at 56-55 gestation in humans and E13.5 in murine (Ruebner *et al.*, 1990). Fate determination of the foregut endoderm into hepatic fate is achieved by three hepatic inducing signals: bone morphogenetic protein (BMP), fibroblast growth factors (FGF) and WNT. Proper dosing of Fgf (Fgf1, Fgf2, Fgf8, Fgf10) is critical to induce hepatic specification as imbalance can shift the development towards lung or ventral pancreatic fate (Parlow *et al.*, 1991; Gualdi *et al.*, 1996; Jung *et al.*, 1999; Rossi *et al.*, 2001). Similarly, coordinated work of Bmp2, Bmp4 and Bmp7 have been shown to induce liver development; Bmp2 signalling repress *Pdx1*, a transcription factor involved in pancreatic specification, yet it is not sufficient to promote liver development (Chung, Shin and Stainier, 2008). In parallel, *Bmp4* mutant mice have shown a delay in liver bud formation, however the correct development can be compensated with Bmp2 signalling (Rossi *et al.*, 2001; Chung, Shin and Stainier, 2008). Nevertheless, the use of either FGF inhibitors or BMP inhibitor (Noggin) have been shown to impair liver bud patterning (Rossi *et al.*, 2001).

Much more crucial than BMP and FGF signalling is the WNT signalling role in hepatic specification, that exhibits a dual opposite functionality during hepatic specification (McLin, Rankin and Zorn, 2007). During gastrulation, WNT promotes formation of the hindgut endoderm at the expense of the foregut endoderm; on the other hand, antagonism of WNT signalling at the anterior endoderm favours foregut endoderm formation (McLin, Rankin and Zorn, 2007; Li *et al.*, 2008). Although WNT appears to repress early stages of liver development, its upregulation is necessary for successful liver formation at later hepatic specification phases. Studies conducted in *Wnt2b* mutant zebrafish have observed liver bud formation deficiency, hence further proving the involvement of WNT/ β -catenin pathway in liver development (Ober *et al.*, 2006). This is not the case for mammalian systems such as mice, in which loss of *Wnt2* and *Wnt2b* did not affect the embryonic liver but only caused lung agenesis, hence indicating *Wnt2* and *Wnt2B* is not required for the specification of the mammalian liver (Goss *et al.*, 2009). However, at later stages of liver development, WNT promotes liver bud formation as demonstrated using antisense β -catenin study in liver mice embryos (Satdarshan P S Monga *et al.*, 2003).

Interaction between FGF, BMP and WNT signalling in the foregut endoderm results in the formation of a bipotent population of progenitor cells called hepatoblasts. These cells have the capacity to differentiate into the main parenchymal cells of the liver: hepatocytes and cholangiocytes; they express markers for both immature hepatocyte such as alpha fetoprotein (*Afp*), adult hepatocyte markers like albumin (*Alb*) and *Hnf4a*, and cholangiocyte marker as (*Ck19*) (Zorn, 2008).

At E9.5 in mice, homeobox transcription factors (*Hhex* and *Prox1*) drive the degradation of the extracellular matrix through the regulation of matrix metalloproteinases (MMPs). This facilitates the migration of hepatoblast from the endoderm to the septum transversum which results in the formation of the liver bud (Bort *et al.*, 2006; Margagliotti *et al.*, 2008). As the liver bud is formed, the hepatic epithelium transits from a simple cuboidal morphology into a pseudostratified columnar epithelium (Houssaint, 1980; Bort *et al.*, 2006).

Maintenance of hepatoblast proliferation is regulated by mesenchymal paracrine signals; being already discussed during the gastrulation phase, FGF and

BMP signalling are still involved in liver bud expansion (Berg *et al.*, 2007). In addition, hepatocyte growth factor (HGF) signalling via the c-Met receptor, promotes hepatoblast proliferation (Defrances *et al.*, 1992).

At E13.5 in mice, hepatoblasts undergo the differentiation into either hepatocyte or cholangiocyte lineage. Depending on the location along the portal-venous axis, hepatoblasts localised in close proximity to the portal tract will differentiate into cholangiocytes, while moving towards the central vein these cells will gradually acquire a hepatocyte fate.

Specification of cholangiocyte phenotype requires a signalling gradient of activin/TGF- β from its highest concentration near the portal vein (Clotman *et al.*, 2005; Clotman and Lemaigre, 2006). In addition, Notch signalling is implicated in biliary development which evidence dates back on studies conducted in patients suffering from Alagille Syndrome in the 1987 (Nishikawa *et al.*, 1987); these patients showed mutations in Notch signalling ligands, *NOTCH2* and *JAG1*, which caused malformations in the intrahepatic bile duct formation (Li *et al.*, 1997; Oda *et al.*, 1997). Furthermore, signals from the mesenchymal compartment promote the expression of biliary transcription factors such as *SOX9*, *HNF6*, *OC2*, and *HNF1 β* , and downregulate *HNF4a* transcription factor expression (Clotman *et al.*, 2002, 2005; Coffinier *et al.*, 2002; Lemaigre, 2003; Antoniou *et al.*, 2009). Additionally, a knockdown study of β -catenin in cultured hepatoblasts observed the impairment of bile duct formation; thus, demonstrating the role of canonical WNT signalling in hepatoblast differentiation towards a cholangiocyte fate (Satdarshan P.S. Monga *et al.*, 2003).

On the other hand, hepatoblasts differentiation into mature hepatocyte relies on the combinatorial activity of transcription factors, cytokines, and signalling molecules. Key transcription factor involved in hepatocyte lineage specification is *HNF4 α* . This is supported by studies conducted on murine lacking *HNF4 α* that exhibited abnormal hepatocyte morphology. Interestingly but mechanistically unclear, *HNF4 α* is involved in periportal hepatocyte differentiation while pericentral hepatocytes are maintained by β -catenin/ WNT signalling (Kamiya *et al.*, 1999; Kamiya, Kinoshita and Miyajima, 2001; Michalopoulos *et al.*, 2003; Cheng *et al.*, 2006; Kymizi *et al.*, 2006). Furthermore, two studies showed the implication of additional

transcription factors involved in hepatocyte lineage specification; they showed that double mutant of two transcription factors, *HNF1 α* and *C/EBP α* , presented abnormal glycogen storage which led to lethality in mice. (Wang *et al.*, 1995; Pontoglio *et al.*, 1996).

Mutational analysis on Oncostatin M (OSM) receptor gp130 and HGF showed an impairment of hepatocyte maturation (Kamiya *et al.*, 1999); hence showing the importance of these two cytokines in liver development.

Similarly, the activity of signalling molecules is likewise important for hepatic specification. As described before, WNT signalling is essential for both early and late stages of liver development. However, its role in hepatoblast differentiation into hepatocytes is far more complicated. Whereas β -catenin/WNT signalling promotes cholangiocyte lineage, stabilisation of β -catenin expression is also involved in hepatocyte differentiation. Indeed, β -catenin covers many roles in hepatocyte maturation including the establishment of hepatocyte polarisation via interaction with E-cadherin, and maintenance of hepatocyte proliferation through HGF/c-Met signalling pathway (Hussain *et al.*, 2004; Decaens *et al.*, 2008; Tan *et al.*, 2008). In contrast to the knowledge that hepatoblasts commitment towards hepatic lineages occurs at E13.5, work conducted by Yang *et al.*, (2017), showed the pre-existence of a transcriptionally heterogenous population of hepatoblast already at E11.5. This observation was further reinforced by the work conducted in our lab by Prior *et al.*, (2019), which demonstrated that hepatoblast functional commitment already pre-existed at E9.5 with the WNT target gene *Lgr5* marking the apex of the hepatoblast pool.

1.2.2 Homeostasis

The adult liver is a slow turnover organ during homeostasis. Under normal physiological conditions, the liver epithelium is preserved primarily through adult hepatocyte proliferation (Duncan, Dorrell and Grompe, 2009). Hepatocytes have a finite lifespan of approximately 400 days, with only 0.025% of hepatocytes able to self-replicate (Magami *et al.*, 2002).

The identification of the source of hepatocyte output remains as an unresolved biological question. In the 80's, considerable focus was given on periportal hepatocytes in a proposed "liver streaming hypothesis" by Zajicek, Oren and Weinreb (1985); which states that the hepatocytes located near the portal tract are the ones capable to slowly migrate along the portal-venous axis and replenish the liver parenchyma. Although this hypothesis was rejected after 10 years (Kennedy *et al.*, 1995), it was recently reinforced by (Furuyama *et al.*, 2011) who lineage traced a subpopulation of biliary cells expressing Sox9. To sustain whole hepatocyte turnover, these cells migrated from the portal tract towards the central vein, with the difference that the source of hepatocyte formation were duct cells and not resident hepatocytes as described by (Zajicek, Oren and Weinreb, 1985). Conflicting evidence showed instead that Sox9+ cholangiocytes are not the drivers of the whole liver parenchyma turnover, but only of periportal hepatocytes and ductal cells (Carpentier *et al.*, 2011). In the same year, opposed to Furuyama *et al.* (2011), Malato *et al.* (2011) showed no evidence of biliary cells giving rise to hepatocytes, hence excluding the hypothesis of a population of biliary progenitor cells sustaining the liver parenchyma under physiological conditions.

More recently, opposed to the hepatic cell streaming hypothesis along the portal-venous axis, a reversed streaming of pericentral hepatocytes was observed from the central vein to the portal vein. Lineage tracing studies showed a subpopulation of pericentral hepatocytes expressing the WNT target gene *Axin2* with the stemness ability to self-renew and sustain homeostatic liver conditions (Wang *et al.*, 2015). This is in agreement with the hypothesis of the liver parenchyma being supported with pre-existing hepatocyte turnover rather than the hypothesis of a stem cell niche at the top of a hierarchical organisation.

However, the evidence of pericentral hepatocytes as the chief cells during homeostasis has been contradicted by Planas-Paz *et al.* (2016) who observed equal proliferative rates among hepatocytes from different zones. However, this is in contrast with a recent study which argued the proliferative capacity of zone 3 pericentral hepatocytes to contribute in liver regrowth compared to zone 1 and zone 2 hepatocytes (He *et al.*, 2021). This is in agreement with another work which identified zone 2 hepatocytes to be an important source for hepatocyte turnover,

hence being in favour of the existence of a zonal hepatocyte heterogeneity to contribute in liver repopulation instead of an homogenous contribution from all zones (Wei *et al.*, 2021).

1.2.3. Regeneration

Although the liver appears to be mitotically inactive during homeostasis, paradoxically it is also renowned for its remarkable capacity to regenerate in response to hepatic injury. Since ancient times, the potential of liver regeneration was described in the Myth of Prometheus by Zeus for revealing the secret of fire to the humankind. As a punishment, his liver was perpetually eaten by eagles whilst eternally regenerated. Today this scenario is classically studied in the model of partial hepatectomy (PH) in which 70% of the liver is surgically removed (Higgins, 1931; Michalopoulos, 2007). As a result, the remaining hepatic cells exit their dormant state and enter the cell cycle to undergo DNA synthesis and proliferation until the original liver weight is restored. In humans the liver will gain its original weight within months, while this process is much faster in rodents, which instead requires approximately a week to fully recover (Higgins, 1931; George K. Michalopoulos* and Marie C. DeFrances, 1997; Michalopoulos, 2007).

Although the regenerative potency of the liver is remarkable upon PH, this capacity is impaired during chronic diseases such as viral hepatitis, cirrhosis, and alcohol induced injury. Being the workhorse of metabolic function in the liver, hepatocytes are continuously exposed to foreign agents, leading to an elevated probability to be damaged. What happens when hepatocytes proliferation is impaired upon injury? Although still a controversial subject, the hypothesis is that hepatic progenitor cells are activated to regenerate the liver parenchyma.

The very first evidence on the existence of progenitor cells was shown on damaged adult rat livers; epithelial cells resembling “oval cells” exhibited the capacity to proliferate and give rise to both cholangiocyte and hepatocyte cells (Farber, 1956).

Today, these facultative progenitor cells are defined as the adult stem cell niche of the adult liver and are presumably located at the biliary compartment of the liver, more specifically located at the canal of Hering. More recently, *Lgr5* has been identified as an adult stem cell marker enriched following injury; cultured *Lgr5*⁺ progenitor cells differentiated into both cholangiocyte and hepatocyte *in vitro* (Huch *et al.*, 2013).

Nevertheless, the existence of a stem cell niche located at the biliary compartment being activated following injury is still uncertain. Lineage tracing targeting biliary markers such as Sox9 and Opn have showed minimal contribution towards hepatocyte formation (Yanger *et al.*, 2013; Tarlow *et al.*, 2014). This further contradicts the previously discussed work conducted by Furuyama *et al.* (2011) on the Sox9 biliary cells committed towards hepatic lineage during homeostasis. However, it is important to delineate that the lineage tracing system adopted, and model of injury differs enormously among the studies, which could have potentially affected the progenitor response.

Further challenging the existence of a biliary stem cell population in favour of a pool of self-replicating hepatocyte during regeneration, arise from the work conducted by Font-Burgada *et al.* (2015) and later by Lin *et al.* (2018). In the model of CCl₄ chronic liver damage, Font-Burgada *et al.* (2015) showed the existence of an “hybrid” population of hepatocytes (HybHP) expressing both biliary (low Sox9 expression) and hepatocyte markers (HNF4) located near the portal tract which become activated during regeneration. Later on, Lin *et al.* (2018) instead showed a new population of hepatocytes with high telomerase expression which they identified throughout the liver lobule. Upon pericentral injury, both population of cells are activated and proliferate to repair the damaged site at the pericentral zone (Font-Burgada *et al.*, 2013.; Lin *et al.*, 2018).

An alternative theory to liver progenitor cells and hepatocyte self-replication to sustain the liver parenchyma upon injury, is the trans-differentiation hypothesis of hepatocytes into cholangiocytes and vice versa. More specifically, upon impairment of one epithelial compartment the other epithelial cell type transdifferentiates into the damaged epithelial population to mediate regeneration. Several papers challenged the strict concept of hepatocyte identity being stable in the liver and

supported the event of hepatocyte to cholangiocyte trans-differentiation. Michalopoulos *et al.* (2002) endorsed this concept by conducting a study on severely periportally injured rat livers expressing the hepatocyte marker dipeptidyl peptidase IV (DPPIV). The work showed a transition of hepatocytes into chimeric cholangiocytes which still retained the expression of DPPIV (Michalopoulos *et al.*, 2002). Similarly, when hepatocyte proliferation is impaired, cholangiocytes transdifferentiate into hepatocytes to replenish the damaged parenchyma (Lu *et al.*, 2015; Raven *et al.*, 2017; Deng *et al.*, 2018).

In summary, whether the main source of liver regeneration upon injury is driven via stem cells, or via the plasticity of the epithelial compartment, it remains an open question in the stem cell field.

1.2.4 Mechanism of hepatocyte plasticity

The plasticity of hepatocyte (Figure 1.2) to trans-differentiate into cholangiocyte or dedifferentiate into progenitor is achieved through the regulation of several signalling pathways. Notch signalling has been confirmed to be implicated in the process; overexpression of Notch intracellular domain (NICD) was enough to induce trans-differentiation of hepatocytes into cholangiocytes in homeostatic condition (Yanger *et al.*, 2013). This is further supported by a study showing deletion of a key component of Notch signalling, *Rbpj*, that decreased the hepatocyte-cholangiocyte conversion in damaged murine livers (Schaub *et al.*, 2018).

In addition to Notch signalling, another signalling pathway involved in hepatocyte-cholangiocyte conversion is WNT signalling. Hepatocytes overexpressing β -catenin exhibited an increase of ductal cell markers expression upon liver periportal injury (Okabe *et al.*, 2016). This transition from an hepatocyte fate into a more progenitor state was observed by Hu *et al.* (2018) that challenged the identity of terminally differentiated hepatocytes to acquire a regenerative potential *in vitro*; primary hepatocytes embedded in Matrigel expanded clonally as organoids in WNT driven culture medium, hence suggesting that the hepatocytes partially acquired a

progenitor state whilst maintaining hepatocyte features (Hu *et al.*, 2018; Zhang *et al.*, 2018).

In addition to Notch and WNT signalling, TGF- β signalling has been shown to play a key role in converting hepatocyte to cholangiocyte fate in the mouse model of human Alagille syndrome; upstream repression of Tgfbr2 receptor or hyperactivation of Tgfbr1 receptor in hepatocytes either blocked or activated the TGF- β signalling, leading to a significant reduction or promotion of hepatocyte to cholangiocyte trans-differentiation, respectively (Schaub *et al.*, 2018).

Gene expression studies have described the importance of another key regulator of hepatocyte trans-differentiation, the Hippo signalling pathway; (Figure 1.3) downstream effector is the Yes1-associated protein 1 (YAP1). The very first evidence of the importance of Hippo signalling in the liver came from studies conducted by Camargo *et al.* (2007) and Dong *et al.* (2007); both works demonstrated a dramatic increase of liver growth upon YAP1 hyperactivation. Of note, YAP1 level of expression differs enormously along the hepatic epithelium; higher YAP1 protein expression is predominantly localised in the biliary compartment and to a lower extent in hepatocytes. This different level of YAP1 activity in the epithelium has emerged as a factor to manipulate hepatic cell fate. The latter evidence arises from Yimlamai *et al.*, (2014) who showed that overexpression of YAP1 in hepatocytes leads to a dedifferentiation process into ductal/progenitor fate. More specifically, approximately 75% of hepatocytes changed their fate upon YAP1 activation *in vivo*. Interestingly, the differentiated cells retained the capacity to revert back to the hepatocyte fate in concomitance with YAP1 activity reduction (Yimlamai *et al.*, 2014). This further endorses the concept of plasticity of the hepatic epithelium to change cellular fate in response to injury. In line with this, a recent study from the same lab unveiled the role of YAP to be a crucial factor for the reprogramming of hepatocytes to biliary-progenitor cells upon injury and to be essential for the maintenance of adult biliary cells in homeostatic conditions. This further indicates the dynamical involvement of YAP signalling in the hepatic epithelium (Pepe-Mooney *et al.*, 2019).

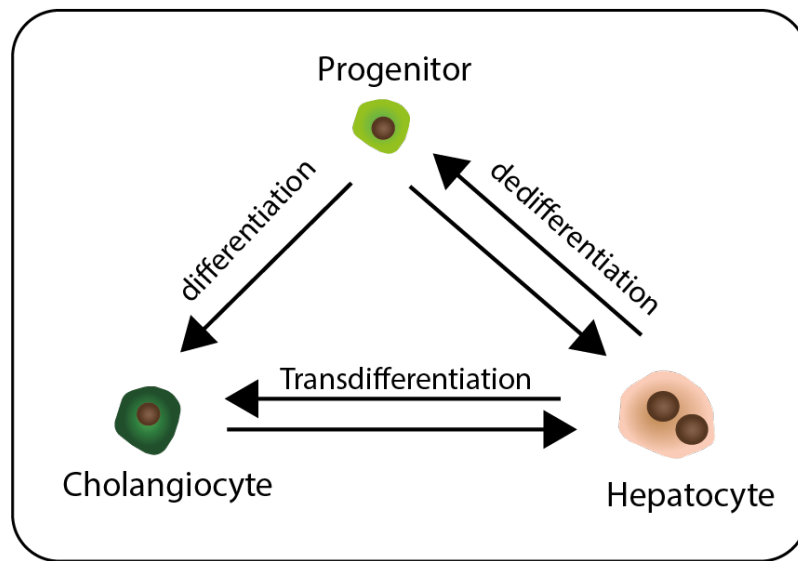


Figure 1.2 **Liver plasticity**. The scheme presents a summary of the remarkable capacity of the liver epithelium to regenerate upon chronic liver injury. Progenitor cells differentiate into hepatocyte and cholangiocyte to regenerate the liver. When the injury become severe, cholangiocytes can transdifferentiate into hepatocyte. Despite the finite proliferative capacity of the hepatocytes in homeostasis, upon liver injury hepatocytes have been shown to have the capacity to dedifferentiate into progenitor cells and to transdifferentiated into cholangiocytes when these cells become depleted.

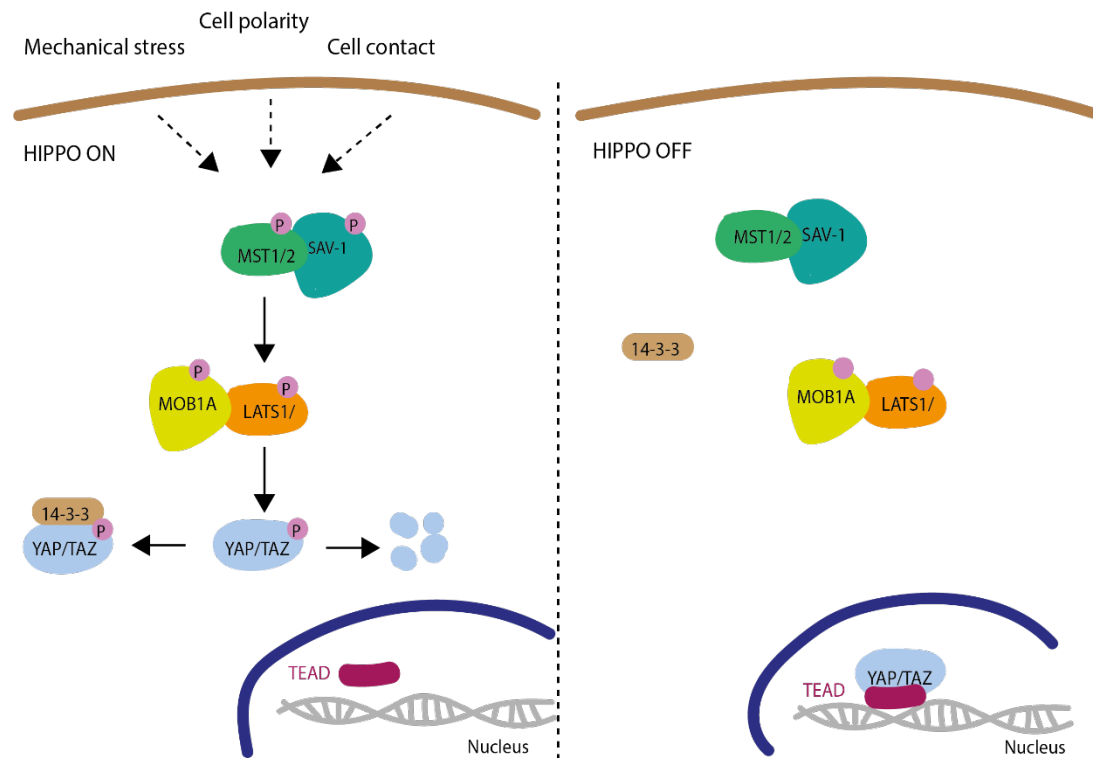


Figure 1.3 **Overview of the Hippo signalling pathway.** When the Hippo signalling pathway is on, stimuli derived from cell polarity, mechanical stress and cell-cell contact, activate a cascade of kinases (MST1/MST2, LATS1/LATS2) that induce the transcriptional inactivation of YAP/TAZ. When the Hippo signalling is off, YAP/TAZ are not phosphorylated, but instead translocate to the nucleus. Once in the nucleus YAP/TAZ bind to the TEAD family of transcription factors and drive the transcription of the YAP target genes.

1.3 The chief hepatic cell: Hepatocytes

Hepatocytes form approximately 80% of the entire liver adult parenchyma and are the most abundant hepatic cell type in the adult liver. Shaped similarly to a polygon, hepatocytes are the dominant functional cells of the liver (Blouin, Bolender and Weibel, 1977; Gebhardt, 1992).

As the liver continuously receives blood supply, it brings in the front-line hepatocytes which are constantly exposed to everything that the organism digest such as nutrients and xenobiotics. Carried via the sinusoids from the portal tract, these substances pass through the space of Disse and reach the hepatocyte cords ('Pathology of the liver: Edited by R.N.M. MacSween, P.P. Anthony, and P.J. Scheuer,

Foreward by H. Popper. 458 pp., Churchill Livingstone, New York, 1980). At this stage, hepatocytes perform two fundamental functions to purify the blood circulation: uptake and breakdown of nutrients such as lipids, and synthesis of bile and blood plasma proteins such as albumin, which contributes to 55% of the total blood plasma proteins (Gebhardt, 1992). As a result, filtered blood is then drained into the central vein and emptied into the inferior vena cava. Although this filtration role is essential, it also exposes the liver to a high risk of damage (Gebhardt, 1992; Lauth, 2009).

To sustain this incessant flow system, hepatocytes have developed into highly polarised cells (Figure 1.4); tight junctions segregate their plasma membranes into two physiologically distinct domains respectively known as basolateral or sinusoidal membrane and apical or canalicular membrane. The basolateral domain is rich in microvilli that face the space of Disse; conversely, the apical membrane faces adjacent hepatocytes. Neighbouring hepatocytes are connected through a complex network of extracellular spaces with a diameter of 1 and 2 μm , called bile canaliculi, which are the terminal branches of the biliary tree. At the lobular level, bile canaliculi ultimately unite with bile ducts at a site defined as Canal of Hering (Rogers and Dintzis, 2012).

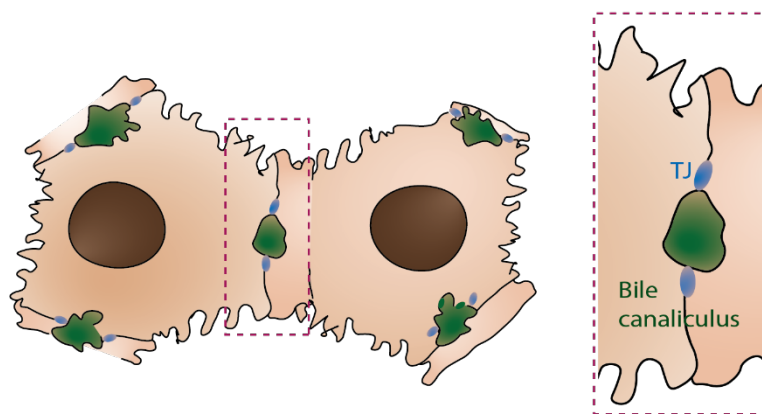


Figure 1.4 **Hepatocyte polarisation.** Hepatocytes secrete bile into the terminal branches of the biliary tree termed bile canaliculi (green), which drain the bile into the bile duct. From this point, the secreted bile is transported through the ductal network until it is stored in the gallbladder.

This unique polarisation differs enormously from the classical polarisation of columnar epithelial cells, including that of the cholangiocytes of which apical domains are oriented facing a central lumen (Strazzabosco and Fabris, 2008).

Each hepatocyte membrane has a distinct function composed of a defined set of membrane proteins. The basolateral (sinusoidal) domain hosts the uptake membrane transporters and a set of tyrosine receptors such as the EGF receptor. At this site, exchange between plasma and cellular content occurs via the sinusoids. On the other hand, the apical (canalicular) domain is populated by the ATP binding proteins, adherens junction and tight junctions. Tight junctions are essential to seal to adjacent hepatocytes and prevent reversal diffusion of bile from the bile canaliculus into the blood system and inside the hepatocyte, as bile accumulation is highly toxic to the cells (Rogers and Dintzis, 2012).

The polarised expression of proteins either at the basal or apical domain is dependent on an intracellular sorting system that allows the segregation of these proteins to the right cellular site. Not surprisingly, the origin of hepatocyte membrane proteins follows the well-known axis from nucleus to endoplasmic reticulum to the Golgi apparatus. At the Golgi, these proteins are modified, packaged into vesicles, transported and exocytosed to the canalicular or sinusoidal domain. Tight regulation of the protein sorting machinery is important to maintain hepatocyte polarisation and function (Gebhardt, 1992; Rogers and Dintzis, 2012).

Despite the uniform appearance at the anatomical level, depending on the location in the hepatic plate along the portal-venous axis, hepatocytes are metabolically heterogenous. This metabolic segregation has been termed as liver zonation. WNT signalling has been identified as an important driver for metabolic zonation, with higher WNT expression in pericentral hepatocytes (Figure 1.5) (Gebhardt, 1992; Jungermann and Kietzmann, 1996). Xenobiotic metabolism is driven by the hepatocytes located near the central vein.

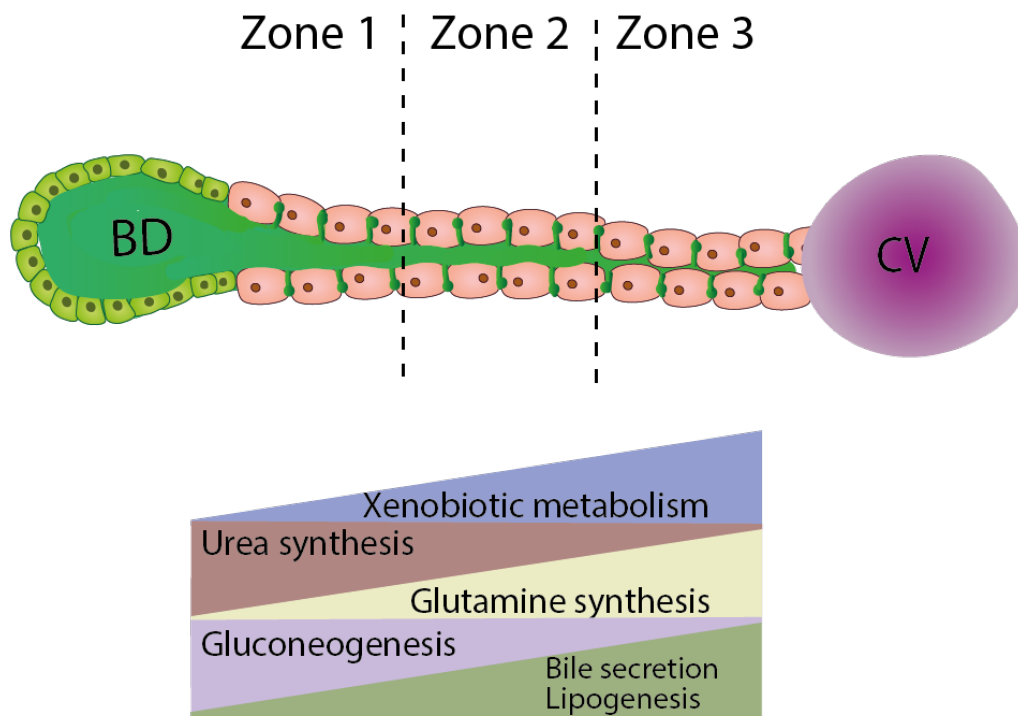


Figure 1.5 **Metabolic zonation of the liver.** Hepatocytes are functionally heterogenous along the portal-venous axis of the live lobule. Zone 1 hepatocytes are closer to the portal area and carry out gluconeogenesis and urea synthesis, while Zone 2 hepatocytes exhibit intermediate features of both Zone 1 and Zone 2 hepatocytes. Zone 3 hepatocytes carry out bile secretion, lipogenesis, and xenobiotic metabolism.

1.3.1 Hepatocytes secretory system

Hepatocytes uninterruptedly work behind the scenes whenever a meal is digested, and one vital task performed is the bile synthesis. It has been estimated that the human liver daily produces between 0.2g-0.6g of bile acids. At its simplest, bile is an aqueous solution composed of 95% water and a mixture of other substances including vitamins, drug metabolites, bile salts, cholesterol, toxins, bilirubin and amino acids. Formation of bile is important for several reasons; to name some it is the primary route of elimination of dangerous toxins and cholesterol; additionally, bile salts facilitate the absorption of lipids into the intestine (Boyer, 2013).

Biosynthesis of bile acids initiates with the hydroxylation of cholesterol mediated by CYP7A1 enzyme, giving rise to two primary bile salts: cholic acid (CA)

and chenodeoxycholic acid (CDCA). To prevent passive re-absorption of bile salts after secretion from the hepatocytes into the biliary tree, bile salts are reinforced with a conjugation step of either a taurine or glycine at their side chains. Once transported into the intestine, conjugated CA and CDCA are then deconjugated by intestinal bacteria forming secondary bile acids, into deoxycholic acid (DCA) and lithocholic acid (LCA). To date, the human bile has had 12 conjugated primary bile acids and secondary bile salts characterised. Deconjugated bile acids can undergo two fates: either excretion into the faeces or re-entering the enterohepatic circulation to be transported back from the intestine into the liver via the portal blood flow (Duane and Javitt, 1999; Hofmann, 2004; Boyer, 2013).

When the metabolic requirement is terminated, the continuous bile flow must also end. To achieve this, the liver has developed a regulatory system to preserve physiological levels of bile acids pool; bile salts act as negative feedback to counteract the activity of CYP7A1, hence controlling the overall rate of bile acids synthesis and homeostasis. Key factor in regulation of the enterohepatic circulation of bile acids involves the action of a nuclear receptor called the farnesoid X receptor (FXR) (Boyer, 2013). Cycling bile salts entering the hepatocyte act as ligands for FXR; this induces transcriptional activation of fibroblast growth factor 19 (FGF19). As a result, FGF19 binds to fibroblast growth factor 4 (FGF4) in the hepatocytes initiating a signalling cascade which downstream effect leads to repression of CYP7A1 bile acid biosynthesis (Zweers *et al.*, 2012). At the same time, induction of FXR transactivates target gene promoters of the family of ATP binding cassette (ABC) transporters known as *ABCB11*, which encodes the bile salt export pump (BSEP) protein, expressed at the apical membrane of hepatocyte (Kipp and Arias, 2000; Ananthanarayanan *et al.*, 2001); BSEP allows secretion of conjugated bile acids into the bile canaliculus and prevents over accumulation inside the cellular environment. The role of FXR on BSEP expression is supported by studies on mice deficient in FXR that showed reduced BSEP expression (Ananthanarayanan *et al.*, 2001; Müller *et al.*, 2002). Given the role of FXR on the apical membrane transporter, in 2016, the food and drug administration (FDA) has approved an FXR agonist drug also called obeticholic acid for the treatment of primary biliary cholangitis (Jones, 2016).

1.3.1.1 The bile salt export pump (BSEP)

Being discovered as sister of P-glycoprotein (*ABCB1*) following an extensive screening in the pig liver by Childs *et al.*, (1998) it was only after remarkable work conducted by Gerloff *et al.*, (1998) that Pgp protein function was elucidated as a bile acid membrane transporter in the rat liver. Following these studies, the protein encoding the *ABCB11* gene was termed BSEP (Figure 1.6).

As part of the family of ABC transporters, BSEP consist of 12 transmembrane regions with conserved sequences called Walker A and B for ATP binding site; its mode of function consists of substrate translocation from the hepatocyte into the bile canaliculi using ATP hydrolysis as a source of energy (Kipp and Arias, 2000; Noé, Stieger and Meier, 2002; Ho *et al.*, 2010). Mutation of the human BSEP leads to familial intrahepatic cholestasis type 2 (PFIC2) disorder; patients suffering from PFIC2 display accumulation of bile acids in the liver with subsequent hepatocellular injury. To date, liver transplantation is the sole treatment for this genetic disorder (Strautnieks *et al.*, 1998; Hayashi *et al.*, 2005).

Expressed exclusively in hepatocytes, BSEP expression is highly dependent on the metabolic demand. It has been shown in rat hepatocytes that the half-life of BSEP is between 4 to 6 days at the apical membrane. Post-transcriptional regulation of BSEP route of localisation at the apical membrane is dependent on many factors which remains under debate; based on vesicular transport studies, BSEP is shuttled either via transcytosis from the basal membrane or exocytosis from the Golgi apparatus (Kipp and Arias, 2000; Kipp, Pichetshote and Arias, 2001).

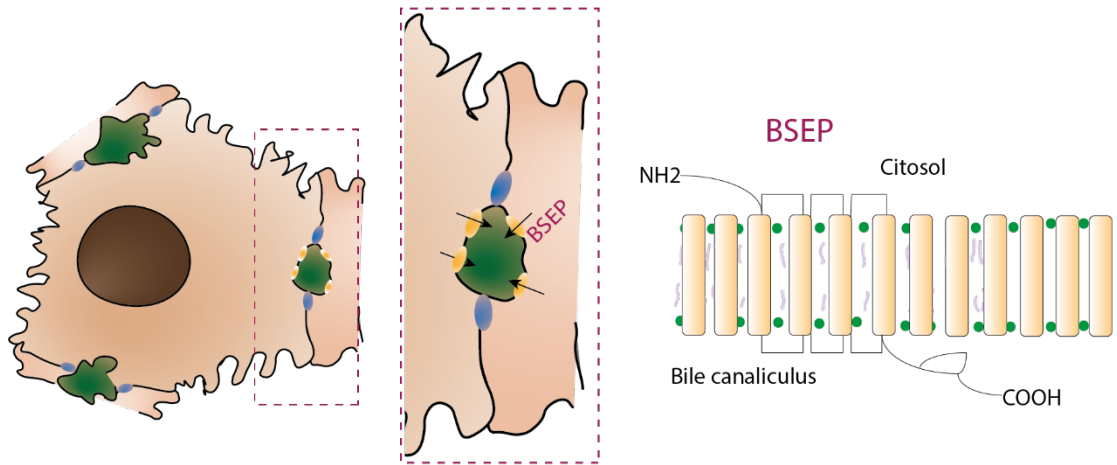


Figure 1.6 **The bile salt export pump.** Functional secretion of bile into the bile canaliculus is achieved via the activity of apical membrane transporters as BSEP. BSEP protein consist of 12 transmembrane regions and drives bile clearance through ATP hydrolysis.

1.3.3 Hepatocyte as centre of drug metabolism

When ingested in the organism, most of the drugs pass through the liver either to be activated or inactivated. To fulfil the drug metabolism tasks, pericentral hepatocytes have adopted a metabolic machinery that allows the enzymatic conversion of drugs into more water-soluble compounds to be excreted out via bile or urine. Drug metabolism is achieved by two fundamental steps: phase 1 and phase 2 metabolism (Figure 1.7) (Iyer and Sinz, 1999).

Phase 1 metabolism

The enzymes involved in the first phase of drug metabolism are called cytochromes P-450. Bound to intracellular membranes of hepatocytes and presenting a prosthetic heme pigment that absorbs light at a wavelength of 450nm, this family of proteins comprise of more than 50 enzymes, yet only six of them (CYP1A2, CYP2C9, CYP2C19, CYP2D6, CYP3A4, and CYP3A5) are involved in 90% of drug oxidation. At its simplest, the product formed after the reaction between a cytochrome and a drug is the addition of a hydrophilic group; this renders the compound easily excretable (Zanger and Schwab, 2013).

Phase 2 metabolism

At this point, the product of phase 1 metabolism serves as point of attachment for phase 2 metabolism. This step requires replacement of a hydrogen atom with conjugation agents. The most important type of conjugation involves uridine diphosphate glucuronosyltransferase (UDPGT) which is the microsome responsible for the type of conjugation called glucuronidation. Once metabolised, the final product can be excreted through the bile or urine (Zanger and Schwab, 2013).

The interference of multiple drugs that share the same metabolic pathway is the caveat of this process. Two drugs taken at the same time may compete for the same CYP450 enzyme resulting either in an augmentation or dramatic decrease of drug concentration in the blood. Therefore, precautions must be taken when administering inducers or inhibitors of CYP enzymes as this can alter the pharmacokinetic and toxicity of drugs (Lafite *et al.*, 2007).

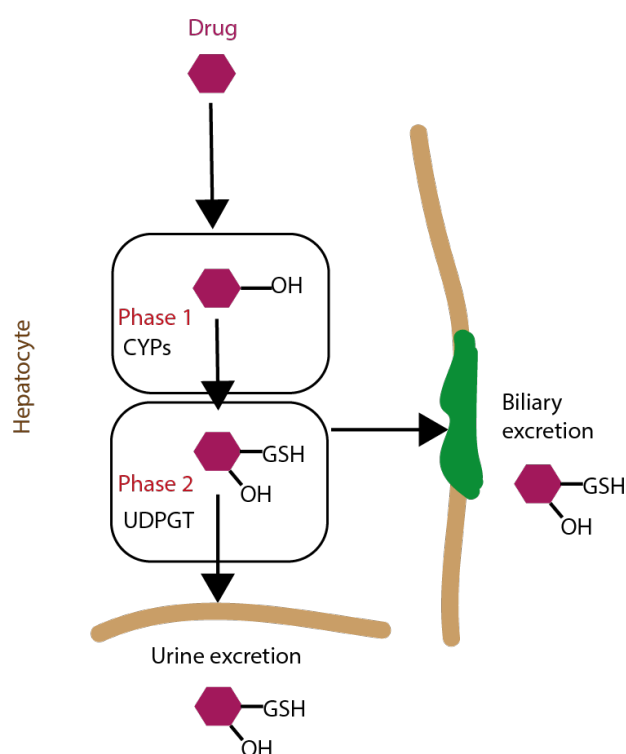


Figure 1.7 **Overview of drug metabolism in hepatocytes.** The process of drug metabolism facilitates the elimination of drugs from the system through a series of chemical reactions which are grouped in two phases. During phase I of drug metabolism, drugs are predominantly oxidised by enzymes of the cytochrome P-450 family. The generated metabolites from phase I or drugs that bypass phase I are rendered water soluble through the action of conjugation reactions of phase II metabolism (glucuronidation, sulfation, methylation, acetylation).

1.4 Drug induced liver injury

The beneficial properties of drugs often is outweighed by the development of adverse drug reactions (ADR) (Lazarou, Pomeranz and Corey, 1998). The major type of ADRs is hepatotoxicity given the primary role of the liver as a drug detoxifying organ. Therefore, assessment of liver safety before a drug is marketed is a key step to avoid the occurrence of unwanted side effects. The unpredictable process of drugs to induce damage to the liver is termed drug induced liver injury (DILI). The occurrence of DILI can either be predictable (intrinsic) when the individual is exposed to toxic doses of the drug given or unpredictable (idiosyncratic) (Watkins, 2005). The latter is far more challenging to diagnose as the cause of hepatotoxicity is dependent on the individual susceptibility. Nevertheless, some other currents of thought consider the two types of toxicity undistinguishable.

DILI is the primary cause of acute liver failure in Western countries due to the wider accessibility to medication compared to poorer countries (Lasser *et al.*, 2002; Watkins, 2005; Reuben, Koch and Lee, 2010). For instance, high doses of acetaminophen (APAP) accounts for approximately 50% of acute liver failure in Western countries (James, Mayeux and Hinson, 2003). However, growing evidence over modern medicine comes from traditional medicines such as herbal supplements, which may result in liver toxicity in developing countries (Amadi and Orisakwe, 2018).

The aetiology of DILI is highly challenging, which is often encompassing of drug type, patient clinical history and genetics. Far more complicated is the lack of standardised methods to recognise DILI; it involves multiple screening methods such as liver biochemistry and bioimaging, but very often it is a diagnosis of exclusion.

Based on the severity spectrum of DILI most patients can either fully recover, require liver transplantation or die at the most extreme (Navarro and Senior, 2006).

1.4.1 Pathogenesis of DILI

The severity of DILI is often due to its misleading clinical manifestations that can resemble non-drug derived liver disease. In general, analysis of hepatic serum enzyme levels is the standard clinical diagnosis to identify any underlying ongoing liver disease. However, very often elevation of liver enzymes occurs only at later stages of hepatic disease when the pathogenesis is irreversible (Dragovic *et al.*, 2016); hence suggesting the need to identify early patterns of liver injury that are specifically induced by drug toxicity. Nevertheless, many studies have identified some common events that can be associated only with the onset of DILI. Based on the clinical pattern, drug toxicity has been classified in five major classes: cholestasis, formation of reactive species, lysosomal disorder, steatosis, and mitochondrial injury (Dragovic *et al.*, 2016) (Figure 1.8).

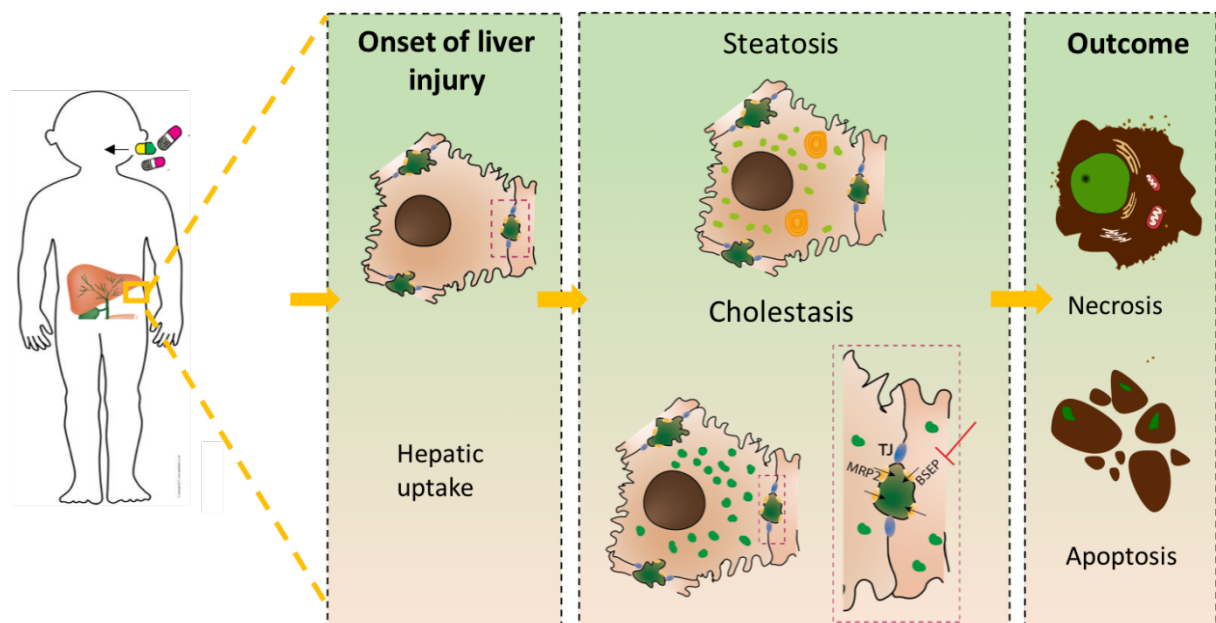


Figure 1.8 **Overview of DILI process.** DILI progression can be subdivided into two phases: early phase and late phase. During the early phase, potential DILI drugs exert toxicity at the organelle level in the hepatocyte. Drugs

can inhibit the biliary flow from the hepatocyte to the bile duct in a process called cholestasis, this leads to excessive bile accumulation in the cell. Additionally, drugs can impair fat metabolism in a process called steatosis. Failure to detect the early phase of DILI, results in hepatocellular damage (late phase).

1.4.1.1. Cholestasis

Bile acid synthesis is an essential hepatic function that serves for digestion of nutrients as well as for the elimination of metabolites (Boyer, 2013). However, obstruction of bile acid secretion from the hepatocytes with subsequent increase of intracellular bile acids leads to the onset of one of the most severe patterns of DILI: cholestasis (Zollner and Trauner, 2008). Concentrations of intracellular bile acids above the physiological levels of 3-7 μ M are associated with hepatotoxicity (Scherer *et al.*, 2009; Tribe *et al.*, 2010).

Drug induced cholestasis (DIC) may mimic other type of non- drug induced liver cholestatic disease; failure to recognise the causative cholestatic drug may lead to an irreversible form of liver injury. On the other hand, immediate recognition, and discontinuation of the cholestatic medication may restore the liver into a healthy state (Zollner and Trauner, 2008). Investigation on the accumulation of cytotoxic bile acids have been associated with several toxic phenotypes in the cell, from the disruption of cellular membranes via formation of reactive oxygen species (ROS), mitochondrial damage, to the endoplasmic reticulum stress (Perez and Britz, 2009). As a result, the prolonged retention of hydrophobic bile acids may lead to hepatocellular injury. More specifically concentration of toxic bile acids in the range of millimolar leads to hepatocyte necrosis, while lower concentration of hydrophobic bile acids in the range of micromolar activates the apoptosis cascade via the death receptors Fas and TRAIL-R2 leading to caspase-8 activation (Faubion *et al.*, 1999; Perez and Britz, 2009)

Drugs with the susceptibility to cause cholestasis have been associated to inhibit BSEP activity (Figure 1.7) (Giacomini *et al.*, 2010; Morgan *et al.*, 2010) (Giacomini *et al.*, 2010). Correlation between known human cholestatic and non-cholestatic drugs have confirmed the higher incidence of cholestatic drugs to promote BSEP inhibition, which led to the suggestion that interference of BSEP activity could

be an important triggering factor of human DILI (Morgan *et al.*, 2010; Dawson *et al.*, 2012)

Several mechanisms may lead to the alteration of BSEP function, drugs may competitively inhibit BSEP activity, disrupt its gene expression via FXR antagonism, and manipulate its translocation to the apical membrane (Soroka and Boyer, 2014). So far, several drugs have been identified as direct competitive inhibitors of BSEP including Rifampicin, Troglitazone, Bosentan and Cyclosporine A (CsA) (Stieger *et al.*, 2000; Fattinger *et al.*, 2001; Funk, Pantze, *et al.*, 2001; Funk, Ponelle, *et al.*, 2001). CsA is an immunosuppressive drug given to post-transplant liver patients to enhance survival. Both *in vitro* and *in vivo* studies have shown CsA interaction with the enterohepatic circulation of bile via inhibition of bile salt synthesis and secretion (Roman *et al.*, 1990; Böhme *et al.*, 1994; Stieger *et al.*, 2000; Román *et al.*, 2003). Another drug associated to DIC, bosentan, caused a dose-dependent accumulation of serum bile salts *in vivo* which potency was further enhanced with co-administration of another drug called glibenclamide (Fattinger *et al.*, 2001). This was also observed *in vitro* with the inhibition of taurocholate transport, a substrate of BSEP (Fattinger *et al.*, 2001)

1.4.1.2. Steatosis

A minimum of 5% fat deposition within hepatocytes is a common feature in patients suffering from non-alcoholic fatty liver disease (NAFLD) (Kanwar and Kowdley, 2016). Accounting for approximately 50% in obese and diabetic patients in Western countries, and to a less extent in the general population, NAFLD may lead from minor forms to more severe hepatic diseases (Bedogni *et al.*, 2005; Sayiner *et al.*, 2016).

On the other hand, drug induced steatosis (DIS) is a rare manifestation of DILI which diagnosis is very often mistaken for NAFLD (Farrell and Larter, 2006; Fromenty, 2017). However, higher incidence of NAFLD may also be justified by the presence of pre-existing steatotic tissue in livers of DILI patients (Tarantino *et al.*, 2007). Several drugs are associated with DIS including amiodarone, tamoxifen and

valproic acid (Lewis *et al.*, 1990; Scott *et al.*, 1991; Gudbrandsen, Rost and Berge, 2006). Depending on the underlining disease, DIS can be histologically subdivided from mild to more severe manifestations. Expansion of a single large vacuole of fat within the whole hepatocyte cellular compartment is often a reversible form of DIS associated to macro-vesicular steatosis (Begrache *et al.*, 2011). On the contrary, more severely, formation of small multiple lipid droplets in the cytoplasmic compartment with mitochondrial injury is associated to micro-vesicular steatosis (Tandra *et al.*, 2011; Zhang, Ouyang and Thung, 2013).

Different sources may contribute to the free fatty acid (FFA) pool in the liver, impairment of such a regulated system leads to excessive fat deposition within the hepatocyte; increased hepatic uptake from circulating FFA, increased *de novo* hepatic lipogenesis, impairment of fatty acid oxidation, and FFA disposal via formation of very low-density lipoproteins (VLDL), all may contribute to increased lipid concentration within the hepatocyte (Donnelly *et al.*, 2005; Bessone *et al.*, 2018). However, more studies are needed to elucidate the exact mechanism of DIS compared to other steatotic diseases.

1.4.1.3. Reactive metabolites

APAP is probably one of the most used over the counter medicine to treat many conditions such as fever, common cold and headaches, as such its mechanism of hepatotoxicity has been widely studied. At therapeutic doses, APAP is converted into non-toxic products via the phase II conjugating enzymes and cleared out with the urine (Feng *et al.*, 2014). A small proportion of APAP is metabolised via CYP2E1 into a reactive metabolite called N-acetyl-p-benzoquinone imine (NAPQI) and then detoxified by the phase II conjugating enzyme glutathione (GSH). However, above the recommended doses the phase II conjugating enzymes are oversaturated, this leads to a surplus production of NAPQI which reduces the levels of GSH. As a result, NAPQI binds to liver proteins leading to oxidative stress and hepatocyte necrosis (Feng *et al.*, 2014).

1.4.2. Current preclinical hepatic models to study DILI

Although many studies have helped in the advancement to understand DILI pathology, still many gaps remain in the field of DILI prediction and therapy. The predisposition of a drug to cause DILI is often identified when a drug is already on the market. A notable example is provided by the discontinuation of a widely used and economically profitable drug called Troglitazone (Nichols *et al.*, 2008). Its termination resulted in a huge economic loss, but it has also negatively impacted the healthcare system. The withdrawal of a drug may also occur at later stage of drug development, after years of preclinical testing, exemplified with a drug designed for type 2 diabetes called Fasiglifam which was discontinued at phase III clinical trials after presenting adverse liver profiles (Marcinak *et al.*, 2018). Therefore, DILI assessment is essential for the successful continuation of a drug development, and for the design of a drug that is safe for the patient. One of the greatest challenges to assess DILI during the preclinical phase of drug discovery is the poor toxic predictivity of available *in vitro* and *in vivo* preclinical models (Olson *et al.*, 2000). Currently, a platform of both *in vitro* and *in vivo* systems is used to investigate DILI.

1.4.2.1 *In vivo* models

Certainly, one would argue that the study of DILI *in vivo* is the most relevant approach to obtain an accurate representation of human DILI. However, significant inter-species differences between preclinical animal models and human in drug absorption, distribution, metabolism, and excretion (ADME), results in outcomes that very often do not equal the liver safety profiles observed in the clinics (Martignoni, Groothuis and de Kanter, 2006). Specifically, 38-51% of potential liver toxic drugs go undetected during the preclinical stages (Olson *et al.*, 2000; Hughes, 2008). An impressive example is provided by the case of fialuridine, a drug developed to treat hepatitis B virus infection. Great hopes were given to the drug as no signs of drug toxicity were seen in multiple animal studies from rats to monkeys, which led to the progression of the drug clinical trials. Similarly, in phase I, patient's response towards the drug showed dramatic decrease of serum hepatitis B level. However, the story

reversed in phase II clinical trials when a treated patient showed aspects of liver injury which resulted in the immediate termination of fialuridine development. Subsequent *in vitro* studies showed that fialuridine is a substrate of nucleoside transporter 1 (ENT1) exclusively expressed in the hepatic mitochondrial membrane (Lai, Tse and Unadkat, 2004; Lee *et al.*, 2006). Expression of ENT1 is the hallmark of fialuridine-induced mitochondrial toxicity. Although mouse Ent1 actively transports fialuridine, it is not expressed in the mitochondrial membrane; hence no mitochondrial toxicity was detected in mice which was the motive for the progression of the drug into the clinical trial step (Lee *et al.*, 2006).

1.4.2.2 *In vitro* models

To respond to the challenges derived using animal models, more focus was given in the identification of human *in vitro* models to address the risk of hepatotoxicity early in the drug discovery process. However, it is important to note that a perfect human preclinical model for one person might not work for another person given the pharmacokinetics heterogeneity between individuals.

Whilst *in vitro* cultures are not entirely representative of normal tissue, these could be adopted as early screening of toxic drugs before proceeding to animal testing and clinical trials. To date, the majority of *in vitro* hepatic liver models are based on the structure and function of the human hepatocytes as these are the workforce of the liver. Immortalised cell lines such as HepG2 and HepaRG cells are widely used as initial indicator of DILI (LeCluyse *et al.*, 2012). These cell lines are derived from hepatocellular carcinoma, as such, these are characterised by extensive proliferative capacity and stable phenotype. In the context of DILI, these cells allow high throughput screening and generation of highly reproducible data, yet their lack of metabolising enzymes and functional hepatic maturation may mislead the interpretation of toxicity data (Xu, Diaz and O'Brien, 2004; Atienzar *et al.*, 2014).

Given the increasing appreciation that immortalised cell lines exhibit low expression of drug metabolising enzymes, the focus shifted towards primary human hepatocytes (PHH), also known as the gold standard model in the field of DILI

prevention (Gomez-Lechon *et al.*, 2005; Knobloch *et al.*, 2012). Freshly isolated PHH are the best tool that closely mimics the human *in vivo* physiology. When isolated and cultured in 2D, PHH display phase I and phase II metabolic enzymes, and hepatocyte functionality, yet PHH rapidly lose their functional and structural hepatocyte phenotype in a process called dedifferentiation, limiting their use for long-term studies (Gomez-Lechon *et al.*, 2005; Knobloch *et al.*, 2012; Godoy *et al.*, 2013).

To combine both the replicative potential of immortalised cell lines and the biological relevance of PHH, hepatocyte-like cells have been derived from induced pluripotent stem cells (iPSC) (Gao and Liu, 2017). iPSC-derived hepatocytes can be expanded for long period in culture while still retaining the donor phenotype. However, current differentiation protocols to induce iPSCs into hepatocyte-like cells are not optimal, as derived hepatocytes fail to recapitulate the PHH maturity with instead high levels of hepatoblast features (Raju *et al.*, 2018).

A common criticism of the above hepatic models is the lack of the complex interplay of cell-to-cell and cell-to-extracellular matrix (ECM) interaction when cells are plated in a two dimensions (2D) configuration (Blau and Miki, 2019). To achieve an improved *in vitro* system, more focus must be given on the cellular arrangement and functionality of hepatocytes *in vivo*. The liver *in vivo* is spatially arranged in a three-dimensional configuration that allows the cells to self-organise in more physiologically relevant manner (Godoy *et al.*, 2013; Matsuzawa, Matsusaki and Akashi, 2015). In addition, hepatocyte cords are highly polarised with specific functional membrane domains, yet these features cannot be retained once hepatocytes are cultured in a 2D configuration. Importantly, the incidence of hepatocyte death occurs at minimal levels *in vivo* during physiological levels, yet stable recapitulation of hepatocyte viability over time is not achievable in 2D culture conditions (Lauschke *et al.*, 2016). Moreover, to further support hepatocytes growth and phenotypic maintenance, media supplements such as amino acids, growth factors, vitamins and sugar are necessary. Of note, despite the fact that serum aids in the overall cell health, its active components can manipulate data interpretation; low serum or serum-free media has been shown to maintain higher levels of cytochrome activity and hepatocyte viability (Lübberstedt *et al.*, 2015; Vorrink *et al.*, 2018).

Therefore, to improve the phenotypic maintenance of hepatocytes over time, several 3D hepatic cultivation methods have been developed. The very first attempt to preserve hepatocyte polarity was adopting a sandwich culture system in which PHH are overlapped with a layer of a natural ECM containing laminin, collagen IV and growth factors, also called Matrigel (Bi, Kazolias and Duignan, 2006; De Bruyn *et al.*, 2013); ECM has proven to act as a scaffolding system to keep cells in place but is also critical for the maintenance of cell fate and function. Despite the retainment of polarity and viability of PHH, a decrease in the levels of PHH maturity is observed over time (Bell *et al.*, 2018).

More advanced 3D culture conditions instead, relied on an ECM-free system. An impressive example is provided by the generation of three dimensional (3D) clusters of cells also called spheroids (Landry *et al.*, 1985; Tong *et al.*, 1992). Spheroid formation is not spontaneous but instead requires specific methods that promote cellular aggregation such as using hanging drop techniques or ultra-low attachment plates; the source of hepatocytes can either be from PHH or from hepatoma cell line (Chang and Hughes-Fulford, 2009; Takahashi *et al.*, 2015; Bell, Delilah F.G. Hendriks, *et al.*, 2016).

In relation to their 2D counterparts, substantial enhancement of hepatocyte phenotype and function is achieved through the spheroid system. PHH and HepaRG spheroids were dosed with chlorpromazine and both showed signs of drug-induced cholestasis (Anthérieu *et al.*, 2013; Bell, Delilah F.G. Hendriks, *et al.*, 2016).

More promising in the field is provided by the generation of 3D microfluidic devices to support the *in vitro* physiological environment (Ewart *et al.*, 2018). The use of chip-like devices enables the incorporation tissue microenvironments that functionally resemble the organ of origin, also called organ-on-a-chip. Recently, a novel liver-on-a-chip was constructed with the simultaneous co-culture of non-parenchymal cells and hepatocytes into liver sinusoidal structures. These devices enable long term maintenance of liver-specific phenotype as well as realistic drug dosing regimen (Dash *et al.*, 2013; Vivares *et al.*, 2015; Kietzmann, 2017; Lee-Montiel *et al.*, 2017; Ewart *et al.*, 2018). A study has shown how using a liver-on-a-chip fully reconstructed the APAP toxicity pathways (Prot *et al.*, 2012). On the other hand, some

limiting technical issues still need to be surmounted, the perfusion system could wash out molecules, drugs may non-specifically bind to the device chambers and the maintenance cost of such a device is extremely high.

Another interesting approach is the development of biological ECM scaffolds based on the decellularization of organs (Hoshiya *et al.*, 2016). With this technique primary rat hepatocytes cultured on a hepatic ECM exhibited an improved viability and functionality (Loneker *et al.*, 2016). However, one limitation of this approach is the huge quantity of tissue needed to create enough decellularized ECM for *in vitro* studies.

Nevertheless, current *in vitro* studies detect only 50% of hepatotoxic drugs, hence stressing the need to find an improved hepatic model (Giuliano *et al.*, 2010). The establishment of an *in vitro* model that can faithfully mimic the human system could bridge the gap between preclinical and clinical stages of drug discovery and bring to the market a drug that is safe and efficient.

1.4.2.2.1 Novel 3D liver models – the era of organoids

Growing interest in the liver safety field is the use of liver progenitor/stem cells to generate complex organotypic models. Substantial advancement in the understanding of stem cell maintenance and differentiation have encouraged the generation of stem cell driven formation of self-renewing and expandable 3D *in vitro* models, called organoids. The very first time the term ‘organoid’ appeared occurred in 1946 and it was associated to a tumour mass in the pararenal tissue (SMITH and COCHRANE, 1946).

However, it was only after successful isolation and maintenance of embryonic stem cells (ESCs) *in vitro* for the first time in 1988 (Thomson, 1998) and later on with the pioneering work that led to the reprogramming of somatic cells into pluripotent stem cells (Takahashi and Yamanaka, 2006; Takahashi *et al.*, 2007) that led to the foundation of organoid research. With the need to re-create the spatial cellular interactions and the structure observed *in vivo*, in 2008 remarkable work conducted

from Sasai's group established for the first time three-dimensional cortical tissue from embryonic stem cells (ESCs) by mechanical self-aggregation (Eiraku *et al.*, 2008). Despite being the very first work of organoid formation, yet the term organoid was not used in Sasai's work.

It was only with the ground-breaking work conducted by Sato *et al.* in 2009 who established for the first-time intestinal organoids from single *lgr5+* adult stem cells that the term organoid was finally established (Barker *et al.*, 2007; Sato *et al.*, 2009). The media for these cultures is rather simple, and its foundation relies on the understanding of the key niche signalling molecules involved in the stem cell maintenance *in vivo*. With the use of R-spondin to drive WNT signalling activation, the use of morphogens, and Nogging (BMP inhibitor), all these signals were essential to promote the formation of organoid structures with a central lumen in the middle surrounded by proliferating epithelial cells. Importantly, external signals alone would not be sufficient to promote organoid formation without the support of the ECM substitute called Matrigel, which mimics the basal lamina (Sato *et al.*, 2009; Sato and Clevers, 2013).

The establishment of such a novel *in vitro* 3D model set new advancements in the stem cell field. A plethora of new organoid models were formed from various tissues based on the alteration of the intestinal organoid media. Today the term 'organoid' refers to the ability to generate *ex vivo* human tissues mimicking the *in vivo* counterpart. These "organs in a dish" can be produced from ESCs, iPSCs and tissue resident adult stem cells (AdSCs), foetal or differentiated cells (Prior, Inacio and Huch, 2019; Kaluthantrige Don and Huch, 2021).

In the hope to improve current *in vitro* liver models, novel hepatic systems were created using the organoid technology. Remarkable work from Takebe *et al.* (2013, 2015) first described the generation of 3D human liver bud structures by co-culturing iPSCs-derived hepatocytes with mesenchymal cells (MSCs) and human umbilication vein endothelial cells (HUVECs). Upon transplantation in mice, the hepatoblasts forming the liver buds organoids differentiated into mature hepatocytes. In 2015, Sampaziotis *et al.* (2015) instead used iPSCs to direct the formation of cholangiocyte organoids. Although IPSCs derived liver organoids are promising tools

to study liver development, however their use in the clinic is debatable due to propensity to form teratoma (Tapia and Schöler, 2016).

Nevertheless, this limitation is circumvented with the use of primary cells as source to generate liver organoids. Interestingly, the evidence of *Lgr5+* being the hallmark of the stem cell pool in the healthy small intestine could also be extended to damaged mouse livers (Figure 1.8). Huch *et al.* (2013) isolated activated *Lgr5+* hepatic cells upon liver damage and generated clonally expandable adult liver organoids. Based on the same principle of WNT activation being the backbone for intestinal organoid expansion, a cocktail of niche factors containing mitogens to promote cellular proliferation – epidermal growth factor (EGF), fibroblast growth factor (FGF) and hepatocyte growth factor (HGF)- supported with R-spondin 1 (RPSO-1), is given to promote the long-term expansion of liver organoids. Interestingly, not only can liver organoids be generated by post- damage progenitor cells, but also by isolated healthy bile ducts (Huch *et al.*, 2013) (Figure 1.9). The same culture system adopted in the mouse model was extended to culture adult stem cells from the human liver. Human liver organoids can be derived either by placing biliary structures or single EPCAM+ cells under the same mouse media conditions, but with the additional induction of the cAMP signalling (Forskolin) to promote duct cell proliferation (Huch *et al.*, 2015; Broutier *et al.*, 2016).

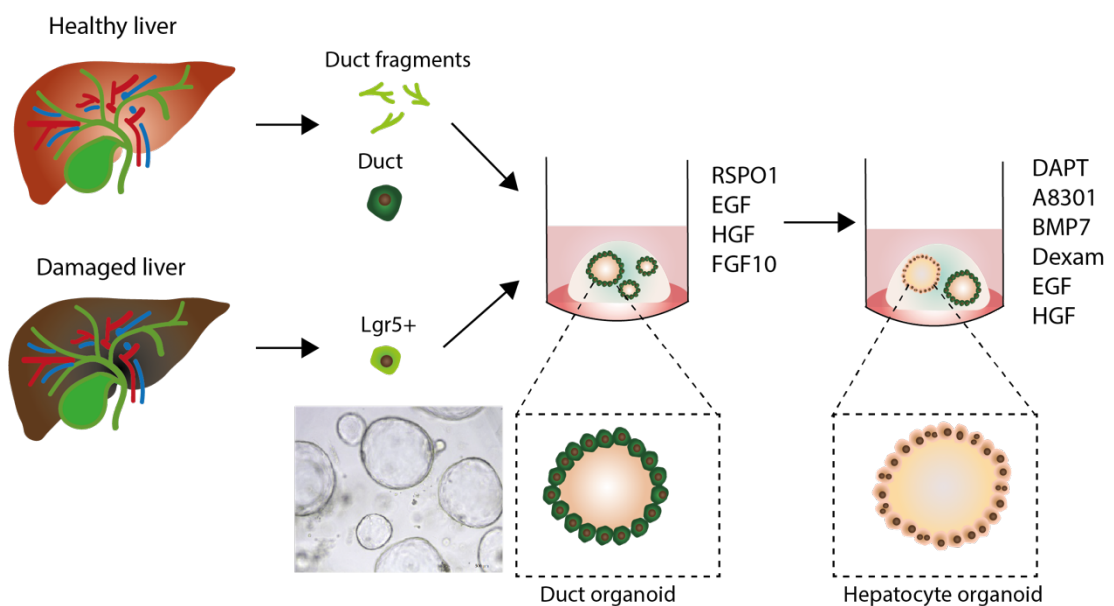


Figure 1.9 Liver organoids as models to study drug toxicity. Single *lgr5*⁺ progenitor cells or healthy biliary fragment or single cells can be isolated from the liver and cultured in a 3D ECM (Matrigel) with a defined cocktails of growth factors that sustain stem cell proliferation (RSPO1, HGF, EGF and FGF10). Once in culture, these cells self-organise into cystic structures, organoids, with a lumen in the middle surrounded by a single layered epithelium of proliferating progenitor and ductal cells. These organoids have the bipotential capacity to differentiate into hepatocyte organoids when TGF- β inhibitor, Notch inhibitor and dexamethasone are added.

As much as the controversy around the liver stem cell pool existence in the biliary compartment *in vivo* is still unresolved, the generation of liver organoids provides a remarkable evidence of the existence of a bipotent population of adult liver stem cells. Indeed, liver organoids are epithelial structures with a lumen in the middle that initially express both biliary (*KRT7 and KRT19*) and progenitor markers (*LGR5 and SOX9*), but with the retained capacity to differentiate into hepatocyte like cells (*CYP3A4 and ALB*) in the presence of FGF19, BMP7, dexamethasone and ductal phenotype inhibitors (A8301 and DAPT) (Huch *et al.*, 2015). As a result of the differentiation process from ductal/progenitor to hepatocyte-like-cells, the differentiated organoids exhibit expression of hepatocyte genes (*CYP3A4, ALB*), and features of hepatocyte functionality including secretion of bile acids, cytochrome activity and albumin secretion. Additionally, transplanted differentiated liver organoids were capable to successfully engraft in CCL₄ treated mice and partially rescue the liver functionality (Huch *et al.*, 2015). However, the yield of hepatocyte maturity following the induction of the differentiation process is not high and fully functional; hence suggesting a requirement to further optimise the differentiation media. Taking into consideration the *in vivo* signalling pathways involved in liver development and cell differentiation could help in the establishment of an optimised differentiation media. In the Huch *et al* 2015 study, cellular differentiation into hepatocyte is based on the inhibition of TGF- β and Notch signalling, however as I have discussed earlier in the introduction, WNT pathway covers an important role cell fate specification.

In the same line to generate more complex *in vitro* hepatocyte models, other studies supported the concept of resident hepatocytes being the source of hepatic cellular turnover *in vivo* (Yanger *et al.*, 2013; Font-Burgada *et al.*, 2015). Specifically, periportal hepatocytes have been identified as drivers of regeneration upon chronic

liver injury in mice (Font-Burgada *et al.*, 2015). Accordingly, a landmark study generated clonally expandable hepatocyte liver organoids from primary mouse/foetal/human hepatocytes and more specifically from Axin2+ pericentral hepatocytes (Hu *et al.*, 2018). Another lab instead established hepatocyte organoids with more focus on promoting long term expansion of mouse hepatocytes *in vitro*, a long withstanding issue (Peng *et al.*, 2018). Based on developmental studies conducted *in vivo*, the use of inflammatory cytokine TNF- α promoted the long-term expansion of hepatocyte organoids *in vitro* (Peng *et al.*, 2018). It is intriguing to speculate that the work from both Peng and Hu could be combined to generate an improved hepatocyte organoid model. Overall, this could indicate that different subpopulation of hepatocyte might have the self-renewal capacity to drive liver regeneration.

These organoids are generated directly from hepatocytes and bypass the differentiation step from ductal cells to hepatocytes, which instead is displayed in the Huch organoids (Huch *et al.*, 2013, 2015); this might be limiting the cross-contamination derived from ductal cells. On the other hand, adult hepatocyte organoids exhibit a very low expansion potential and low organoid formation efficiency compared to Huch organoids, hence suggesting the difficulty to use these models for long-term experimental studies.

Overall, the improved expansion potential and the recapitulation of the *in vivo* phenotype make the liver organoid a promising tool to study drug toxicity.

1.5 Imaging techniques to study 3D biological systems

Dynamic visualisation of biological processes is still an ongoing challenge for complex 3D *in vitro* systems. Current state of the art imaging techniques are more suitable for simple 2D models. On the other hand, 3D samples such as organoids are far more complicated with multiple layer of cells, exhibiting greater thickness and high cellular dynamics. Emerging biological imaging methods to study 3D models have been developed that could overcome the limitation of conventional imaging single photon methods (Centonze and White, 1998; Conchello and Lichtman, 2005)

Two-photon excitation scanning microscope (2P) has been used as an alternative to the confocal microscope as it allows higher 3D imaging resolution of live and thick samples by reducing light absorption and scattering. As light absorption is decreased, less photobleaching and phototoxicity occurs above and below the plane of focus (Denk, Strickler and Webb, 1990).

The phenomenon of two-photon excitation arises from the simultaneous absorption of two infrared photons in a single event. If two photons arrive at the molecule of interest at the same time, both photons can be absorbed and excite the molecule to produce fluorescent light (Pawley, 1996). The energy of each photon has half the energy compared to a single-photon absorption event, thus the fluorescence emission after two-photon excitation is the same as the one produced by a one-photon event. In addition, the wavelength required for 2P excitation is approximately twice that for single photon excitation (due to the energy of a photon being inversely proportional to the wavelength) (Zipfel, Williams and Webb, 2003). Thus, longer wavelengths mean less light scattering from the according to Raleigh scattering law in which states that the amount of scattering is inversely proportional to the wavelength to the power of 4 (Twersky, 1964; Denk *et al.*, 1994). Thus, in a two-photon excitation event, twice the wavelength means 16 times less Raleigh scattering. For this reason, as less light scattering occurs, more of the excitation light penetrates deeper in the specimen at plane of focus. Thus, this offers deeper 3D imaging of thick sample over confocal microscopy.

Absorption of two photons at the same time is very unlikely but can be achieved using high power and pulse laser sources. These lasers short (100 fs) and rapid (80 MHz) pulses at which peaks the power reach ~10s to 100s mW are high enough to generate significant two-photon excitation. The titanium-sapphire (ti-sa) laser with pulse duration around 100 fs can produce rapid pulses, thus photon can arrive at the sample approximately at the same time.

Because two coincident photons are required to excite a fluorescent molecule, the intensity level necessary to cause fluorescence is much higher than with one-photon excitation. Thus, the fluorescence is highly localized to the focal point and therefore very little out of focus 2-photon absorption occurs (Denk, Strickler and

Webb, 1990; Centonze and White, 1998; Zipfel, Williams and Webb, 2003). For this reason, a pinhole is not required in 2PM. In addition, because the 2P excitation is nonlinear, this reduces background signal and increases the viability of the biological sample by reducing photobleaching and phototoxicity.

To summarize, two-photon allows deep tissue sectioning of thick sample compared to the confocal microscopy for the following reasons:

1. Absence of out-focus absorption permits localization of excitation light at one focal plane
2. The use of longer wavelength such as red and infrared allows less scattering

Although the 2P has several advantages in imaging thick samples compared to the confocal, spatial resolution is higher in the confocal microscopy system. As the resolution of a microscope is inversely proportional to the wavelength of light, as described by the Abbey's Law, in a 2P twice the wavelength means half the resolution (Denk, Strickler and Webb, 1990). In addition, as higher light intensities are used at one focal plane, this could also lead to toxic and bleaching effects on the specimen.

2P has been widely used for *in vivo* imaging of zebrafish, mouse models and deep imaging of neuronal tissue (Schummers, Yu and Sur, 2008; Olivier *et al.*, 2010; Looney *et al.*, 2011). With the enhanced capacity to penetrate deeper in the tissue, 2P can simply breach the mouse skin, follow subcutaneous tumours, and track cellular processes.

On the other hand, the use of 2P to study organoids dynamic is still an emerging field. Very recently in 2017, a multi-imaging approach was adopted to reconstruct the dynamics of a mammary gland organoid formation from a single basal cell (Jamieson *et al.*, 2017). The use of 2P as a tool to study the dynamics of liver development and drug treatment in liver organoid has not been investigated yet.

1.6 Aims

DILI is a long-standing problem in the drug development field and clinics. Translation of liver safety outcomes from the pre-clinical phase to the clinics is very often confounded by the biological differences between pre-clinical hepatic models and humans to detect potential human hepatotoxins. For this reason, a growing demand in liver safety field is the identification of a human *in vitro* system that can closely mimic the human liver *in vivo*. The organoid technology could be fundamentally relevant to toxicology due to its inherent capacity to proliferate and retain some of the aspects of the *in vivo* physiology, yet it is still an unexplored system for the study of DILI. In this Thesis I aim to:

- 1) Develop an optimised differentiation protocol of ductal/progenitor organoids into functional hepatocyte organoids. Current differentiation protocol of hepatocytes organoids *in vitro* does not fully achieve a homogenous induction of ductal organoid differentiation towards a hepatocyte fate. We hypothesise that ductal cells differentiation should be driven with additional signalling molecules involved in the hepatocyte maintenance *in vivo*.
- 2) Characterise hepatic specific function and structure of the newly differentiated organoids. To validate any hepatic *in vitro* model for drug toxicity studies, it is essential to assess the biological features involved in hepatic functionality. For this purpose, several parameters will be investigated: a) drug distribution inside the liver organoid b) bile canaliculi formation c) drug efflux transport.
- 3) Recapitulate early clinical manifestations of DILI pathogenesis using known human hepatotoxins. This will confirm the sensitivity of the organoid system to detect DILI. Specifically, we hypothesise that differentiated organoids will be able to recapitulate cholestasis and steatosis *in vitro*. A set of DILI compounds will be used, and the results compared to published *in vivo* scenario.

4) Implementation of a time-lapse imaging system to study organoid proliferation. Modulation of cellular proliferation is an emerging parameter to study DILI. Many DILI studies rely on endpoint imaging rather than a temporal imaging setting, hence losing valuable data. Here we will establish a novel imaging system to study organoid proliferation using the two-photon laser excitation microscopy.

Chapter 2

Material and Methods

2. 1 Organoid cultures

2.1.1 Isolation of human hepatic ductal cells organoid formation and maintenance

Human liver organoids were established as described in (Huch et al, 2015). Healthy livers biopsies (~1cm³) were obtained during liver transplantation. All patients provided informed consent and samples were procured and studies were conducted under Institutional Review Board approval prior to tissue acquisition. Samples were confirmed to be tumour or normal based on pathological assessment.

Patient	Gender	Age	
Donor 3	M	23	Healthy
Donor9	M	50	Healthy
Donor 13	F	77	Healthy

Briefly, human tissue biopsies were washed thoroughly in phosphate buffer saline (PBS), placed on a petri dish to dissect out the gall bladder and minced with a razor blade until small pieces of ~1 mm³ were obtained. Enzymatic digestion was carried out for 2-3 hours at 37°C with the digestion solution containing 0.0125% (mg/ml) collagenase (SIGMA, C9407), 0.0125% (mg/ml) dispase II (GIBCO, 17105-041) and 1% foetal bovine serum (FBS) (GIBCO) in DMEM/Glutamax (GIBCO, 31966-021) supplemented with HEPES (Invitrogen, 15630-056) and Penicillin/Streptomycin (Invitrogen, 15140-122). During the enzymatic incubation, the progress of the digestion is monitored by transferring small volumes of the supernatant into a petri dish and checking formation of duct structures under the microscope. Once appearance of ducts is visible under the microscope, the enzymatic digestion is interrupted, and enrichment of ductal tree fragments obtained by hand-picking. Finally, the isolated duct fragments are seeded in 50 µl Basement Membrane Extract Type 2, Pathclear (BME), droplets. Once the BME has solidified, the donor samples

were overlaid with expansion medium (EM) based on AddMEM/F12 (ThermoFisher) supplemented with basal media (1% B27 (Invitrogen), 1% N2 (Invitrogen), 1.25 mM N-acetylcysteine (Sigma-Aldrich)), 10 nM gastrin (Sigma-Aldrich), 50 ng/ml hEGF (Peprtech), 10% RSPO1 conditioned medium (homemade - [Table 2.1](#)), 100 ng/ml FGF10 (Peprtech), 10 mM nicotinamide (Sigma-Aldrich), 25 ng/ml HGF (Peprtech), 5 μ M A8301 (Tocris) and 10 μ M FSK (Tocris). Additionally, the EM was also supplemented with 30% Wnt3a conditioned media (homemade - [Table 2.1](#)), 10 μ M Rho-kinase inhibitor - Y27632 (Tocris), and 25ng/ml Noggin (Peprtech) to aid stem cell survival for the first week only. Once organoid structures appear, media was replaced with EM only. Medium was changed every 2 -3 days.

Once the organoid cultures reached a high confluency, passaging was performed by mechanical dissociation into small fragments, achieved with the use of narrowed glass Pasteur pipets. The resulted organoid fragments were embedded in BME in the form of droplets. For the maintenance of organoid line, frozen stocks were also prepared as follows. Organoids cultures were mechanically dissociated and instead of being transferred to fresh BME, the small organoid fragments were mixed with recovery cell culture freezing medium (GIBCO) and frozen following standard procedures. To recover frozen stocks, standard procedures were followed. Briefly, frozen samples were quickly thawed at 37°C and transferred into 10 ml of AddMEM/F12 (ThermoFisher) supplemented with 1% B27 (Invitrogen), 1% N2 (Invitrogen), 1.25 mM N-acetylcysteine (Sigma-Aldrich), and cultured as previously described. For the first two weeks 10 μ M Rho-kinase inhibitor - Y27632 (Tocris) was supplemented to the EM.

Table 2.1 Wnt3a and Rspo1 conditioned medium recipe and protocol.

<p>Wnt3a conditioned medium</p> <p><u>Growth medium:</u> DMEM supplemented with 10% FBS, 1% Penicillin/Streptomycin and 300µg/ml Zeocin. Store at 4 °C for up to one week.</p> <p><u>Harvest medium:</u> DMEM supplemented with 10% FBS and 1% Penicillin/Streptomycin. Store at 4 °C for up to one month.</p> <ol style="list-style-type: none">1 Plate 1.5-2x10⁶ cells of the L-Wnt3a cell line into a T150 flask in 35ml of growth medium, pre-warmed to 37 °C.2 Expand cells in growth medium by passaging when cells are at ~75% confluence. Passage by removing medium and incubating in 3ml TrypLE, pre-warmed to 37 °C.3 Incubate for 2-3min until all cells are in suspension, then add ~5ml of growth medium to the flask. Pool cells and re-seed 1.5x10⁶ cells per T150 flask in 35ml of growth medium as in step 1.4 When there are 20-30 T150 flasks each at ~75% confluence, passage cells as in step 2 but re-seed 500cm plates with 4.5x10⁶ cells per plate in 100ml of growth medium.5 When plates are ~70% confluent then change growth medium to 100ml harvest medium per plate. Incubate in this medium for 1 week6 Remove medium into 50ml tubes. Centrifuge at 500g for 5min to remove cells.7 Filter medium using 500ml filter cups. Mix and aliquot into 25ml aliquots. Wnt3a conditioned medium can be stored at 4 °C for up to 6 months.
<p>Rspo1 conditioned medium</p> <p><u>Growth medium:</u> DMEM supplemented with 10% FBS and 150µg/ml Zeocin. Store at 4 °C for up to one week.</p> <p><u>Harvest medium:</u> Advanced DMEM/F12 supplemented with 1% Penicillin/Streptomycin, 1% Glutamax, and HEPES 10mM. Store at 4 °C for up to one month.</p> <ol style="list-style-type: none">1 Plate 1.5-2x10⁶ cells of the 293T-HA-Rspo1-Fc cell lines into a T150 flask in 35ml of growth medium, pre-warmed to 37 °C.2 Expand cells in growth medium by passaging when cells are at ~75% confluence. Passage by removing medium and incubating in 3ml TrypLE, pre-warmed to 37 °C.3 Incubate for 2-3min until all cells are in suspension, then add ~5ml of growth medium to the flask. Pool cells and re-seed 1.5x10⁶ cells per T150 flask in 35ml of growth medium as in step 1.4 When there are 20-30 T150 flasks each at ~75% confluence, change growth medium to 35ml harvest medium per flask. Incubate in this medium for 1 week5 When plates are ~70% confluent then change growth medium to 100ml harvest medium per plate. Incubate in this medium for 1 week6 Remove medium into 50ml tubes. Centrifuge at 500g for 5min to remove cells.7 Filter medium using 500ml filter cups. Mix and aliquot into 5ml aliquots. Rspo1 conditioned medium can be stored at -20 °C for up to 6 months.

2.1.2 Organoid dissociation into single cells

Liver organoids were mechanically dissociated as previously described. To make single cells, the dissociated organoid fragments were incubated with TrypLE Express (Gibco) for 10 min at 37°C. The cell suspension was filtered through 40 µm strainer and then counted using disposable counting chambers (Immune systems) as stated in the manufacturer's protocol.

2.1.3 Ductal organoid differentiation into hepatocyte organoids

Organoids were grown in EM media supplemented with recombinant human bone morphogenic protein – 7 (BMP-7) (Peprotech) as shown in (Huch et al, 2015). On day 5, organoids were mechanically dissociated as described above in a ratio of 1:3 and seeded in differentiation media – DM, DM+ and DM+VP (Table 2.2). Media was refreshed every 2 days for a total of 15 days. Images were taken with either a Leica M80 stereoscope and Leica MC170 HD camera or with an inverted microscope Leica

DMIL and Leica DFC 450C camera. Organoid quantification in one single drop of Matrigel/BME was quantified using an in-built ImageJ plugin.

Table 2.2 List of differentiation media.

Media name	Components	Concentration	Comments
DM Huch et al, 2015	Advanced DMEM/F12 +++ Basal media (2x) hEGF (Peprotech) Gastrin (Tocris) hHGF (Peprotech) BMP7 (Peprotech) FGF19 (Peprotech) Dexamethasone (Sigma) DAPT (Sigma) TGFBi=A83-01 (Tocris)	50% 1x 50 ng/ml 10 nM 25 ng/ml 25 ng/ml 100 ng/ml 3 uM 10 uM 500 nM	1. Grow organoids for 5 days in EM+BMP7 (25ng/ml) 2. Add DM at day5 3. Refresh DM every 2/3 days for a period of 15 days
DM +	Advanced DMEM/F12 +++ Basal media (2x) hEGF Gastrin hHGF BMP7 FGF19 Dexamethasone DAPT TGFBi=A83-01 IWP-2 CHIR iCRT3	50% 1x 50 ng/ml 10 nM 25 ng/ml 25 ng/ml 100 ng/ml 3 uM 10 uM 0.5 uM 3 uM 3 uM 25 uM	1. Grow organoids for 5 days in EM+BMP7 (25ng/ml) 2. Split 1:3 at day 5 3. Add DM+ 4. Refresh DM+ every 2/3 days for a period of 15 days
DM + VP	Advanced DMEM/F12 +++ Basal media (2x) hEGF Gastrin hHGF BMP7 FGF19 Dexamethasone DAPT TGFBi=A83-01 IWP-2 CHIR iCRT3 Verteporfin (Sigma)	50% 1x 50 ng/ml 10 nM 25 ng/ml 25 ng/ml 100 ng/ml 3 uM 10 uM 0.5 uM 3 uM 3 uM 25 uM 100 nM	1. Grow organoids for 5 days in EM+BMP7 (25ng/ml) 2. Split 1:3 at day 5 3. Add DM+VP for 24h 4. Add DM+ at day 6 5. Refresh DM+ every 2/3 days for a period of 15 days

2.1.4 Hepatocyte organoid formation from cryopreserved hepatocytes

Cryopreserved PHH were kindly obtained from Dr. Carla Newmann at GlaxoSmithKline. PHH were thawed as standard procedures and transferred in a 15ml falcon tube containing 10 ml of William's E medium (ThermoFisher) and 10%FBS. Cells were centrifuged at 100g room temperature for 10 minutes. The pellet was checked for viability and counted using a nuclear counter. Cell were resuspended in William's E medium (ThermoFisher) and 10% FBS and different cell densities were extrapolated from the cell suspension. The seeding densities assessed to identify at which concentration hepatocyte organoids would form were 5000, 30.000 and 60.000 cells. After counting the number of cells needed, each condition was embedded in BME and overlaid with hepatocyte media described in Hu *et al.* (2018) and in Peng *et al* (2018) which we will refer as Hu and Peng media respectively. The Hu media consist of AddMEM/F12 (ThermoScientific) supplemented with basal media, 10% RSP01 conditioned medium (homemade), 50 ng/ml hEGF (Peprotech), 10 nM gastrin (Sigma-Aldrich), 25 ng/ml HGF (Peprotech), 50 ng/ml FGF10 (Peprotech), 50 ng/ml FGF7 (Peprotech), 3 μ M CHIR99201 (Sigma), 1 μ M A8301 (Tocris), 10 mM nicotinamide (Sigma-Aldrich), 10 μ M Rho-kinase inhibitor - Y27632 (Tocris). The Peng media consist of all the above media components with the addition of TNF- α 100 ng/ml (Peprotech). Media was replaced every 2-3 days.

As controls, cells were embedded in a 2D conformation and in BME in William's E medium (ThermoFisher) and 10 %FBS only.

Seeding density was calculated as follows:

$$\text{Total number of cells} / 60.000 \text{ cells} = \text{DF}$$

$$\text{Total volume of cell suspension (6ml)} / \text{DF} = \text{Volume of cells}$$

Organoid pictures were taken using the CQ1 microscope (Yokogawa) at GlaxoSmithKline.

2.1.5 Organoid immunostaining

Organoids were grown as described before. For whole mount organoid staining, organoids were carefully removed from Matrigel by adding the BD cell recovery solution (Corning) on top of the bubble and incubated for 30min on ice. Organoids were either fixed with ice-cold 4% paraformaldehyde (PFA) (Electron Microscopy Sciences, 15713-S) or 10% formalin (Sigma-Aldrich) for 30 min on ice depending on the primary antibody used. Fixed organoids were blocked/permeabilised for 2h in a buffer – referred to as PBSTD - containing 0-1% Triton X-100 (SIGMA, T8787), 1% dimethyl sulfoxide (SIGMA, D8418), 1% bovine serum albumin (BSA, A8806) and 2% donkey serum (SIGMA, D9663) diluted in PBS. Primary antibodies were added overnight at 4°C in 1:100-diluted PBSTD buffer and were washed three times prior to adding secondary antibodies raised in donkey (ThermoFisher) at 1:250 dilution for 2h at room temperature in PBS-0.05% BSA. After washing the secondary antibody in PBS-0.05% BSA twice, Alexa Fluor 647 Phalloidin (ThermoFisher) was incubated at a dilution of 1:150 in PBS-0.05% BSA for 1.5 hours at room temperature. Next, nuclei were counterstained with Hoechst 33342 (Thermo Scientific, H3570) for 15 min at room temperature. For the complete list of primary and secondary antibodies used refer to [Table 2.3](#).

For YAP staining, organoids were fixed for 24 hours in 2%PFA and then blocked in 0.1% Tween-20 with 10% donkey serum for 30 minutes at room temperature. 1:20 diluted primary antibody was then incubated for 24h in the blocking solution. Next day organoids were washed three times in blocking solution and secondary antibodies applied for 1h at room temperature. From this point, the protocol follows as previously described.

Table 2.3 List of primary antibodies.

Primary antibody	Catalogue number	Company	Host	Dilution
ALB	sc-271605	santa cruz	Mouse	1:100
β -catenin	sc7199	Santa Cruz	Mouse	1:100
BSEP Antibody (F-6)	sc-74500	Santa Cruz	Mouse	1:100
DPPIV/CD26	AF1180-SP	R&D systems	Goat	1:50
Krt19	troma-III	Hybridoma bank	Rat	1:200
YAP (D8H1X) XP	14074	Cell Signalling	Rabbit	1:20
ZO-1	61-7300	Invitrogen	Rabbit	1:100

2.1.6 Bile acid transport assay

To monitor canalicular secretion, cell tracker green 5-chloromethylfluorescein diacetate (CMFDA) (ThermoFisher) was used. Organoids were cultured in 8 well glass bottom IBIDI dish and on the day of the assay incubated with 5 μ M CMFDA for 40 minutes at 37C 5% CO₂. Next, CMFDA solution was removed and organoids washed with 1X PBS. Organoids were fixed with 4% PFA for 40 minutes on ice and then washed with 1X PBS. F-actin filaments and nuclei were visualised with Alexa Fluor 647 Phalloidin (ThermoFisher) diluted in 1X PBS 1:150 and Hoechst 33342 (Thermo Scientific, H3570) (1:1000).

2.1.7 Cytotoxic assay

Cell viability was assessed using the Viability/Cytotoxicity Assay Kit for Animal Live & Dead Cells (30002-T, Biotum). Organoids were washed twice in 1X PBS and were incubated with 2 μ M calcein AM and 4 μ M EthD-III for 30 min at room temperature as indicated in the manufacturer's protocol. The staining solution was then replaced with growth medium and the cells were imaged using a confocal microscope (Leica, Sp8). The calcein and EthD-III dyes were excited using the 488 and 568 lasers respectively. The percentage of live and dead cells was quantified using the ImageJ software.

2.1.8 3D cell viability

Cell viability was assessed using the CellTiter-Glo® 3D Cell Viability Assay (Promega – G9681). Organoids were grown in a 48 well plate and assayed for cell viability as follows. 100µl of 3D cell viability reagent was added on top of the organoids in 100ul of media and the plate agitated using an orbital shaker to promote cell lysis. 100ul of the lysate was transferred in a white flat bottom 96 well plate for luminescence in duplicates and incubated for 20 minutes at room temperature protected from the light. Media alone was used as blank control. Luminescence was recorded using the Perkin Elmer Envision machine at 1s integration time. The readout was normalised to the total number of single cells derived organoids. IC50 and IC10 values were calculated using the GraphPad Prism 8.

2.1.9 Total bile acid assay

Organoids were grown in a 24 well plate as previously described. Supernatant was collected from the organoid cultures, spun at 10.000g for 10 min at 4°C and stored at -80. The organoids cultures which supernatant was taken from were dissociated into single cells and the total number used to normalise the total bile acid measured. Total bile acids were measured using the Total bile acid kit (Cell Biolabs – STA-631) as explained in the manufacturer protocol. Media only was used as background control. Absorbance was measured at 450nm using the Perkin Elmer Envision machine.

2.1.10 Albumin ELISA

Albumin secretion was measured using the Human albumin assay kit (AssayPro) according to the manufacturer's instructions. Supernatant was collected from the organoid cultures, spun at 10.000g for 10 min at 4°C and processed as indicated in the manufacturer's protocol. The organoids which supernatant was taken from were dissociated into singles cells and the total number used to normalise the amount of

albumin secreted according to the cell number. Absorbance was measured at 405nm using the Perkin Elmer Envision machine at 1s integration time.

2.1.11 CYP3A4 activity assay

CYP3A4 activity was measured using the P450-Glo CYP3A4 assay (Promega). Organoids were collected as previously described using BD cell recovery solution (Corning) and washed in washing buffer based on Hepatozyme media (ThermoFisher) supplemented with 10% foetal bovine serum and 1% penicillin-streptomycin (Life Technologies). Organoids and media only were then incubated with Luciferin-PFBE enzyme (1:40 dilution) in the washing buffer supplemented with 50 ng/ml hEGF (Peprotech), 10 nM gastrin (Sigma-Aldrich), and 25 ng/ml HGF (Peprotech), for 8 hours at 37C 5% CO₂. After 8 hours organoids were collected and spun at 2000 RPM for 5 minutes. 25ul of the supernatant was transferred in a white 96 flat bottom plates supplemented with 2X luciferin reagent and incubated for 25min at room temperature protected from light. Luminescence was recorded using the Perkin Elmer Envision machine at 1s integration time. The pellet was processed for dissociation into single cells and the total number counted used to normalise the amount of CYP3A4 activity.

2.2 Immunohistochemistry

2.2.1 Tissue OCT sections preparation

Human healthy liver samples were collected as previously described and fixed overnight in PFA. The following day, tissues were processed for OCT embedding as follows. Tissues were washed three times in 1X PBS for 5 min each and then process in a sucrose gradient, 15% sucrose for 30 min at room temperature and then 30% sucrose overnight at 4°C. Next day, tissues were placed into cryomolds and embedded in OCT (VWR, 361603E) compound and snap frozen in dry ice. OCT blocks were then either stored at -80 or processed for cryo-sectioning. Tissue blocks were sectioned at

a thickness of 8 μm using a cryostat and mounted on glass slides for immunohistochemical analysis.

2.2.2 Immunohistochemistry of OCT sections

OCT sections were thawed at room temperature for 30min, and blocked in 0.3% Triton (SIGMA), 2% donkey serum (SIGMA) in PBS for 2h. Primary antibodies were diluted in 1:100 blocking solution and incubated overnight at 4°C. For primary antibodies dilution refer to the Table 2.2. Next day, tissues were washed three times in 1X PBS and incubated in secondary antibodies (ThermoFisher) diluted in 1:250 together with Hoechst 33342 (ThermoScientific) for 2h at room temperature. Slides were washed in 1X PBS and mounted using with VectaShield mounting media (Vector lab). Slides were then processed for imaging using a Leica confocal microscope (SP8).

2.3 qRT-PCR

Total RNA was purified from organoids using the Qiagen RNAeasy Mini RNA Extraction Kit (Qiagen) according to the manufacturer's protocol including a 15 min digestion step with DNase to remove traces of genomic DNA. The amount of purified RNA was counted using a standard nanodrop. The purified RNA (200-500 ng) was reverse-transcribed using random primers (Promega) and the Moloney Murine Leukemia Virus reverse transcriptase (M-MLVRT) (Promega). The generated cDNA was amplified using the iTaq™ Universal SYBR® Green Supermix (Bio-Rad) on the CFX Connect™ Real-Time PCR Detection System (Bio-Rad). The list of primers used for qRT-PCR is summarised in [Table 2.4](#). Gene expression levels were normalised to the housekeeping gene *HPRT* and *18S*.

Table 2.4 List of qPCR primers.

Gene symbol	Species	Forward primer	Reverse primer
<i>ALB</i>	Human	CTGCCTGCCTGTTGCCAAAGC	GGCAAGGTCCGCCCTGTCATC
<i>ABCB11</i>	Human	ATAGTCCAAGCTGCCAAGGA	CTGGCGATAGCTACCCTTTG
<i>ABCC2</i>	Human	CCTTGGGCTTCCTATGGCTC	GAAGAAAACCAACGAATACCTGCT
<i>ABCG2</i>	Human	GCCATAGCAGCAGGTCAGA	GAAGCCATGACAGCCAAGAT
<i>CYP3A4</i>	Human	TGTGCCTGAGAACCAGAG	GTGGTGGAAATAGTCCCGTG
<i>CYP2C8</i>	Human	GAGGACCGTGTTC AAGAGGA	AACGGAGCAGATCACATTGC
<i>CYP2C9</i>	Human	CCTCTCCCAGTGATTGAAA	GCACCACTATGGGTTTCAGG
<i>CTGF</i>	Human	ACCGACTGGAAGACACGTTTG	CCAGGTCAGCTTCGCAAGG
<i>KRT19</i>	Human	CGCGGCGTATCCGTGTCCTC	AGCCTGTTCCGTCTCAAACCTGGT
<i>KRT7</i>	Human	CTCCGGAATACCCGGAATGAG	ATCACAGAGATATTCACGGCTCC
<i>SULT1A1</i>	Human	AGGAGTTCATGGACCACAGC	GCCATCTTCTCCGCATAGTC
<i>HPRT</i>	Human	AAGAGCTATTGTAATGACCAGT	CAAAGTCTGCATTGTTTTGC
<i>18S</i>	Human	GTAACCCGTTGAACCCATT	CCATCCAATCGGTAGTAGCG

2.4 Imaging

2.4.1 Confocal imaging of organoids and image processing

Immunoassayed organoids were processed for confocal imaging following standard procedures. Images were acquired using a confocal microscope (Leica SP8) and processed using ImageJ software.

2.4.2 Transmission electron microscopy (TEM) analysis

Samples were fixed in 2 % glutaraldehyde/2 % formaldehyde in 0.05 M sodium cacodylate buffer pH 7.4 containing 2 mM calcium chloride overnight at 4°C. After washing 5x with 0.05 M sodium cacodylate buffer pH 7.4, samples were osmicated (1% osmium tetroxide, 1.5 % potassium ferricyanide, 0.05 M sodium cacodylate buffer pH 7.4) for 3 days at 4°C. After washing 5x in DIW (deionised water), samples were treated with 0.1 % (w/v) thiocarbohydrazide/DIW for 20 minutes at room temperature in the dark. After washing 5x in DIW, samples were osmicated a second time for 1 hour at RT (2% osmium tetroxide/DIW). After washing 5x in DIW, samples

were block stained with uranyl acetate (2 % uranyl acetate in 0.05 M maleate buffer pH 5.5) for 3 days at 4°C. Samples were washed 5x in DIW and then dehydrated in a graded series of ethanol (50%/70%/95%/100%/100% dry) 100% dry acetone and 100% dry acetonitrile, 3x in each for at least 5 min. Samples were infiltrated with a 50/50 mixture of 100% dry acetonitrile/Quetol resin (without BDMA) overnight, followed by 3 days in 100% Quetol (without BDMA). Then, the sample was infiltrated for 5 days in 100% Quetol resin with BDMA, exchanging the resin each day. The Quetol resin mixture is: 12 g Quetol 651, 15.7 g NSA, 5.7 g MNA and 0.5 g BDMA (all from TAAB). Samples were placed in embedding moulds and cured at 60°C for 3 days.

TEM sections (90 nm thickness) were cut by ultramicrotome (Leica Ultracut) and placed on 300 mesh bare copper grids. Samples were imaged in a Tecnai G2 TEM (FEI/ThermoFisher) run at 200 keV accelerating voltage using a 20 µm objective aperture to improve contrast; images were acquired using an AMT digital camera.

2.4.3 Mass spectrometry imaging analysis

Experiments were conducted at the National Physical laboratory (NPL) in London. Organoids were treated pre-treated with 10 µM Amiodarone (Sigma) for 24h and gently removed from the BME drop without disrupting the morphology using BD cell recovery (Corning) as previously described. To remove any traces of extracellular matrix, organoids were further washed with cold 1X PBS for 40 min in ice. Next, organoids were centrifuged at a lower speed of 40g for 3 minutes and supernatant removed.

2.4.3.1 Sample preparation for mass spectrometry imaging

Organoids were washed 3 times with 150 mM Ammonium formate buffer at pH 7.4 and deposited in a sandwich of polyhydroxylated methylmethacrylate (PHPMMA) embedding material. The PHPMMA embedding material was prepared at 150mg/mL. A small amount was added to the embedding mould so it was around half full and then that was placed on dry ice until it was fully frozen. Organoids were then

placed on that embedding material layer, allowed to freeze and then sandwiched with another layer of PHPMMA and stored at -80C until fully frozen. The material was then sectioned using a Cryostat, at a thickness of 16 μm .

2.4.3.2 ToF-SIMS 5

Experiments were conducted using a ToF-SIMS 5 mass spectrometer (ION-TOF, Munster, Germany) in a dual-beam setup with an electron gun used for charge compensation, imaging was performed using a Bi_3^{2+} analysis beam at 60 keV, and an Ar_{3000}^+ sputtering beam at 10 keV in a non-interlaced mode. Pulsed delayed extraction of secondary ions was employed for improved mass resolving power. The 3D images were collected in positive ion mode over a variable surface area depending on the size of the organoid and 256×256 pixels. In each analysis phase, the Bi_3^{2+} ion dose was 5.9×10^{10} ions/ cm^2 , and an Ar_{3000}^+ dose of 9.1×10^{13} ions/ cm^2 was used to erode the cells between analysis phases. The data analysis was performed in SurfaceLab (ION-TOF, Munster, Germany) (version 6.5).

2.4.3.3 OrbiSIMS

Control and Amiodarone treated organoids were imaged using the 3D OrbiSIMS instrument (ION-TOF GmbH, Münster, Germany) equipped with a time-of-flight mass (ToF) mass analyzer and a Q Exactive HF (Thermo Fisher, Bremen, Germany) with an Orbitrap mass analyzer. All acquisitions were performed using the Q Exactive analyser and a 20 keV Ar GCIB as a primary ion source and in positive polarity. Mass calibration of the Q Exactive HF instrument was performed on the day of analysis using silver cluster secondary ions. Orbitrap mass spectrum was acquired using 20 keV Ar_{2594}^+ (I_{GCIB} : 26.14pA at 45.00 % duty cycle and 200 μs cycle time) for analysis with the Orbitrap mass analyzer (mass-resolving power 240 000, injection time 1000 ms, mass range m/z 100–1500). The field of view was $150 \mu\text{m} \times 150 \mu\text{m}$ (75×75 pixel). The sample probing was performed using sawtooth rastering. For all acquisitions, an electron floodgun (I_{floodgun} : -10 μA) was used to compensate charging

effect over the surface of the sample complemented by Ar gas flooding at a pressure of 9.8×10^{-7} mbar.

For the 3D depth profiling of organoids, control and treated organoids surfaces were acquired using the profiling mode 3D OrbiSIMS instrument (ION-TOF GmbH, Münster, Germany) equipped with a time-of-flight mass (ToF) mass analyzer and a Q Exactive HF (Thermo Fisher, Bremen, Germany) with an Orbitrap mass analyzer. All acquisitions were performed using the Q Exactive analyser and a 20 keV Ar GCIB as a primary ion source. Mass calibration of the Q Exactive HF instrument was performed on the day of analysis using silver cluster secondary ions. Orbitrap mass spectrum was acquired using 20 keV Ar_{2594}^+ (I_{GCIB} : 26.14 pA at 45.00 % duty cycle and 200 μs cycle time) for analysis with the Orbitrap mass analyzer (mass-resolving power 240 000, injection time 1000 ms, mass range m/z 100–1500). The field of view was $200 \mu\text{m} \times 200 \mu\text{m}$ (66×66 pixel). The sample probing was performed using random rastering and for 80 scans (70 seconds). For all acquisitions, an electron floodgun (I_{floodgun} : $-10 \mu\text{A}$) was used to compensate charging effect over the surface of the sample complemented by Ar gas flooding at a pressure of 9.8×10^{-7} mbar. Three spectra were acquired per sample.

2.4.4 Live imaging of organoids using 2-photon excitation microscopy

Live imaging of organoids was conducted using an Upright 2-photon scanning fluorescence microscope (LaVision Biotec TriM Scope II - 25x 1.05 NA water dipping lens built in house at the Cambridge Advanced imaging Centre). The system has a tunable laser of 710-1300 nm and a fixed laser at a wavelength of 1040 nm with an incubation system for temperature and CO_2 adjustment for live imaging.

Mouse nTnG organoids were dissociated into single cells as previously described. Single cells were counted (18,000) and then embedded in Matrigel (15 μl drop) in a 35 mm dish (IBIDI) and fully filled with EM supplemented with 30% Wnt3a conditioned media (homemade), 10 μM Rho-kinase inhibitor - Y27632 (Tocris), and 25ng/ml Noggin (Peprotech). Parafilm was applied on top of the dish to avoid any

bubble formation, enclosed with lid and then inverted. The sample was inserted in the 2 Photon excitation scanning microscope (25x 1.05 NA) incubation system set at 37°C, 5% CO₂ and 95% humidity. Oil with the same refractive index of H₂O (RI=1.3) was applied on top of the sample dish to match the requirements of the objective lens. A 400x400x400 μm³ volume of Matrigel was imaged. Images were taken at 15 minutes time interval for about 4 days. For each timepoint, a Z-stack was taken at 1 μm Z step. Time-lapse videos were generated using ImageJ software. Single cells were tracked using the IMARIS software and plots generated using the GraphPad Prism 8.

The mouse strain used to generate mouse organoids in this study is listed in [Table 2.5](#).

Table 2.5 List of mouse lines.

Mouse strain (allele ID)	Allele symbol
<i>nTnG</i>	<i>Gt(ROSA)26Sortm1(CAG-tdTomato*,-EGFP*)Ees</i>

2.5 Compound dosing

Organoids were grown in the DM+ or DM+VP protocol as previously described. On day 10 post differentiation, organoids were treated with two doses of known human DILI compounds at day 10 and day 12 for a total duration of 4 days. The list of compounds and concentration used is summarised in [Table 2.6](#).

Table 2.6 List of compounds used.

Compound name	Source	Reconstitution solution	Concentration tested
Acetaminophen	Sigma	DMSO	1000 μM; 3000 μM; 4000 μM; 5000 μM
Amiodarone	Sigma	60 % Methanol : 40% H ₂ O	1 μM; 5μM; 10 μM; 20 μM
Bosentan	Sigma	DMSO	10 nM; 100nM; 50 μM; 100 μM; 300 μM
Diclofenac	Sigma	DMSO	1 μM; 10 μM; 50 μM; 100 μM; 200 μM; 400 μM
Cyclosporin A	Santa Cruz	DMSO	10 nM; 100nM; 1 μM; 10 μM; 20 μM

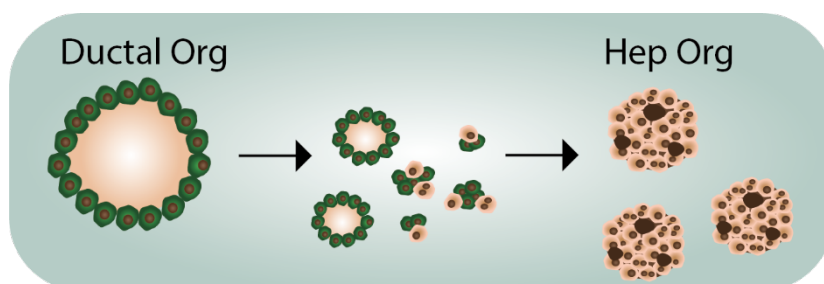
2.7 Statistics

Data were analysed using the Mann–Whitney non-parametric test. $P < 0.05$ was considered statistically significant. $P < 0.05$ (*), $P < 0.01$ (**), $P < 0.001$ (***), $P < 0.0001$ (****). Calculations were performed using the Prism 8 software package. In all cases, data from at least three biological replicates was used (N=biological replicate/different human donors). Experiments were performed in organoids with a passage number ranging from 2-8 (p2-p6).

Chapter 3

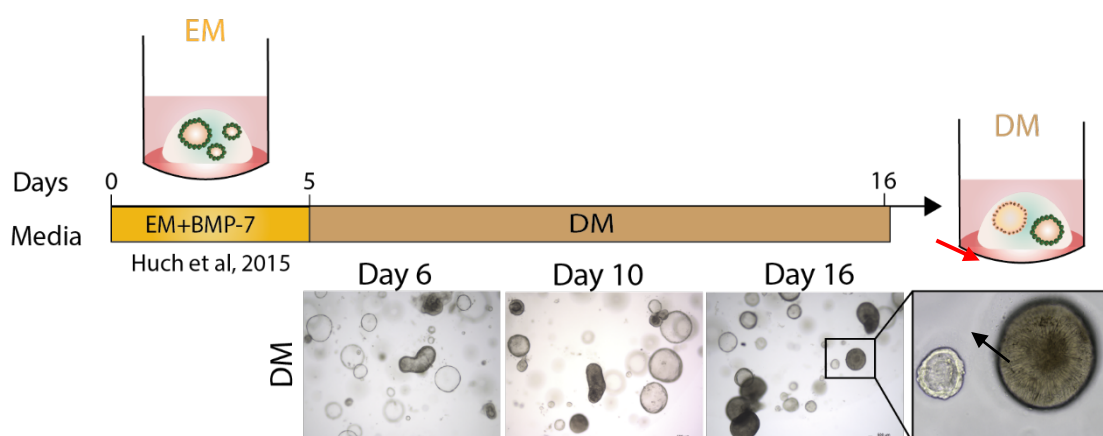
Results I:

Targeting of the WNT pathway
combined with inhibition of YAP
activation facilitates cholangiocyte
organoids differentiation into
hepatocyte fate



3.1 Targeting WNT enhances hepatocyte fate specification in cholangiocyte organoids

The *in vitro* study of DILI requires a hepatic system that recapitulates hepatocyte identity, including at a functional level, and is able to be maintained in culture overtime. With the advent of hepatocyte organoids generated from the differentiation of the ductal organoids (Chol. Orgs) (Huch et al., 2015), the interest of using this hepatic system in the liver toxicology field has heightened. The current state-of-the-art differentiation protocol referred as DM (Figure 3.1) (Huch et al., 2015) established the bipotentiality of Chol. Orgs, in which ductal cells can give rise to both cholangiocytes and hepatocytes. However, with the current DM protocol the differentiation into a hepatic lineage is still insufficient, as they retain features of both lineages, ductal and hepatocyte-like cells. Here we established a new differentiation protocol to further promote the differentiation of ductal cells into an hepatocyte fate, with the aim of establishing better functional hepatocyte organoids that better recapitulate key features of the *in vivo* liver.



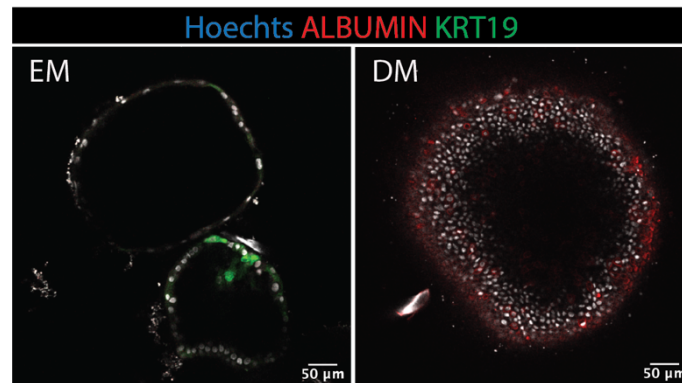


Figure 3.1 **Schematics of the DM protocol.** Chol. Orgs are grown for 5 days in their growth media (EM) supplemented with BMP-7. On day 5 organoids are mechanically dissociated and incubated in DM for a total of 11 days. The brightfield images show the growth of organoids in DM overtime. The zoom-in image shows the simultaneous presence of Chol. Orgs (black arrow) and differentiated organoids (red arrow). Scale bar = 500 µm. The immunostaining analysis show KRT19 expression in Chol. Orgs and ALBUMIN expression in DM Orgs.

The DM protocol relies on the chemical inhibition of two key pathways for the suppression of a ductal phenotype: the Notch pathway, inhibited by DAPT, and the TGF- β pathway, inhibited by A8301 (Huch et al., 2015). Nevertheless, the inhibition of these pathways is not sufficient since the retainment of the ductal phenotype is still observed following differentiation. This suggests that additional signalling factors are likely required to suppress further the ductal fate. *In vivo*, following an injury, the liver triggers a regeneration program by which the activation of WNT signalling drives the expansion of ductal cells – commonly referred as ductal reaction. This is recapitulated *in vitro* with the expansion of Chol. Orgs via the activation of WNT through exogenous RSP0-1 (LGR5 ligand – see Introduction). Here, we hypothesised that in addition to ductal fate suppression via the inhibition of Notch pathway and the TGF- β pathway, targeting the WNT pathway could enhance the transition from a ductal/progenitor state to an hepatocyte fate. For this purpose, we tested two WNT chemical inhibitors called IWP-2 and ICRT-3 which respectively inhibit upstream and downstream of the WNT pathway (for a detailed mode-of-action see Figure 3.2). More recently, it was shown that inhibition of the glycogen synthase kinase-3 (GSK-3) promoted the transition of human adipose stem cells into hepatocytes (Huang et al., 2017). Thus, along with IWP-2 and ICRT-3, we tested the effects of inhibiting GSK-3 using the chemical agent called CHIR99201 (CHIR).

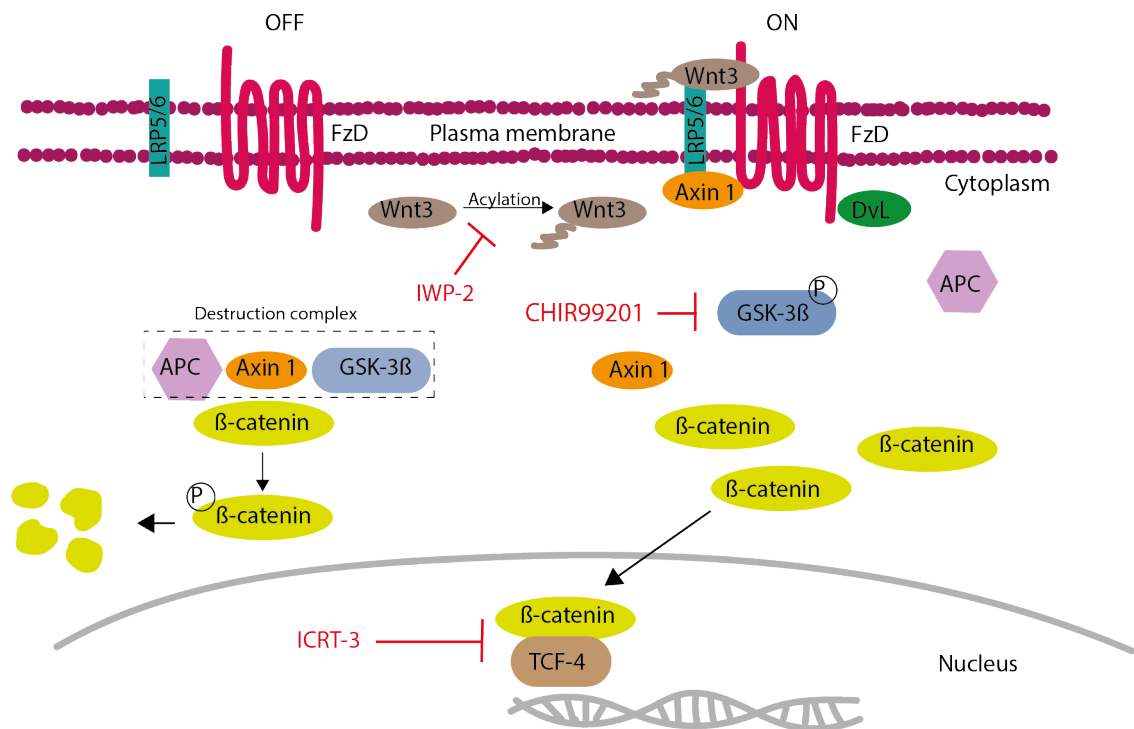


Figure 3.2 Targeting the canonical WNT signalling pathway. In the absence of WNT (OFF), the signalling pathway is inactive, and β -catenin is phosphorylated by the destruction complex. Phosphorylated β -catenin is then targeted for degradation. In the presence of WNT, the pathway is active (ON) – by binding to Frizzled (FzD) and LRP5/6, WNT prevents the formation of the destruction complex allowing the nuclear translocation of β -catenin and the triggering of the WNT target gene transcription. The two WNT inhibitors (in red) suppress the pathway at different stages: IWP-2 inhibits the activity of porcupine (Porcn), a membrane bound O-acyltransferase, essential for the lipidation of WNT ligands (Hofmann, 2000; Dodge et al., 2012); ICRT-3 interferes with β -catenin/TCF mediated transcription (Gonsalves et al., 2011). CHIR inhibits GSK-3, thereby inducing WNT signalling activation (Ying et al., 2008).

Accordingly, we supplemented the DM with ICRT3, IWP2 and CHIR99201 and named this new formulation as DM+ (Figure 3.3A). The DM+ protocol follows the DM protocol with the initial growth of Chol. Orgs for 5 days in EM, supplemented with (BMP-7) (Huch et al., 2015). BMP-7 was shown to be important for hepatocyte growth during liver development *in vivo* (Sugimoto et al., 2007). On day 5, Chol. Orgs were incubated on DM or DM+ for a total of 10-11 days (Figure 3.3B). At the end of the differentiation process, we assessed the level of differentiation in organoids grown in DM (DM Orgs) vs

DM+ (DM+ Orgs). In agreement with what was shown in Huch *et al* 2015, at day 13 post differentiation, the morphology of the DM Orgs revealed the presence of an heterogeneous population of organoid, with features of both ductal and hepatocyte cells. The ductal organoids retained a distinct ductal morphology evidenced by the presence of a lumen surrounded by a single layered epithelium, while few organoids exhibited a pseudostratified epithelium, a distinct morphological feature of a hepatocytes (Figure 3.3C). On the other hand, more of the DM+ Orgs presented a hepatocyte-like morphology, yet still there were organoids that retained a ductal phenotype (Figure 3.3C).

At the mRNA level, DM+ Orgs expressed higher levels of key hepatocyte markers Cytochrome P-450 3A4 (*CYP3A4*) and Albumin (*ALB*) when compared to DM+ Orgs; a small tendency for increased expression was also observed for other cytochrome genes, Cytochrome P-450 2C8 (*CYP2C8*) and Cytochrome P-450 2C9 (*CYP2C9*) in DM+ Orgs (Figure 3.3D). Additionally, we also observed a small increase of hepatocyte apical membrane transporter gene expression, ATP Binding Cassette Subfamily B Member 11 (*ABCB11*) and ATP Binding Cassette Subfamily G Member 2 (*ABCG2*) (Figure 3.3D).

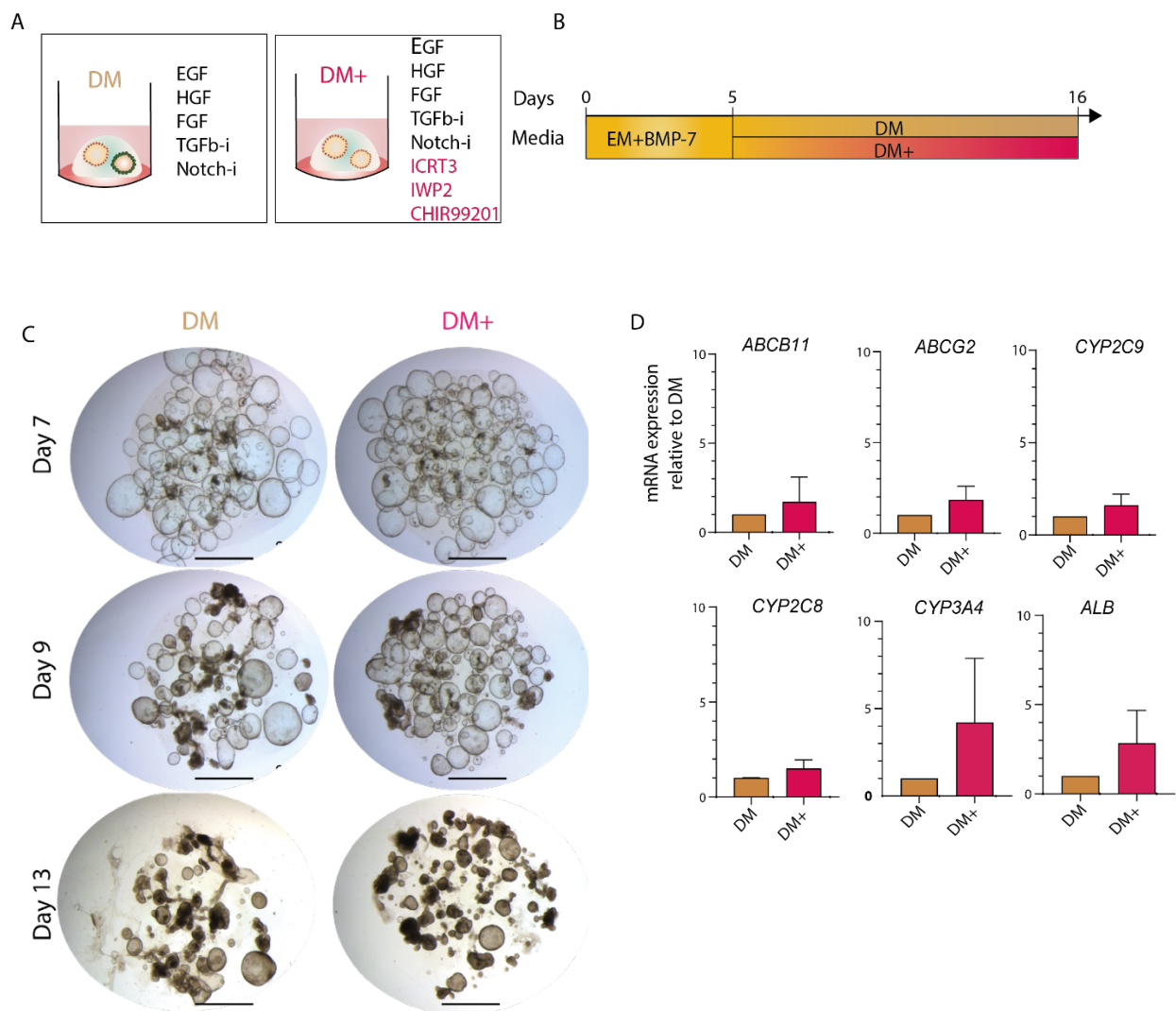


Figure 3.3 DM+ Orgs show an increase of hepatocyte-like morphology and a tendency for higher expression of hepatocyte markers. A) Detailed composition and protocol for DM v DM+. **B)** Timeline of DM and DM+ protocol. **C)** Brightfield images of DM/DM+ Orgs. Scale bar: 2mm, organoid p5 **D)** qPCR analysis of hepatocyte markers in DM and DM+. mRNA expression of each marker was normalised to the housekeeping gene *HPRT* and are represented as fold change relative to DM. N=3, error bars denote \pm SEM.

Since certain organoids still retained a ductal phenotype despite the DM+ protocol, we reasoned whether all cells were exposed to the media and whether increasing their exposure would induce their differentiation. We underwent mechanical dissociation of Chol. Orgs to generate smaller structures before incubating in either DM or DM+. Within 5 days of dissociation, Chol. Orgs grown in EM+BMP-7 were either left intact (Figure 3.4A) or dissociated into smaller fragments in a 1:3 ratio (Figure 3.4B). With this approach, we compared non-dissociated DM and DM+ Orgs (Figure 3.4A) and dissociated DM and DM+ Orgs (Figure 3.4B). For this experiment, the samples will be referred to as DM and DM+ non-dissociated or DM and DM+ dissociated Orgs.

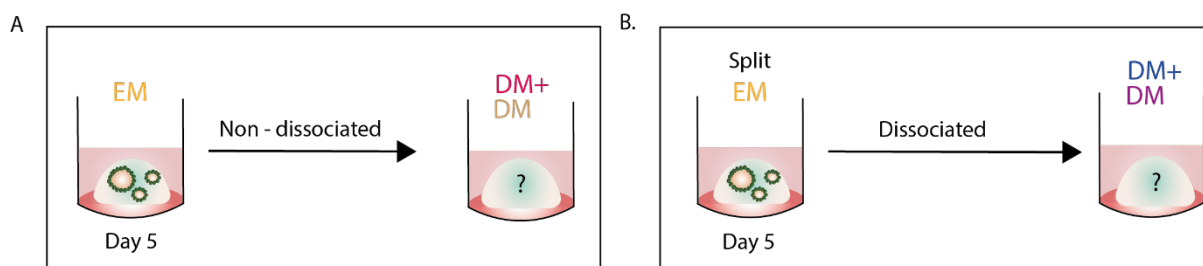


Figure 3.4 **Assessment of mechanical dissociation in DM and DM+ Orgs.** **A)** Addition of DM and DM+ on day 5 cholangiocyte organoids with no dissociation. **B)** Addition of DM and DM+ on dissociated organoid day 5 Chol. Orgs.

The results showed that, as expected, in the dissociated condition, organoids were reduced in size in both DM and DM+ (Figure 3.5B), compared to the non-dissociated ones (Figure 3.3C). By day 7, we observed a morphology more similar to that of hepatocyte organoids, as shown by the formation of a pseudo-stratified epithelium compared to the single layered epithelium typical of Chol. Orgs in both DM and DM+ dissociated Orgs (Figure 3.5B). Yet this was predominant in the DM+ (Figure 3.5B), suggesting that targeting WNT in parallel with mechanical dissociation promotes a faster differentiation of ductal cells. By day 9, all the DM+ dissociated Orgs exhibited the differentiated hepatic-like morphology while the DM dissociated Orgs still presented ductal “contaminants” (Figure 3.5B), which was maintained by day 13 (Figure 3.5B). Quantification of ductal and hepatocyte-like phenotypes showed an increase of hepatocyte-like morphology in the

DM+ dissociated condition (Figure 3.5D). Overall, compared to non-dissociated Orgs (Figure 3.3C), prior dissociation of Chol. Orgs and incubation in the DM+ enhanced the differentiation of Chol. Orgs towards a hepatocyte fate.

To confirm the efficiency of DM+ organoids in promoting hepatocyte formation either in the dissociated or non-dissociated condition, we performed gene expression analysis of hepatocyte markers and ductal markers (Figure 3.5B). The levels of several of the hepatocyte markers analysed – cytochromes (*CYP3A4*, *CYP2C8*, *CYP2C9*), apical membrane transporters (*ABCB11* and *ABCG2*) and *ALB* – were upregulated in the DM+ dissociated condition when compared to all the other condition (DM Non-diss., DM diss. and DM+ Non-diss. - Figure 3.5B). Indeed, a trend towards increased expression was observed for all the hepatocyte markers, with the highest expression in the DM+ dissociated. Overall, these data support that a combination of WNT inhibition and mechanical dissociation enhances the differentiation of Chol. Orgs into a hepatocyte fate. While dissociation improved the cell's transition to a differentiated state in the DM condition, it was still less effective than the differentiation achieved in the DM+ alone, without any dissociation, once again supporting that sole inhibition of the ductal phenotype via the Notch and TGF- β inhibition is not sufficient to promote the transition from a progenitor to a hepatocyte fate.

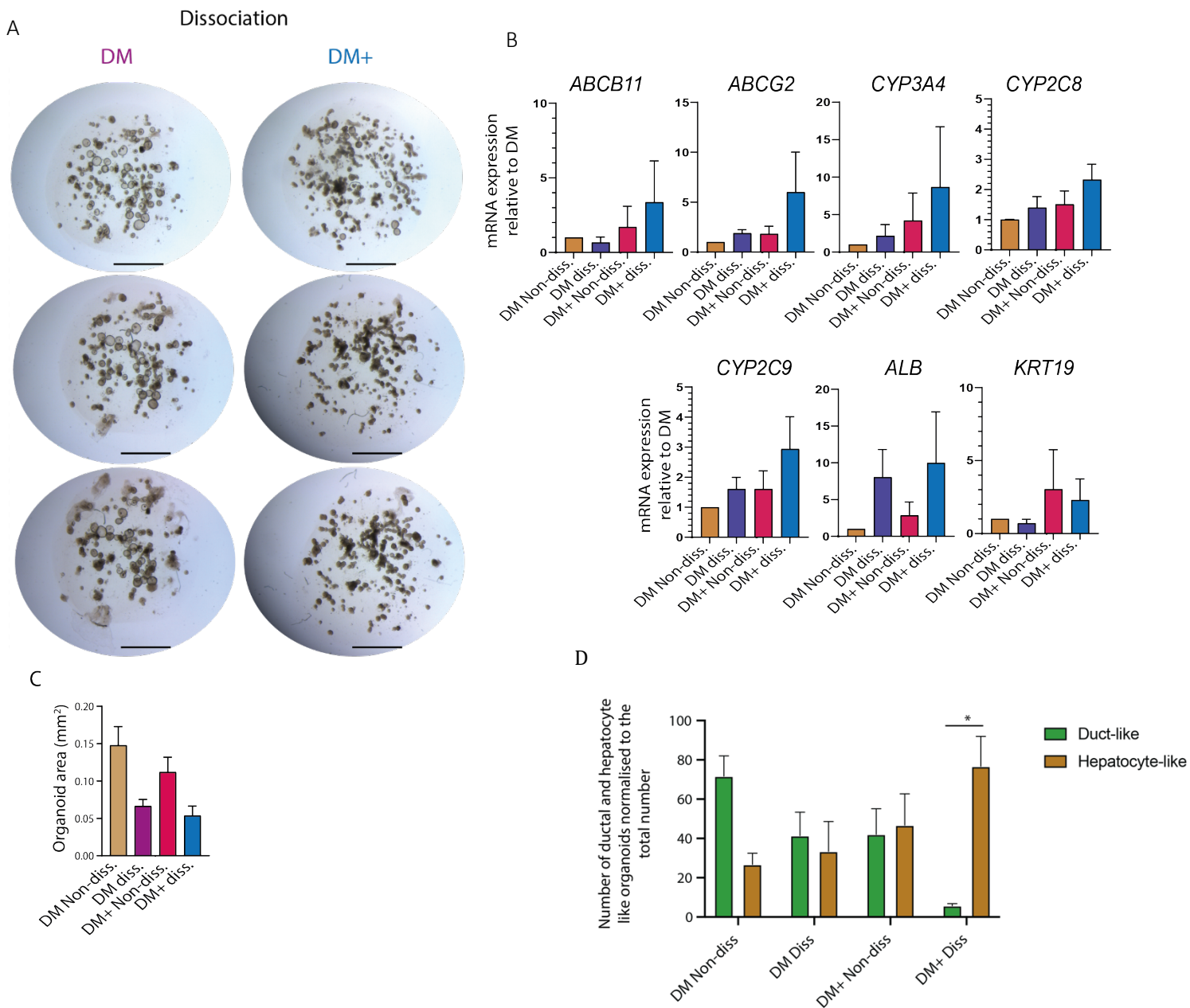


Figure 3.5 Organoid dissociation and WNT inhibition enhances ductal cells differentiation towards hepatocyte fate. **A)** Brightfield images of dissociated organoids (DM/DM+) during the differentiation process. Scale bar: 2 mm, organoids p5 **B)** Quantification of organoids area (mm²). N=3 **C)** qPCR analysis of hepatocyte markers. mRNA expression of hepatocyte marker was normalised to the housekeeping gene HPRT and is represented as fold change relative to DM non-dissociated (Non-diss) Orgs. N=3; error bars denote \pm SEM. Hepatocyte markers: cytochromes-*CYP3A4*, *CYP2C8*, *CYP2C9*; apical membrane transporter - *ABCB11* and *ABCG2*; *ALB*. **D)** Measurement of ductal and hepatocyte-like morphology, N= 2, Mann-Whitney non-parametric test P value < 0.05.

Having identified an improvement in the differentiation of Chol. Orgs into hepatocyte organoids, from this point DM+ dissociated Orgs and DM non-dissociated Orgs (Huch et al., 2015) will be used for the next experimental studies and will be referred as DM+ Orgs and DM Orgs only. Next, we performed functional assays to assess whether the increase in expression of hepatic markers with the newly developed differentiation protocol is paralleled by an enhancement of hepatocyte functions. As described previously (see 1.3 section of introduction) two of the key functions of hepatocytes is to secrete bile and serum protein albumin. To confirm that the new differentiation protocol (Figure 3.6A-B) resulted in more functional hepatocytes, we quantified the secretion of bile and albumin secreted Chol. Orgs, DM Orgs and DM+ Orgs. The secretion of both albumin and bile was markedly superior in the DM+ Orgs compared to DM Orgs and even more when compared to Chol. Orgs (Figure 3.6C-D). Of note, the albumin secretion levels in DM Orgs are lower compared to the previous study (Huch *et al.*, 2015), a difference which might be derived by the heterogeneity of human donors adopted. Taken together, we have optimised the DM+ protocol based on mechanical dissociation to improve ductal differentiation into hepatocyte fate.

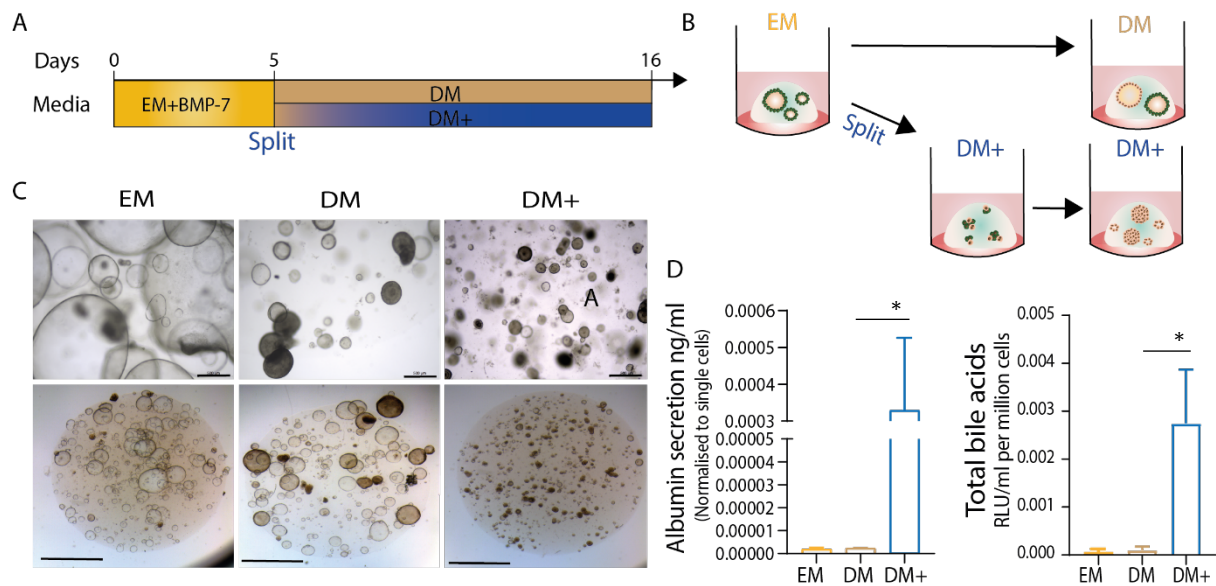


Figure 3.6 DM+ Orgs recapitulate enhanced hepatocyte specification compared to DM Orgs. **A/B)** Overview of DM and DM+ protocols. **C)** Brightfield images of Chol Orgs (EM), DM and DM+ Orgs at day 16. Scale bar: 500 μ m; 2mm **D)** Albumin and total bile acid secretion measured on day 16. Albumin secretion was quantified as ng/ml and results were normalised to the total number of cells in each condition. Secretion of total bile acids is expressed as RLU/ml after normalisation to the total number of cells in each condition. N=3, data are represented as mean \pm SEM. Mann-Whitney non-parametric test P value < 0.05.

3.2 GSK-3 inhibition promotes DM+ Orgs growth and enhances hepatocyte fate specification

We have shown that addition of IWP-2 and ICRT-3, WNT inhibitors, and CHIR, GSK-3 inhibitor, led to an improved differentiation of ductal cells into hepatocytes. How could inhibition of WNT signalling and its activation potentiate the differentiation towards the hepatocyte fate? A recent study, suggested that inhibition of GSK-3 facilitated the differentiation of human adipose stem cells to hepatic fate (Huang et al., 2017). GSK-3 is a serine/threonine protein kinase, primarily regulated through suppression of its own activity by phosphorylation. It is a downstream target of several signalling pathways including WNT (Peifer, Pai and Casey, 1994; He et al., 1995), in which its inhibition triggers activation of WNT signalling. To answer the above question, we investigated how

inhibition of GSK-3 impacted the differentiation of Chol. Orgs into DM+ Orgs by removing the GSK-3 inhibitor - CHIR - from the DM+ (from now on called DM+(-CHIR)). Morphological analysis revealed an increase in size of the DM+ Orgs compared to the DM+(-CHIR) ([Figure 3.7](#)), indicative of a potential increase in cellular proliferation.

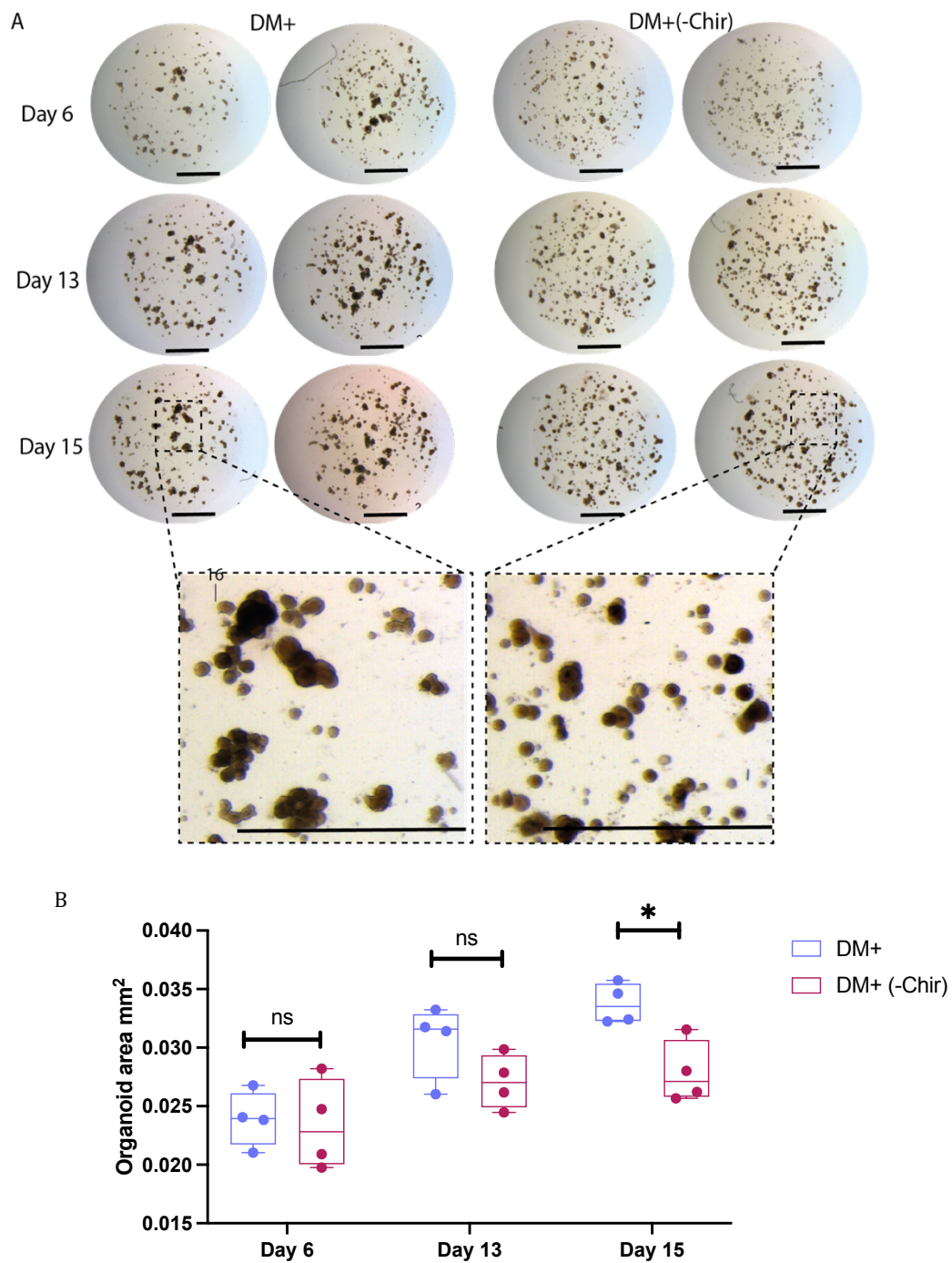


Figure 3.7 Enhanced organoid growth upon GSK-3 inhibition. A) Brightfield images of DM+ and DM+(-CHIR) Orgs overtime during the differentiation process. Scale bar: 2 mm **B)** Measurement of organoid area (mm²) in time: day 6, day 13 and day 15. DM+ Orgs present a higher organoid area compared to DM+ (-CHIR) overtime. Box and whiskers plot, dot represent technical replicates; middle line equals mean. N= 2, Mann-Whitney non-parametric test P value < 0.05.

Since we observed a potentially enhanced organoid growth in DM+ Orgs compared to DM+(-CHIR), we questioned whether higher cellular proliferation derived by GSK-3 inhibition could impact the differentiated state of the hepatocyte into a more progenitor state. However, the expression of key markers of hepatocyte's metabolic functions- *CYP2C8*, *CYP3A4* and *CYP2C9* – was upregulated in the DM+ (which is CHIR supplemented) compared to DM+(-CHIR) (Figure 3.8), supporting that CHIR supplementation enhances the transition towards an hepatocyte functional fate. The results goes in line with the observation of GSK-3 inhibition promoting functional hepatocyte specification (Huang et al., 2017).

Additionally, upregulation of hepatocyte markers following DM+ supplemented with CHIR, coincided with a decrease in the expression of the cholangiocyte marker *KRT7* (Figure 3.8), once again in support of CHIR as a booster of hepatic fate. Based on these results, from now on we used DM+ supplemented with CHIR as our differentiation media.

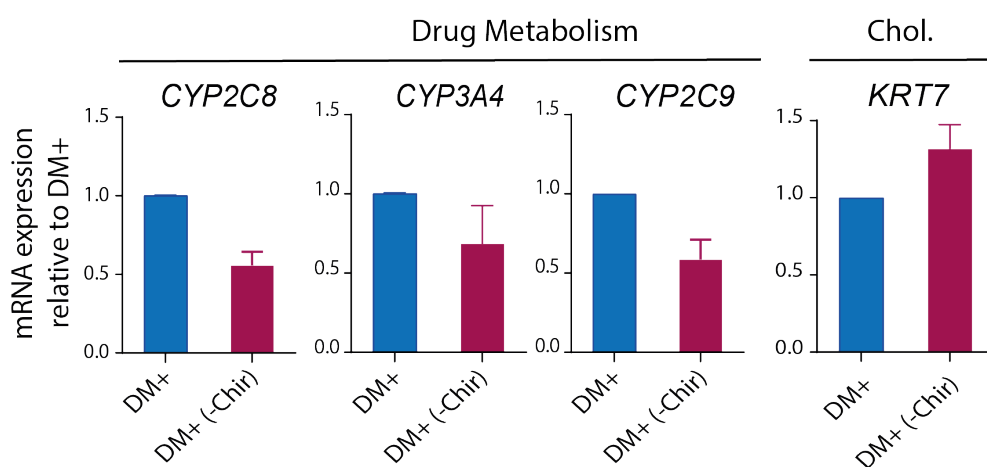


Figure 3.8 **GSK-3 inhibition favours hepatocyte fate specification.** qPCR analysis of hepatocyte markers in DM+ and DM+(-CHIR). mRNA expressions are normalised to the housekeeping gene *HPRT* and are represented as fold change relative to DM+ organoids. N=3; error bars denote \pm SEM. DM+ organoids show an upregulation of hepatocyte markers involved in drug metabolism: *CYP2C8*, *CYP3A4*, *CYP2C9*, while cholangiocyte marker *KRT7* is decreased compared to DM+(-CHIR).

3.3 Inhibition of YAP activity in Chol. Orgs enhances the differentiation towards a functional hepatocyte fate.

Cells can sense changes from the extracellular environment and neighbouring cells. The perceived mechanical stimuli result in changes in gene expression that translate into changes in cell fate, rate of cell proliferation and cell death until a mechanical balanced is reached. YAP, key downstream effectors of the Hippo signalling pathway (refer to [Figure 1.3](#) for an overview of the Hippo pathway), has been identified as a mechano-transducer involved in translating such mechanical forces into transcriptional responses (Huang et al., 2005; Dong et al., 2007). *In vivo* studies have shown that the intra-biliary compartment present higher YAP activity compared to hepatocytes (Yimlamai et al., 2014). This led us to question the potential role of the Hippo signalling pathway, and of YAP, in the differentiation of ductal cell to hepatocyte. Therefore, first we assessed whether the upregulation of YAP expression is recapitulated in our *in vitro* Chol. Orgs cultures.

Since we showed previously (see [Figure 3.5](#)) that Chol. Orgs mechanical dissociation enhances their differentiation, we performed immunostaining analysis for YAP protein before and after dissociation and quantified the % of YAP in the nucleus, a sign of the pathway's activation, vs cytoplasm. In Chol. Orgs grown in EM+BMP-7 for 5 days and prior to any mechanical dissociation, YAP was predominantly cytoplasmic (EM day 5 - [Figure 3.9A](#)). On the contrary, upon dissociation, we observed a major translocation of YAP into the cell's nucleus (EM 24H - [Figure 3.9A](#)). In fact, within 24h of dissociation 30% of cells expressed nuclear YAP ([Figure 3.9B](#)). The result is concomitant

with the expression of YAP target gene *CTGF* (Figure 3.9C). This suggests that organoid mechanical dissociation might trigger YAP activity, which could coincide with the initial proliferative capacity of ductal cells to self-organise into organoid structures.

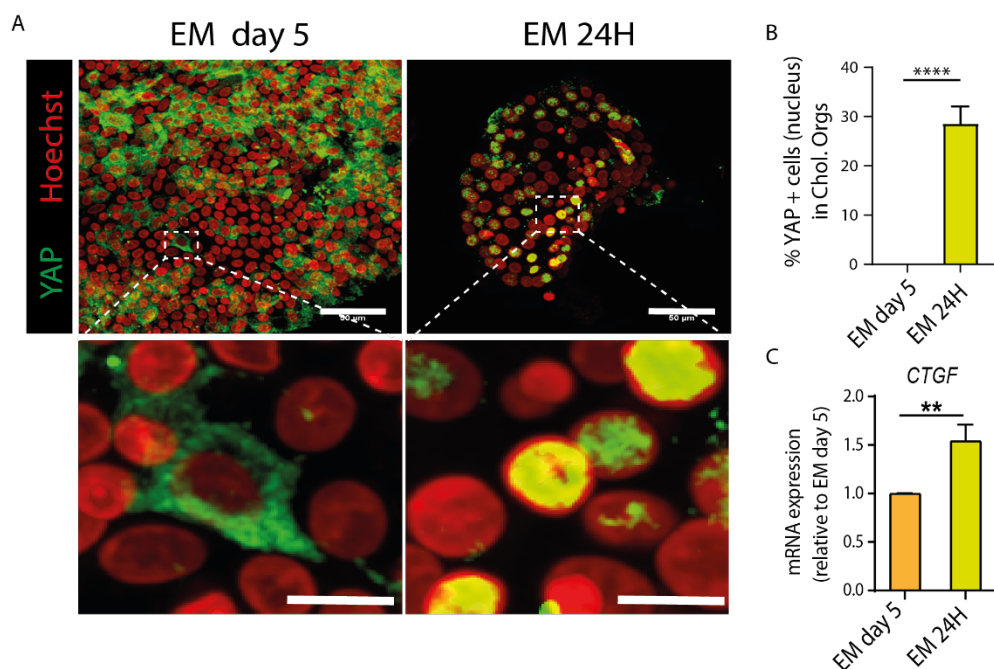


Figure 3.9 YAP is activated in Chol. Orgs following mechanical dissociation. A) Immunostaining analysis of YAP (green) shows that its expression is mainly restricted to the cytoplasm of cell of Chol. Orgs in culture for 5 days. Within 24h after mechanical dissociation, YAP is translocated into the nucleus (EM 24h). Scale bar = 50 μ m; Scale bar zoom = 10 μ m **B)** Quantification of nuclear YAP+ cells after 5 days in EM+BMP7 and 24h after mechanical dissociation. $P < 0.0001$ (****). **C)** qPCR analysis of YAP target gene *CTGF* shows its upregulation after 24H dissociation (EM 24H). mRNA expression of *CTGF* is normalised to the housekeeping gene *HPRT* and is represented as fold change relative to EM day 5. $N=5$, error bars denote \pm SEM. $P < 0.001$ (**).

To further validate the role of YAP in Chol. Orgs proliferation, we inhibited YAP activity at the point of organoid dissociation using a small molecule called Verteporfin (VP), previously shown to act as a YAP inhibitor in intestinal organoids (Wang et al., 2016). Chol. Orgs were grown in EM supplemented with one of two concentration of VP – 100 nM and 1 μ M – for 24h following their mechanical dissociation (Figure 3.10A). The number of Chol. Orgs showing a morphology characteristic of a hepatic fate was markedly higher with increasing concentrations of VP (Figure 3.10A), supporting activation of YAP in the maintenance of a ductal fate. While at the highest concentration all Chol. Orgs showed a hepatic-like morphology, we observed signs of toxicity based on the phenotype, these included signs of lower viability marked with shrinkage and formation of debris surrounding the organoids possibly suggesting apoptosis. For this reason, we continued our studies with 100 nM VP after confirming that this lower concentration was already efficient at downregulating YAP's activation, as shown by a marked decrease in the expression of its target gene *CTGF* (Figure 3.10B). Overall, our data suggest a role of YAP in the maintenance of Chol. Orgs in agreement with was previously shown *in vivo* (Yimlamai et al., 2014).

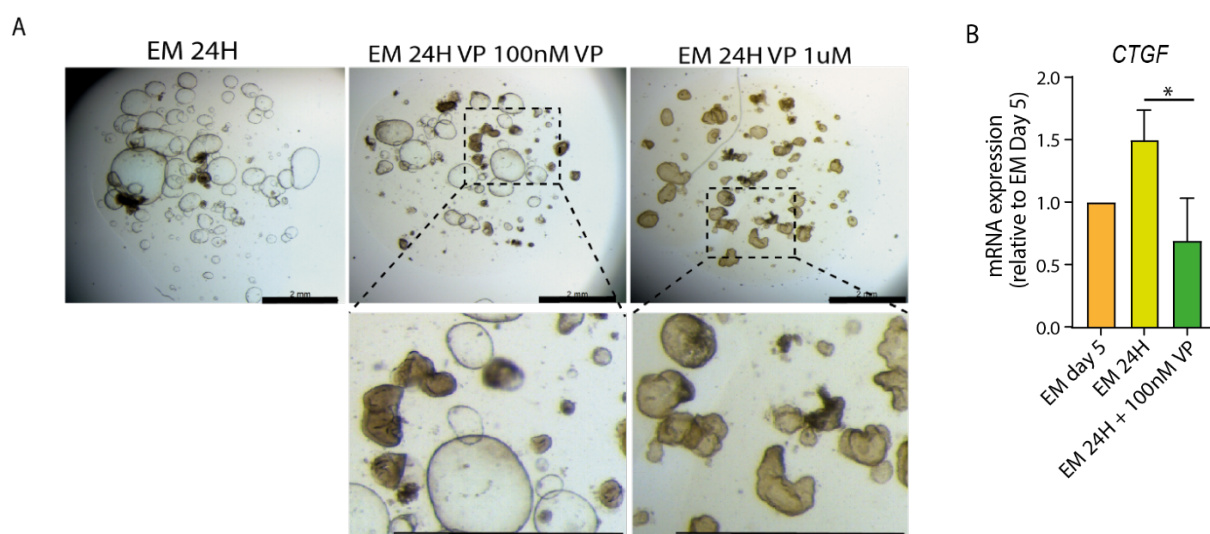


Figure 3.10 **YAP inhibition impairs Chol. Orgs maintenance.** **A)** Brightfield images of Chol. Orgs dissociated and treated for 24h with two concentrations of VP – 100 nM and 1 μ M – versus EM 24H. EM 24H VP 1 μ M presented a clear differentiated phenotype. Scale bar = 2mm. Scale bar zoom = 1 mm **B)** qPCR analysis showed downregulation of YAP target gene *CTGF* when treated with VP. mRNA expression of *CTGF* is normalised to the housekeeping gene *HPRT* and is represented as fold change relative to EM day 5. N=5, error bars denote \pm SEM. Mann-Whitney non-parametric test $P < 0.01$ (*).

Since our results in EM suggested a role of YAP activation in the maintenance of a ductal phenotype, we then asked how YAP activity is in DM+. We observed an increase of YAP localisation in the cytoplasm – indicative of an active Hippo signalling – after incubation in DM+ for 24h (Figure 3.11). A previous study showed that WNT signalling is implicated in the activation of the Hippo pathway with subsequent YAP cytoplasmic retention (Azzolin et al., 2014).

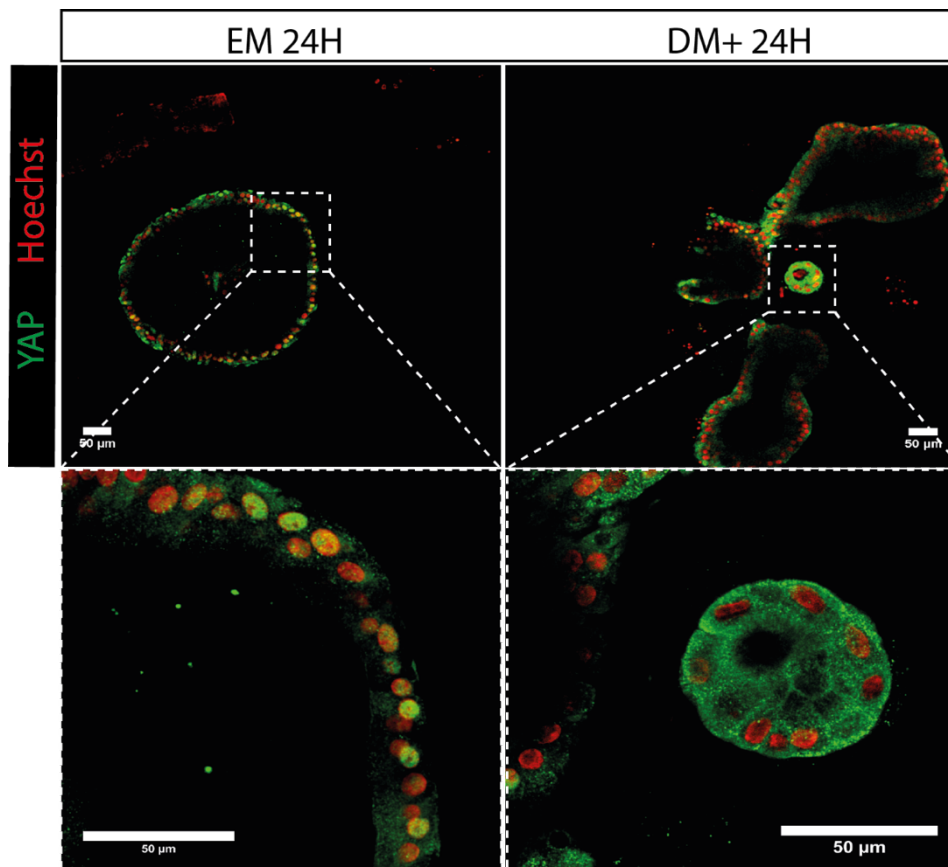


Figure 3.11 YAP is predominantly located in the cytoplasm in DM+ Orgs. Immunostaining of YAP (green) and nuclei (red) in Chol. Orgs (EM 24H) and DM+ 24H Orgs showed a reduction of YAP nuclear localisation in DM+ 24h Orgs. Scale bar: 50 μ m.

Although, YAP nuclear translocation is significantly reduced in DM+ Orgs after 24h (Figure 3.11), yet some cells still retained YAP nuclear expression (Figure 3.13A). Based on previous findings on the dynamics of YAP signalling in the hepatic epithelium (Yimlamai *et al.*, 2014; Pepe-Mooney *et al.*, 2019) and having observed the acquisition of a differentiated morphology upon YAP inhibition in Chol. Orgs (Figure 3.10A), We hypothesised whether YAP inhibition could improve Chol. Orgs differentiation into hepatocyte organoids. Therefore, to further inhibit YAP activity we supplemented the DM+ media with VP.

DM+ Orgs were first treated with 100 nM VP and assessed for their morphology (Figure 3.12). At VP 100 nM we observed structural features of organoid collapsing compared to Chol. Orgs exposed to the same concentration (Figure 3.10A), suggesting a possible role of YAP inhibition in promoting a rapid transition from a less differentiated state into a terminally differentiated state. In addition, long term exposure of VP for 48h caused a drop in organoid viability (Figure 3.12). For this reason, 100 nM VP treatment for a period of 24h only was selected as concentration and regimen to be tested on DM+ Orgs.

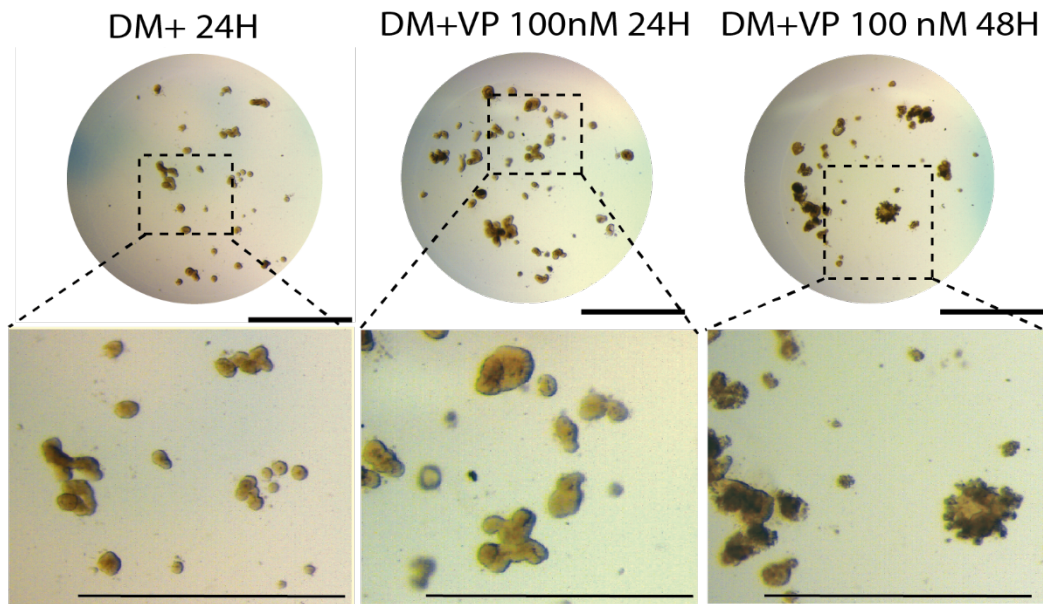


Figure 3.12 **Long term exposure to VP in DM+ Orgs leads to organoid toxicity.** Brightfield images of 24h post-dissociated DM+ Orgs exposed to 100 nM VP for 24h and 48h. Longer exposure to VP beyond 24h leads to organoid collapsing. Scale bar: 1 mm.

Supplementation of DM+ with VP 100 nM for 24h led to a marked reduction in the translocation of YAP in the nucleus (Figure 3.13A-B).

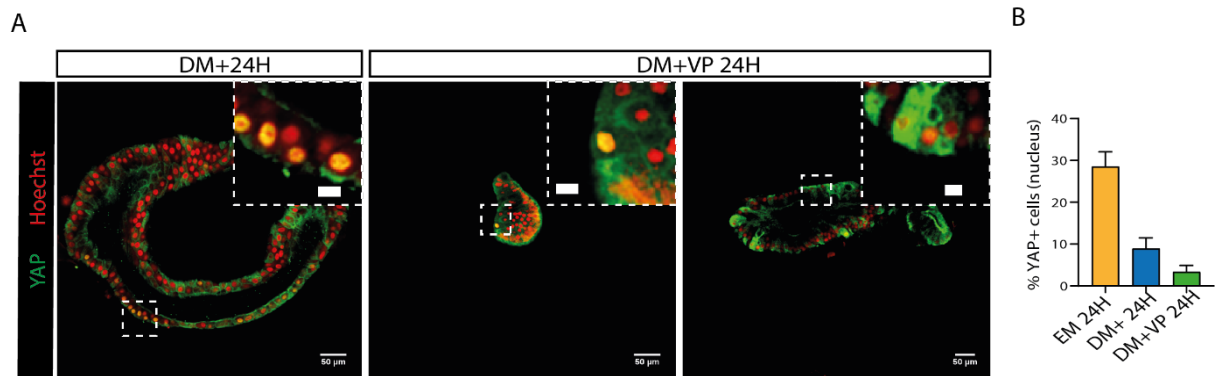
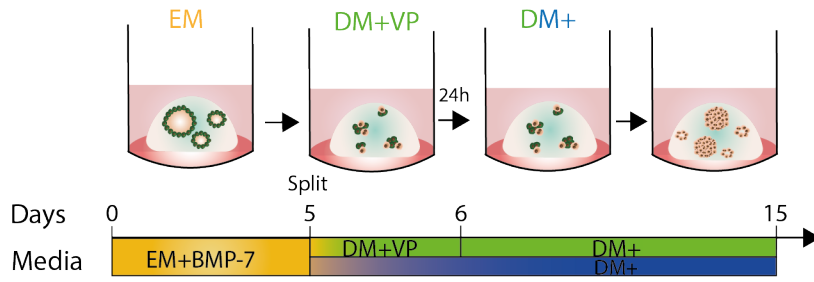


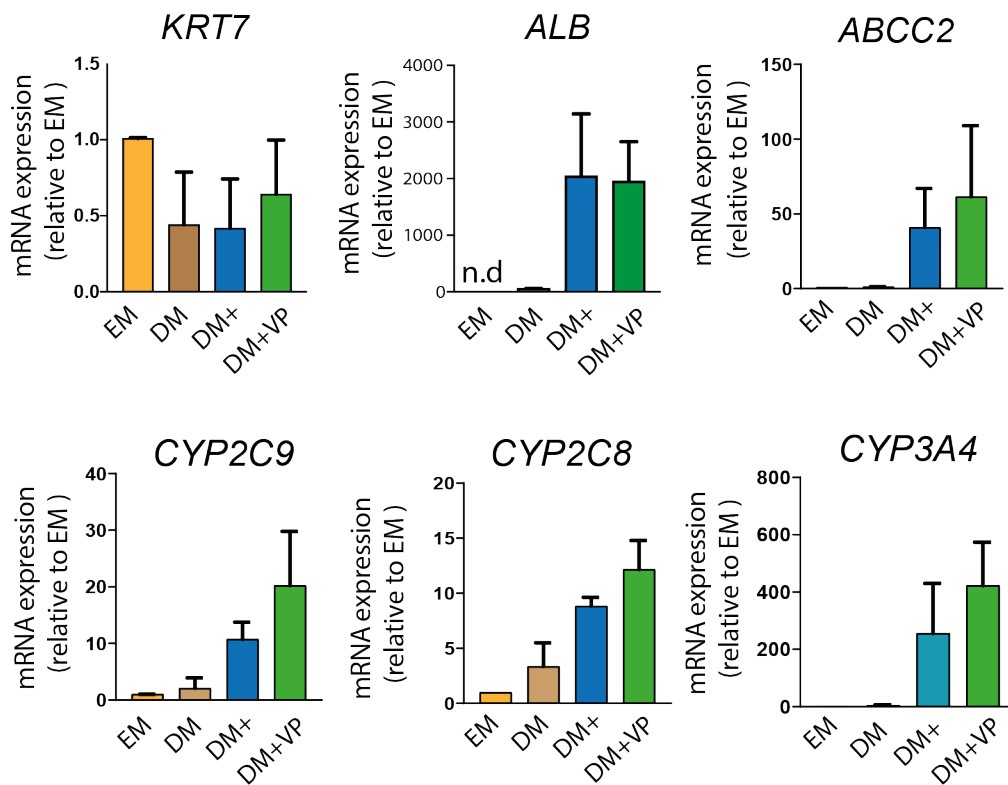
Figure 3.13 YAP activity is inhibited following VP treatment in DM+ Orgs. A) Immunostaining analysis of YAP (green) and nuclei (red) in DM+ 24H and DM+VP 24H Orgs. Scale bar: 50 μ m. Zoomed in image scale bar: 10 μ m. **B)** Quantification of % of YAP+ in the nuclei normalised to the total number of cells. A decrease of 5% of YAP+ nuclei is observed following VP treatment.

These results prompted us to hypothesise whether YAP inhibition could be an important addition in the DM+ protocol to further enhance the differentiation of ductal cell to hepatocyte fate. Similarly, to the DM+ protocol, in the DM+VP protocol (100nM VP 24h) organoids were grown for 5 days in EM+BMP7 and dissociated after 5 days. At day 5, organoids were incubated in DM+VP ([Figure 3.14A](#)). After 24h, media was refreshed to DM+ only, and kept until day 16. These organoids will be referred hereafter as DM+VP Orgs. On day 16, mRNA analysis showed an upregulation of hepatocyte markers (*CYP2C9*, *CYP2C8* and *CYP3A4*) in DM+VP Orgs compared to DM+ Orgs ([Figure 3.14B](#)). Functional assays showed that DM+VP Orgs had higher levels of bile secretion, albumin secretion, and cytochrome activity compared to DM+ Orgs ([Figure 3.14C](#)). Expression of the ductal marker *KRT7* expression was maintained both in DM+ and DM+VP Orgs ([Figure 3.14B](#)), supporting the existence of a pool of ductal/progenitor cells that resist differentiation. However, analysis of another ductal marker, KRT19 protein, was only seen in DM Orgs but not in DM+ orgs and in DM+VP Orgs ([Figure 3.15](#)).

A



B



C

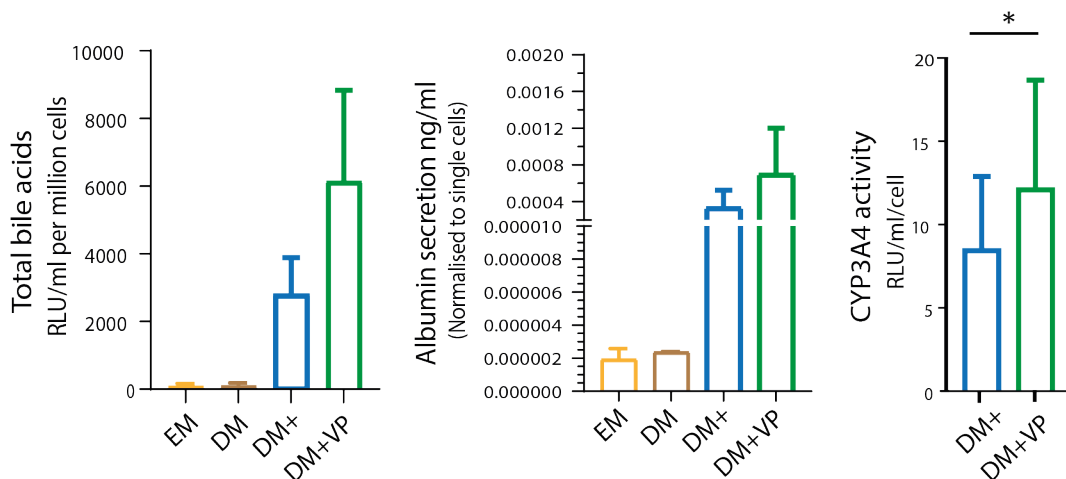


Figure 3.14 VP supplementation to DM+ results in increased expression of hepatocyte markers **A)** Model of DM+ and DM+VP protocols. **B)** qPCR analysis between Chol Orgs (EM), DM, DM+ and DM+VP Orgs showed upregulation of cytochromes such as *CYP2C9*, *CYP2C8* and *CYP3A4* in DM+VP Org. Ductal marker *KRT7* expression is upregulated in DM+VP Orgs. mRNA expression values are normalised to the housekeeping gene *HPRT* and are represented as fold change relative to EM. N=5, error bars denote \pm SEM. **C)** Quantification of albumin, total bile acid secretion and cytochrome activity measured on day 16. Albumin secretion was quantified as ng/ml and results were normalised to the total number of cells in each condition. Secretion of total bile acids is expressed as RLU/ml after normalisation to the total number of cells in each condition. Cytochrome activity is expressed as RLU/ml and the readout normalised to the total number of cells. DM+VP Orgs had higher levels of bile secretion, albumin secretion, and cytochrome activity compared to DM+ Orgs N=3, error bars denote \pm SEM. Mann-Whitney non-parametric test $P < 0.05$.

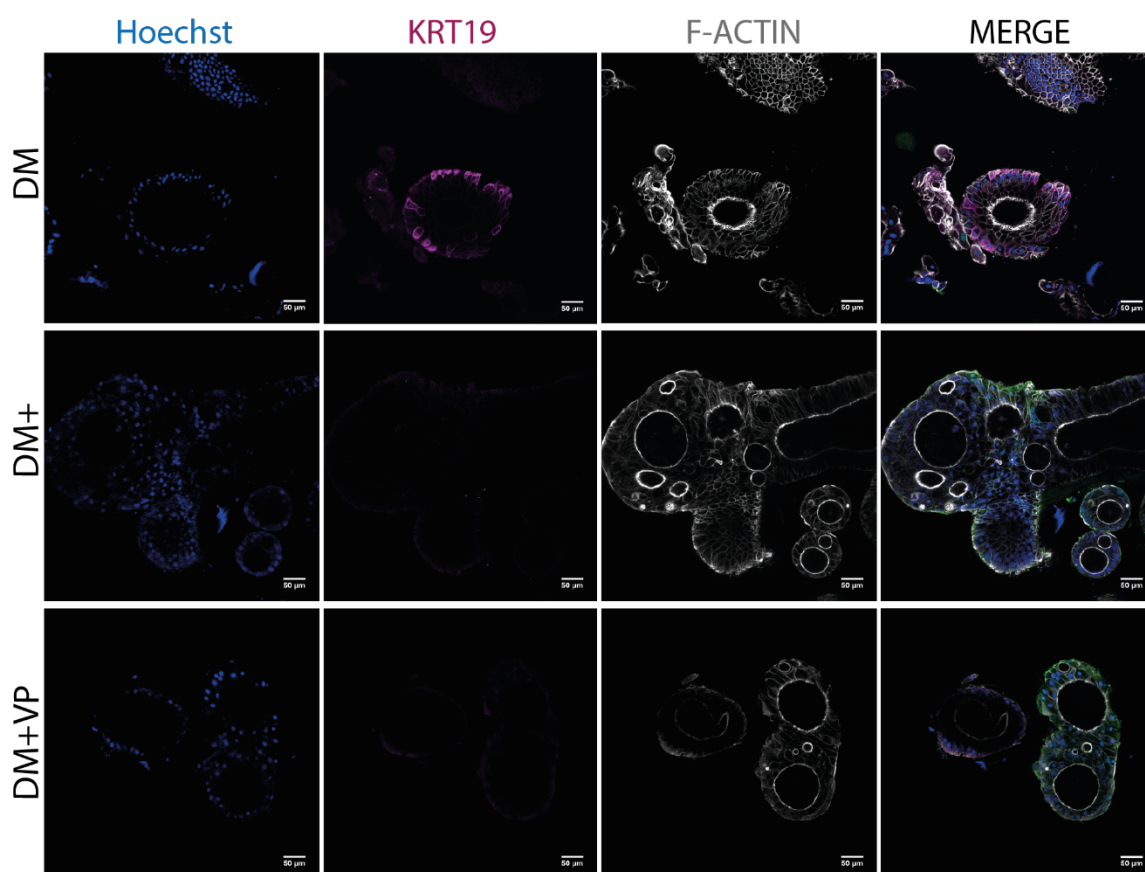


Figure 3.15 KRT19 protein expression in DM Orgs but not in DM+ and DM+VP Orgs. Immunostaining analysis of KRT19 (purple), F-actin (grey), nuclei (blue). Scale bar: 50 μ m.

Since DM+VP Orgs showed upregulation of drug metabolising genes such as *CYP3A4*, we chose DM+VP as our standard protocol to differentiate ductal cells to hepatocytes.

3.4 Comparing human cholangiocyte derived DM+VP Orgs vs new model of human hepatocyte organoids.

While we developed a new media that enhances the differentiation of Chol. Orgs toward a hepatocyte lineage, the effectiveness of differentiation is still highly heterogeneous, a marked impairment for its application in DILI studies. In addition, despite hepatocytes derived ductal/progenitor cells exhibited hepatocyte features both at the RNA and protein level, how close they resemble *in vivo* hepatocyte is still unclear. Recently, two landmark studies have successfully reported the establishment of hepatocyte organoids (Hep Org) directly from hepatocytes (Hu et al., 2018; Peng et al., 2018). These studies have successfully generated Hep Org using isolated hepatocytes from adult mouse livers (Hu et al., 2018; Peng et al., 2018), foetal human livers and human cryopreserved hepatocyte (Hu et al., 2018).

We generated human Hep Orgs using commercially available cryopreserved human adult PHH, kindly provided by GlaxoSmithKline. To identify the optimal initial seeding density to generate hepatocyte organoids, we tested different seeded numbers of hepatocytes, from 10.000 to 60.000 cells (Figure 3.16A) in the two medias, Hu and Peng (Hu et al., 2018; Peng et al., 2018) (See Methods and Materials). As a control, hepatocytes were either embedded in BME or in a 2D conformation in Williams'E + 10 % FBS (Figure 3.16A). We only observed well-defined organoid structures in the 60.000 cell seeding condition (Figure 3.16B); whilst at lower seeding densities organoid formation was low, suggesting that higher cellular density enhances organoid formation efficiency. In these conditions, organoid formation was observed only in the Hu media (Hu Orgs) and not when hepatocytes were treated with Peng media (Figure 3.16B). Of note, the Peng media was used only in mouse hepatocytes which might explain the lack of organoid formation observed in Figure 3.16B. Albumin protein expression supports the hepatocyte-like identity of the Hu Orgs (Figure 3.16C).

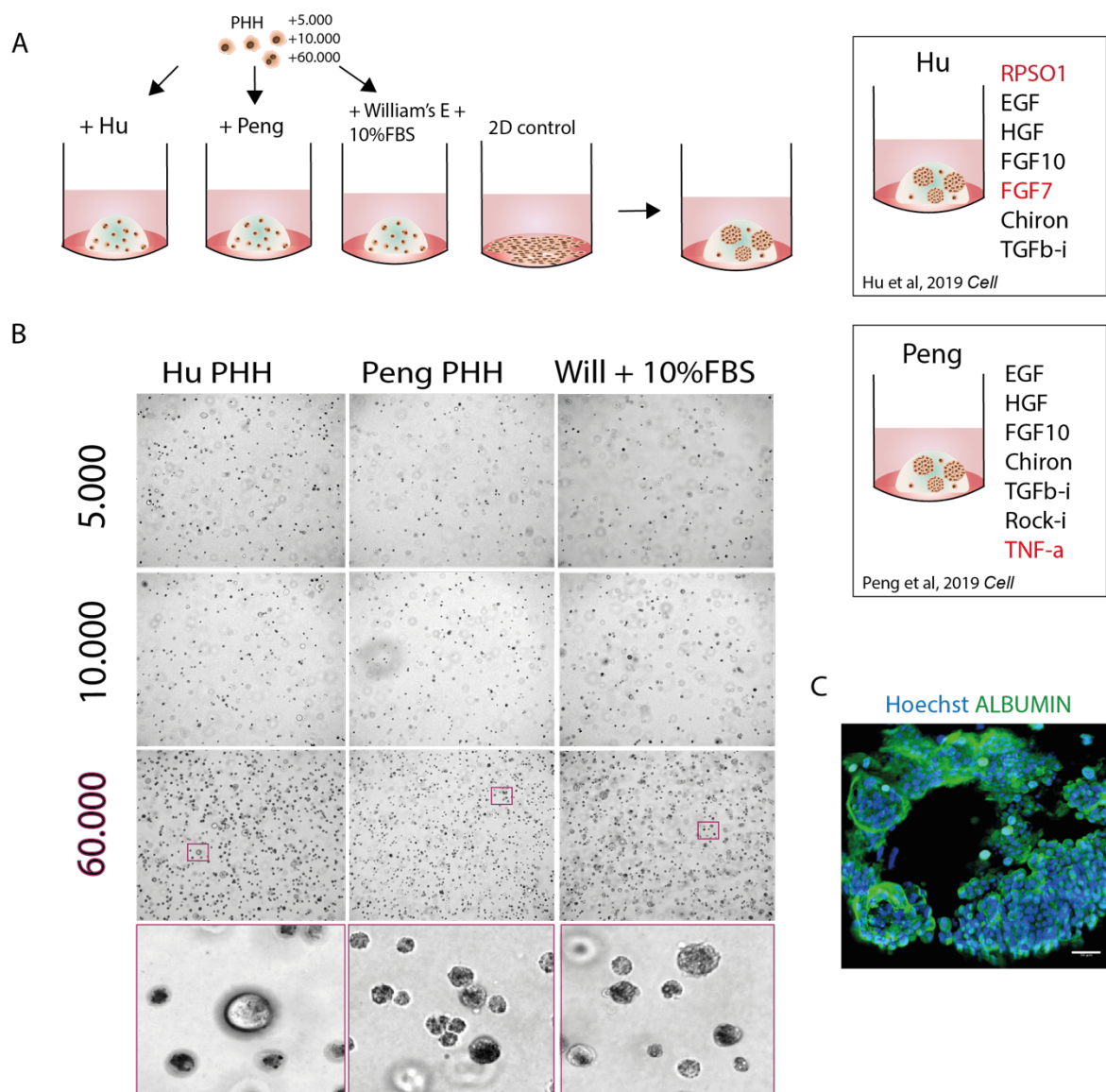


Figure 3.16 Establishment of human Hep Org using PHH. A) Experimental model. Different initial seeding densities of PHH were used from 5,000 to 60,000 cells and incubated in different hepatic media: Hu (Hu et al, 2019), Peng (Peng et al, 2019) and William's E + 10% FBS. PHH were also seeded in monolayer (2D) and incubated in William's E + 10% FBS medium. **B)** Brightfield images of hepatocytes in different seeding densities. Hep Org formation was only observed in the condition of 60,000 cells. N=3 **C)** Immunostaining analysis of Albumin expression (green) in Hu Orgs. Scale bar: 50 μ m. N=3

As previously shown in the Hu *et al.*, (2018) we observed an upregulation of hepatocyte markers in Hu Orgs compared to DM Orgs, whilst the result was the opposite when compared to DM+VP Orgs and to 2D hepatocytes (Figure 3.17B). These results

support that our DM+VP media achieves a higher degree of hepatocyte maturation. Conversely, expression of ductal markers, *KRT7* and *KRT19*, was still significantly higher in the DM+VP compared to the Hu media (Figure 3.17B). This suggests that using hepatocytes as the initial cells to generate Hep Orgs might reduce the risk of more chimeric organoids, in which ductal and hepatocyte-like cells co-exist. Additionally, this also indicates that perhaps different subpopulations of ductal cells might be more prone to differentiate into hepatocyte, while some “resistant” ductal population might favour self-renewal or differentiation towards the cholangiocyte fate.

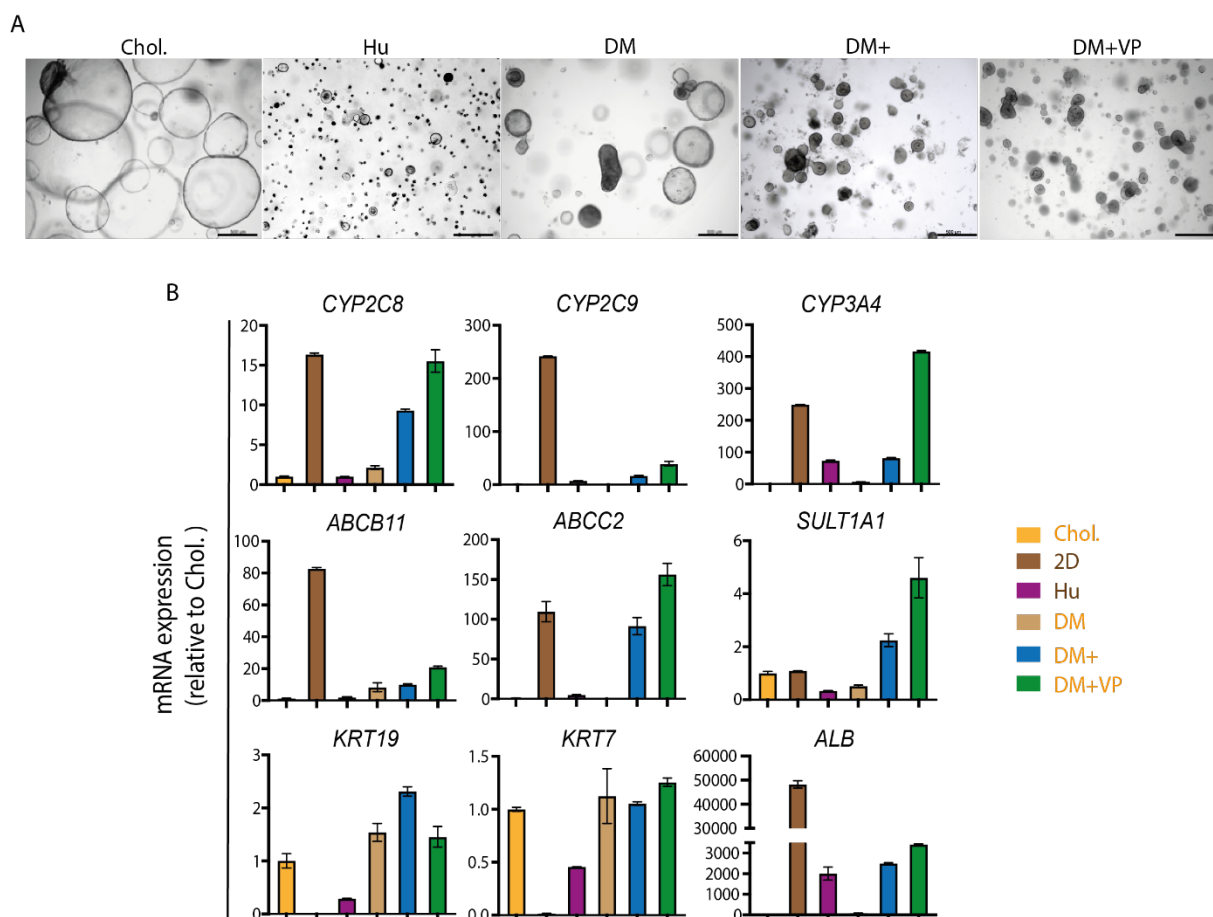


Figure 3.17 mRNA expression analysis of hepatocyte markers in cholangiocyte and hepatocyte derived Hep Orgs. A) Brightfield images of the different hepatic organoid systems. Scale bar: 500 μ m. **B)** qPCR analysis of hepatocyte markers and ductal markers across the different organoid systems. Hu Orgs expressed lower hepatocyte markers compared to DM+VP Orgs, yet expression of ductal markers was significantly lower. mRNA levels for each gene were normalised to the housekeeping gene *HPRT* and are represented as fold change relative to Chol. N=1, two technical

replicates, error bars denote \pm SEM. Legend: Cholangiocyte derived - DM, DM+, DM+VP Orgs; Hepatocyte derived - 2D and Hu.

I noted that some organoid structures in the Hu media, however, resemble the Chol. Orgs (Figure 3.18), suggesting that either I had a “ductal contaminant” in our PHH (highly unlikely) or that hepatocytes incubated in the Hu media to generate organoids undergo a certain level of de-differentiation. Further to assess the cholangiocyte nature of the luminal structures in the Hu media, I have mechanically dissociated them and incubated the organoids in the EM media, which favours the ductal/progenitor growth. Analysis of these cultures showed that indeed they expanded as Chol. Orgs, hence implying that the presence of luminal structures in the Hu condition are true Chol. Orgs (Figure 3.18).

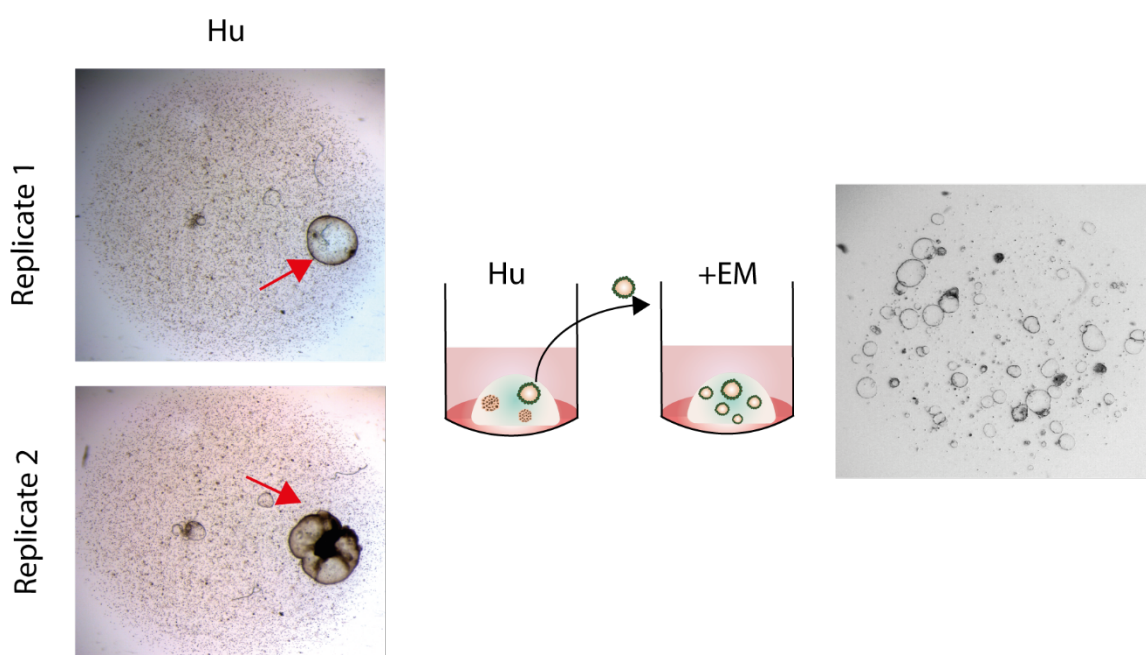


Figure 3.18 **Formation of Chol. Orgs from PHH cultures in Hu media.** Brightfield images of Hu Orgs cultures. Luminal structures were handpicked, dissociated, and grown in EM. N=3 biological replicates..

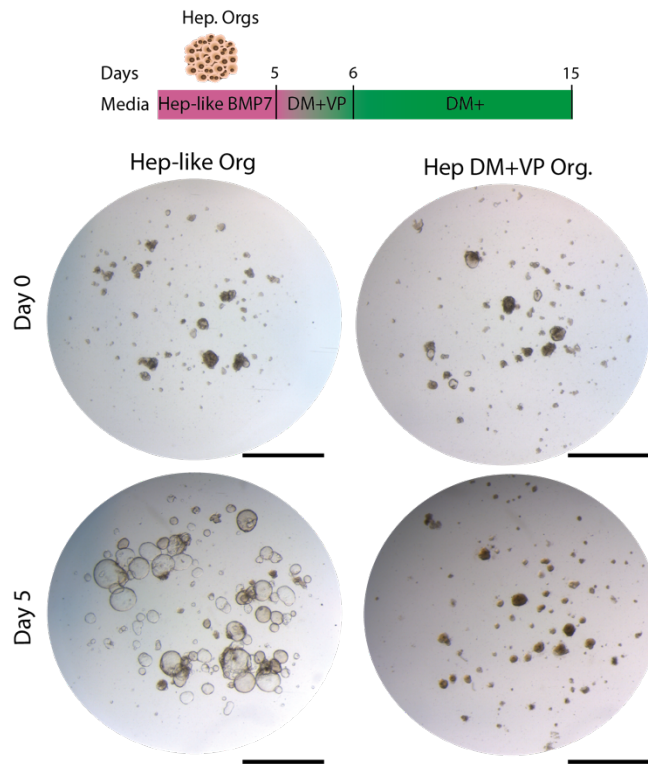
Our lab has undergone efforts to enhance the effectiveness of the establishing Hep Orgs from hepatocytes isolated from human liver tissue resections, and henceforth called Hep-like Orgs. Similar to the Hu Orgs, the Hep-like Orgs seem to acquire a cholangiocyte phenotype with time in culture (Figure 3.18A). Based on the observations of Figure 3.17 and from the Hu *et al.*, (2018) study, the ability of Hep Orgs to clonally expand from a single hepatocyte suggest a cell fate transition from a differentiated state to a progenitor state. This could impact hepatocyte maturation in favour of ductal and progenitor expansion.

To enhance hepatocyte maturation, I treated the Hep-like Orgs with DM+VP (Hep DM+VP Orgs) (Figure 3.19A-B). Briefly, Hep-like Orgs were grown for 5 days in BMP-7 and treated with DM+VP for 24h following dissociation on day 5. On day 6, the media was switched to DM+ and refreshed in DM+ for a total of 10 days (Figure 3.19A). 5 days post-treatment in DM+VP, the Hep-like Orgs exhibited a similar morphology, characteristics of hepatocytes, as the Chol. Orgs grown in DM+VP Orgs (Figure 3.19A-B). On the contrary, the untreated Hep-like Orgs acquired a characteristic ductal phenotype (Figure 3.19A-B Hep-like Org_1).

While Hep Orgs are less heterogeneous, without increased expression of ductal markers, their maturation however into hepatocyte fate is still impaired when compared to Chol. Orgs grown in DM+VP. This suggest that further research is required to identify additional factors to improve the Hep Orgs culture condition.

Overall, our results show that the newly developed media for differentiation, DM+VP, enhances the differentiation of human liver organoids into a hepatocyte-fate, supporting their use for DILI studies. I will assess the effectiveness of Chol. Orgs grown in DM+VP Orgs for DILI in the next chapter.

A



B

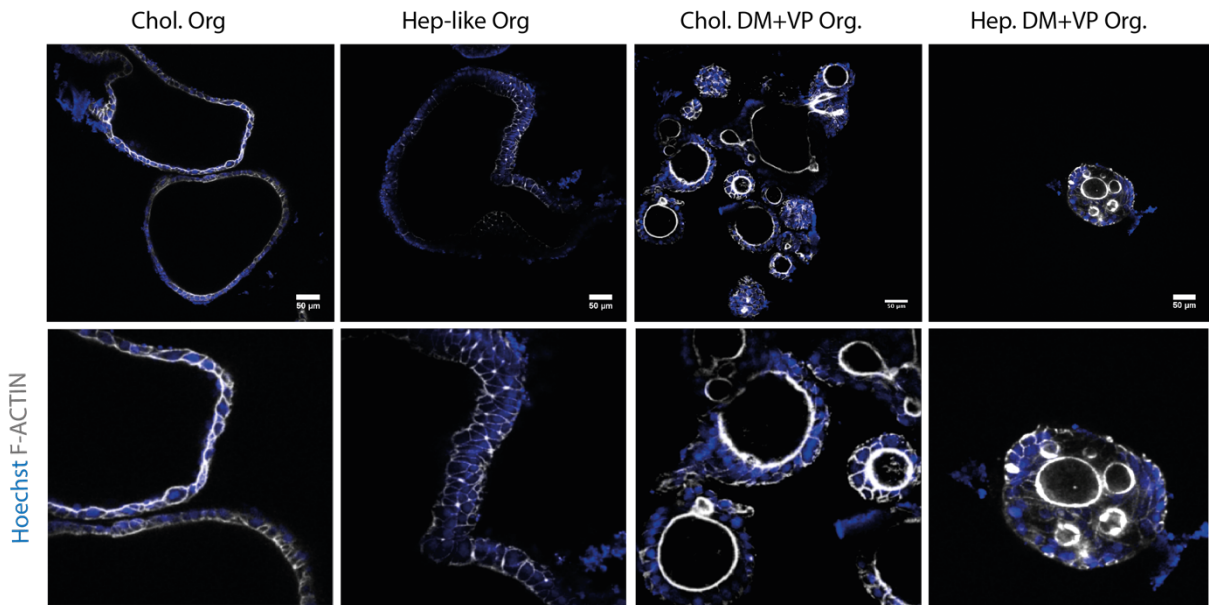
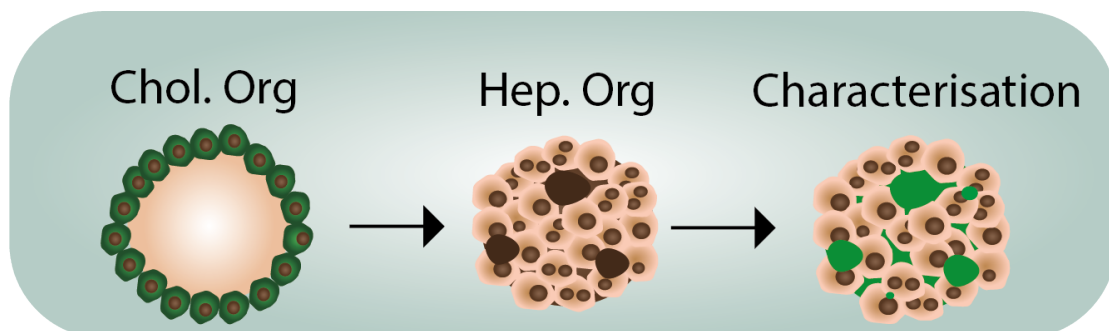


Figure 3.19 Differentiation of Hep-like Orgs following DM+VP treatment. A) Hep-like Orgs were grown for 5 days in BMP-7 and treated with DM+VP for 24h following dissociation on day 6. At day 7, media was switched for DM+ and refreshed for a total of 10 days. Hep-like Orgs treated with DM+VP maintained a differentiated morphology, whilst Hep-like Orgs acquired a ductal morphology over 5 days. Day 0= treatment with DM+VP, day 5= 5 days post-treatment. Scale bar: 2mm. **B)** Immunostaining analysis of F-actin filaments (grey) in Chol. Orgs, Hep-like Orgs and cholangiocyte and Hep-like derived DM+VP Orgs. Upon differentiation in DM+VP, both systems derived either from cholangiocytes or hepatocytes presented similar morphology, with circular actin structures. Scale bar: 50 μ m.

Chapter 4

Results II:

Validating human liver organoids for
DILI studies



4.1 Human differentiated liver organoids can be maintained in culture for two weeks.

To validate a hepatic system for drug toxicity studies, one important parameter to evaluate is the viability of the cells in time. In fact, drug testing must be performed during the timeframe in which cells are viable to distinguish the drug induced toxic responses over biological cell responses to culture conditions. With this aim, I assessed the long term viability of DM+VP Orgs in culture generated from the differentiation of Chol Orgs.

Cellular membrane integrity was assessed via the use of viable and cytotoxic markers, a membrane permeable dye namely Calcein (green) and a membrane impermeable dye namely Ethidium Homodimer III (red) (Figure 4.1A). A decline in organoid viability was observed at day 18 marked with a reduction of Calcein+ cells (Figure 4.1A-B). The results obtained coincide with the number of metabolically active cells in proportion to ATP formation (Figure 4.1C). Indeed, ATP levels drop at day 18, further strengthening the results from the observation that DM+VP Orgs are viable for almost two weeks in culture (Figure 4.1C).

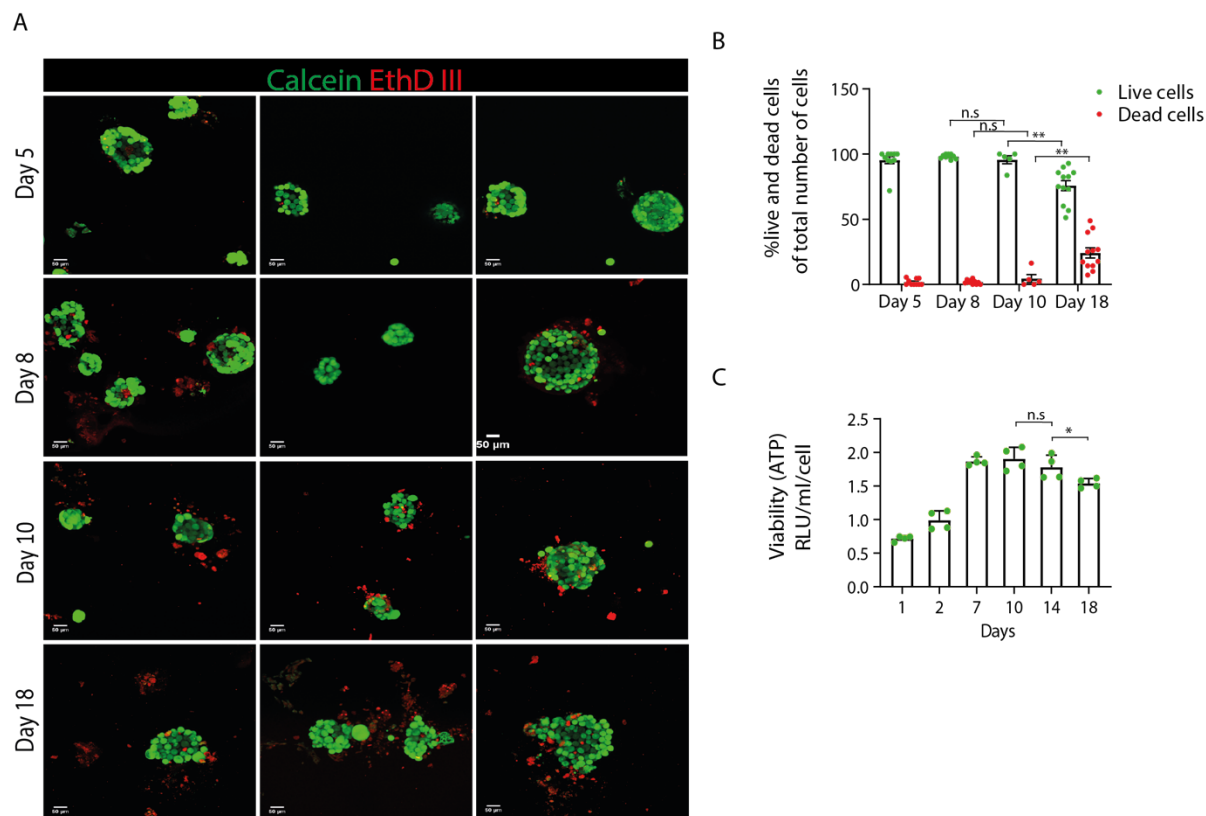


Figure 4.1 DM+VP Orgs are viable for two weeks. A) Live and death staining of DM+VP Orgs. Calcein (green) marks viable cells and Ethidium Homodimer III (red) marks dead cells. Gradual increase of dead cells over time from day 5 to day 18. Scale bar: 50 μ m. **B)** Quantification of live and dead cells normalised to the total number of cells. Each dot represents one organoid. Error bars denote \pm SEM. $P < 0.01$ (**), $P < 0.05$ (*). **C)** ATP quantification of metabolic active cells in DM+VP Orgs normalised to the total number of cells. $N=2$, error bars denote \pm SEM. At day 18 post-differentiation a significant drop in cell viability is observed.

Given the progenitor nature of Chol. Orgs, it has been shown that this system can be maintained in culture for up to 1 year (Huch et al., 2013, 2015) via repeated cycles of organoid dissociation and maintenance. Therefore, I was interested to test the possibility to maintain DM+VP Orgs beyond the two weeks viability via repeated steps of organoid dissociation. However, (in Figure 4.2), I have observed that upon dissociation, DM+VP Orgs can only be maintained for approximately 5 days. This suggests the need of repeated cycles of differentiation from Chol. Orgs to obtain hepatocyte organoids for drug testing. The data raise the requirement to identify culture conditions that could aid in the maintenance of differentiated organoid over time without affecting cell identity.

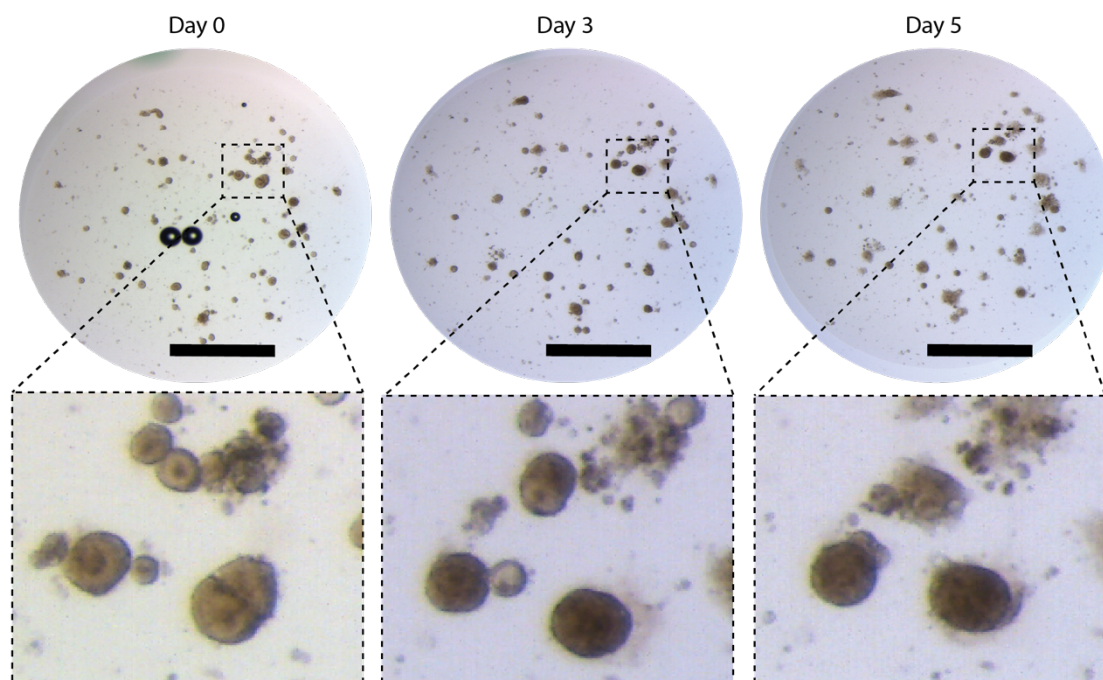


Figure 4.2 **Post-differentiated DM+VP Orgs cannot be maintained overtime in culture.** Brightfield images of post-dissociated day 15 DM+VP Orgs in time. Organoid viability persists for approximately 5 days. Scale bar: 2 mm.

Based on the data in [Figure 4.1C](#), stable levels of ATP are observed from day 7, suggesting that the analysis of drug toxicity could be performed from this point onwards. Since the differentiation process from Chol. Orgs to hepatocyte organoids has a duration of 10-11 days, I have selected day 10 and day 12 as the two timepoints for drug dosing for a total of 4 days incubation.

4.2 Functional uptake of drugs inside the organoid system

Organoids are complex multicellular biological systems embedded in artificial extracellular matrix, and as such this could result in an impediment for drug intracellular uptake and distribution. To address this aspect in collaboration with GlaxoSmithKline and the National Physical laboratory in London, we used the mass spectrometry imaging technology. Specifically, we used the time-of-flight Mass spectrometer imaging system

(TOF-SIMS). This technology allows the chemical mapping of a compound inside a biological tissue. Amiodarone, an anti-arrhythmic drug well-known to be a human hepatotoxin, has been selected to test the uptake efficiency inside the organoid structure.

With this aim, amiodarone was incubated in both Chol. Orgs and DM+VP Orgs at a concentration of 1 μ M for 24h and processed for mass spec imaging (as described in the Methods section). The result showed amiodarone detection only outside the organoid. (Figure 4.3). Two possible explanations could be drawn from the above observation: a lack of specific membrane uptake transporters in the organoid or the amiodarone signal detected outside the organoid might outweigh the signal detected inside the system.

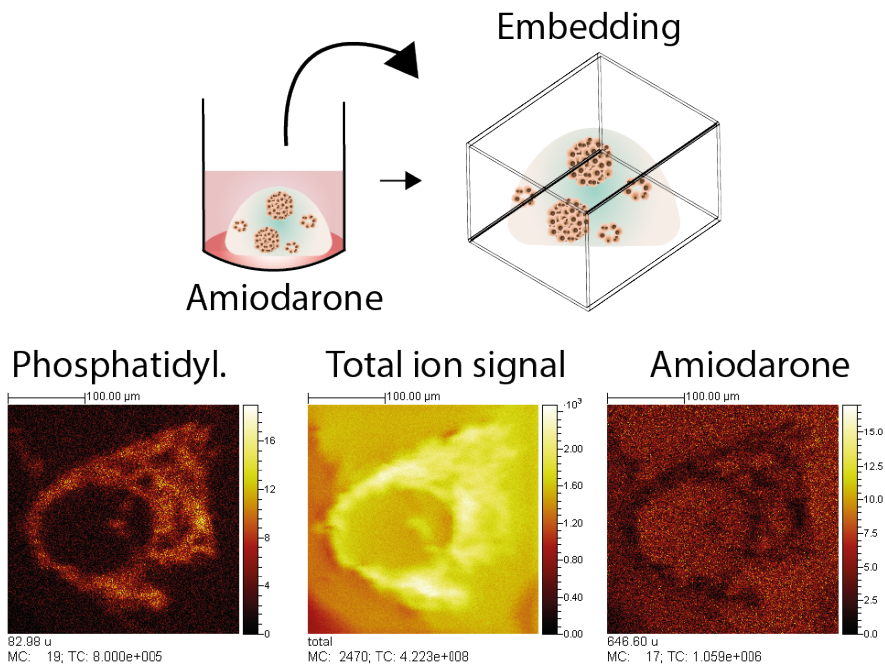


Figure 4.3 **Amiodarone is not detected inside the organoids.** Representative images of treated organoids embedded in ECM and processed for Mass spec imaging. Mass to charge ratio signal of phosphatidylcholine (to mark the cell membrane) and amiodarone. Amiodarone is detected outside the organoid.

To test the latter, I adopted a new experimental approach as described In the Methods section. Complete removal of the ECM prior to mass spec imaging in both treated and untreated samples, resulted in amiodarone detection inside the organoid while no detection was observed in the untreated sample (Figure 4.4). This supports the hypothesis that the signal from the ECM masked the signal within organoid.

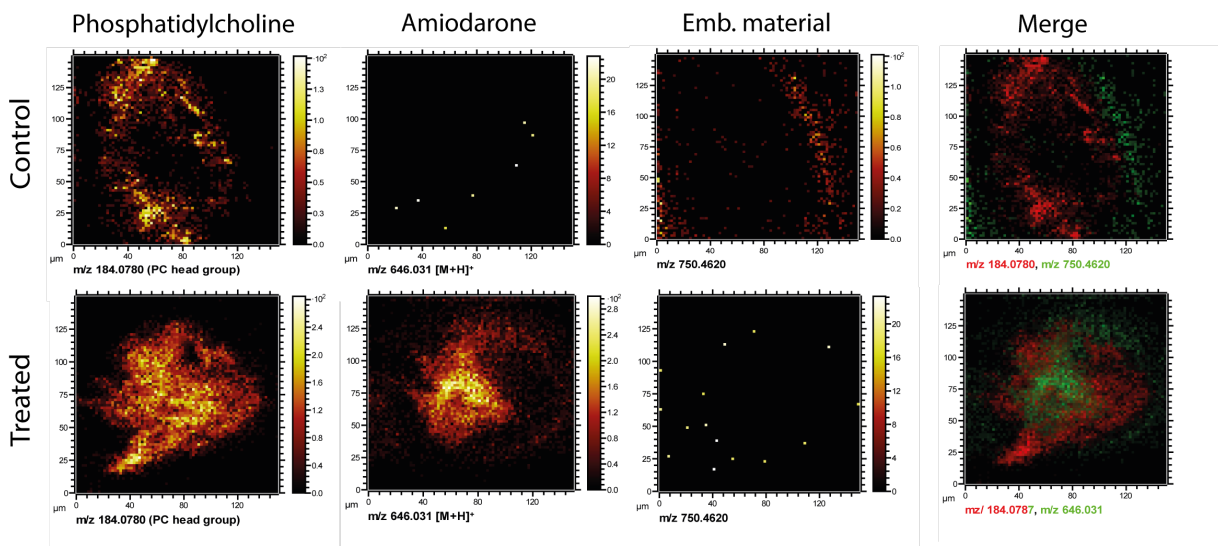
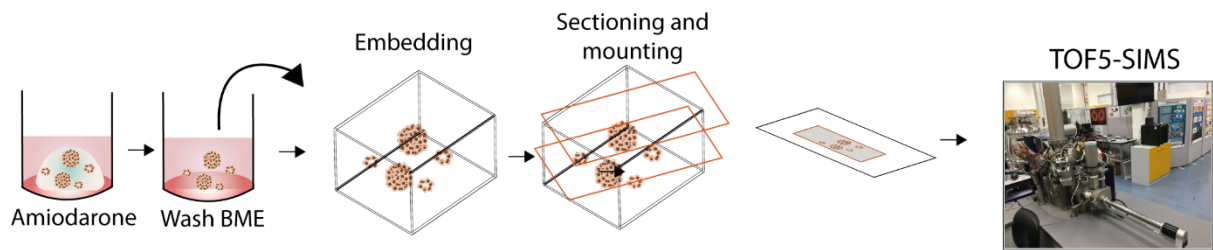


Figure 4.4 Removal of ECM prior to mass spec imaging enables the detection of amiodarone particles inside the organoid. Representative images of mass to charge ratio intensities for cell membrane (phosphatidylcholine), amiodarone and embedding material for treated and untreated samples. Amiodarone (merge – green) is detected inside the organoid whilst in the control it is detected outside.

Interestingly, a depth profiling analysis also showed that the localisation of the drug highly correlated with the outer layer of the organoid, suggesting that the metabolic active cells might be predominantly localised externally and not internally (Figure 4.5), which could be dependent on the degree of exposure to culture conditions. Taken together the data indicates that the liver organoids are able to uptake exogenous compound.

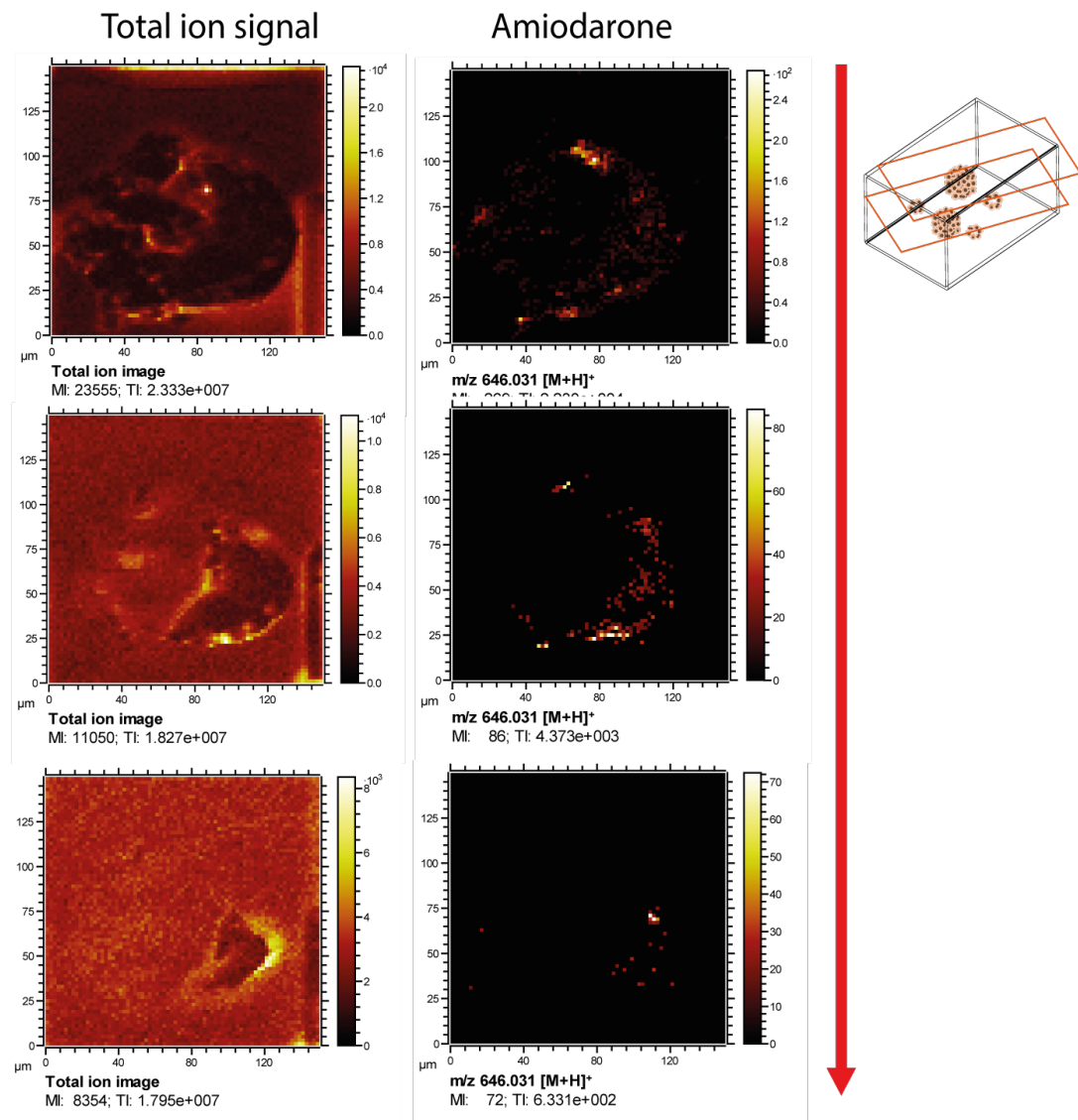


Figure 4.5 Amiodarone is predominantly detected in the outer layer of organoids. Depth profiling mass spec images of treated organoids with amiodarone. Red arrow indicates the progression of amiodarone localisation from the outer later to the inner layer of the organoid. Amiodarone is predominantly detected in the outer layer.

4.3 Human differentiated liver organoids present functional hepatic secretory system

Another important key biological parameter to validate the DM+VP Orgs as a model for drug testing is the assessment of the hepatocyte secretory system. The route of drug metabolism within a hepatocyte follows the axis of uptake, metabolism and clearance (See introduction). Failure of this process will result in intracellular metabolite accumulation which leads to hepatocyte damage. I have first assessed the expression of the BSEP transporter, one of the main apical membrane transporters involved in bile and metabolite secretion from the hepatocyte to the bile canaliculi. Immunostaining analysis in human liver tissue exhibited BSEP expression both in the cytoplasm and on the membrane ([Figure 4.6](#)).

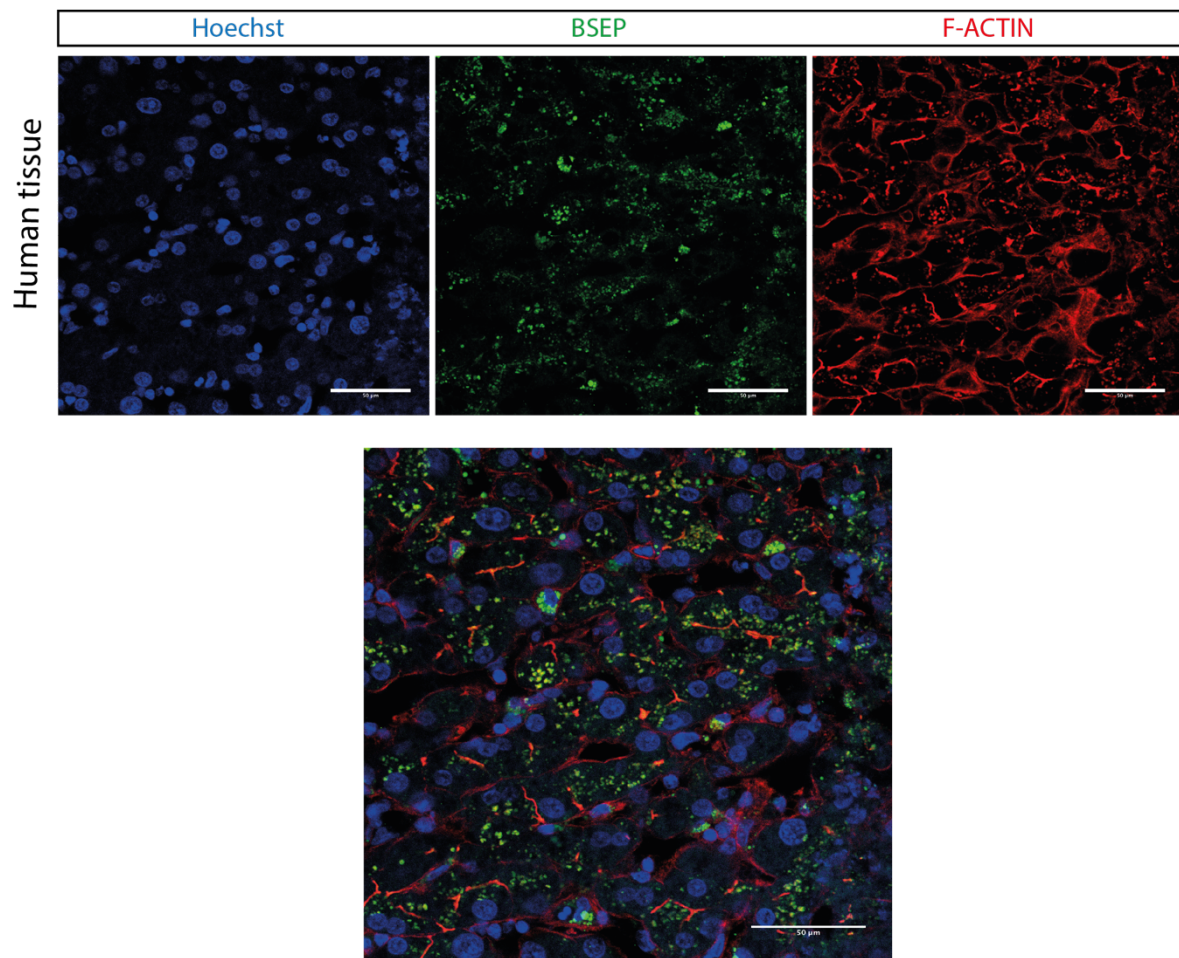


Figure 4.6 **Validation of BSEP expression in human liver tissue.** Immunostaining analysis showed BSEP (green) expression in human liver tissue. Scale bar: 50 µm.

Similar pattern of BSEP expression was observed *in vitro* in the DM+VP Orgs (Figure 4.7). However, compared to the human tissue, I have also noted BSEP localisation on a different pattern of actin filaments which resemble circular structures (Figure 4.7).

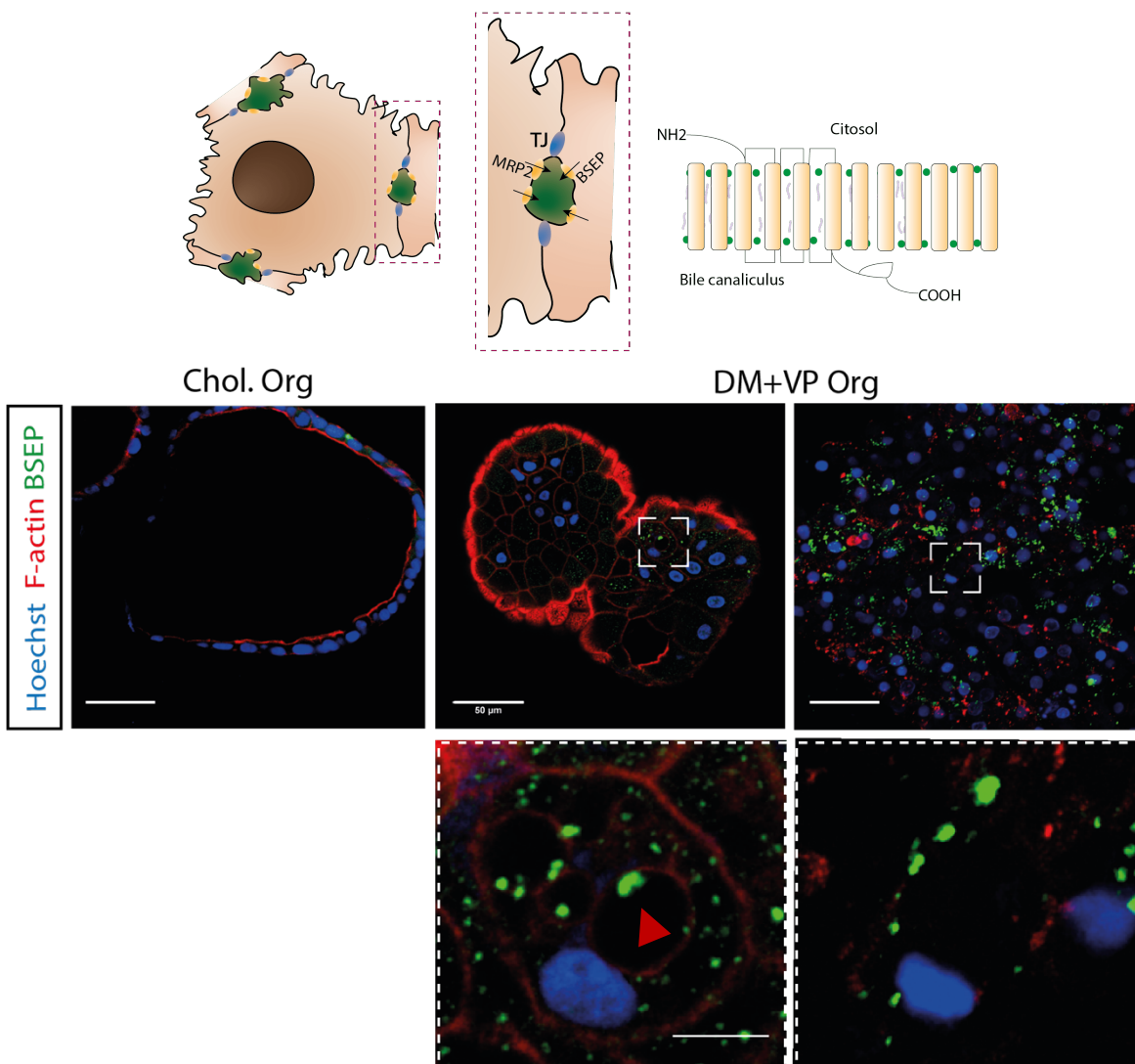


Figure 4.7 **BSEP is expressed in DM+VP Orgs.** Immunostaining of BSEP (green) and F-actin (red) in Chol. Org and DM+VP Org. No BSEP expression is detected in Chol. Orgs. Red arrow points to BSEP expression located on the circular actin filament structures. Scale bar: 50 μm .

Next, I have analysed the expression of tight junctions marked by the protein Zonula occludens-1 (ZO-1). Tight junctions are key structural components needed to maintain the formation of the bile canaliculus between two adjacent hepatocytes (see Introduction). I have observed ZO-1 expression within the F-actin circular structures and between cells (Figure 4.8) which denotes the formation of tight junctions between

neighbouring cells but also the indication that the circular actin morphology might have a biological function.

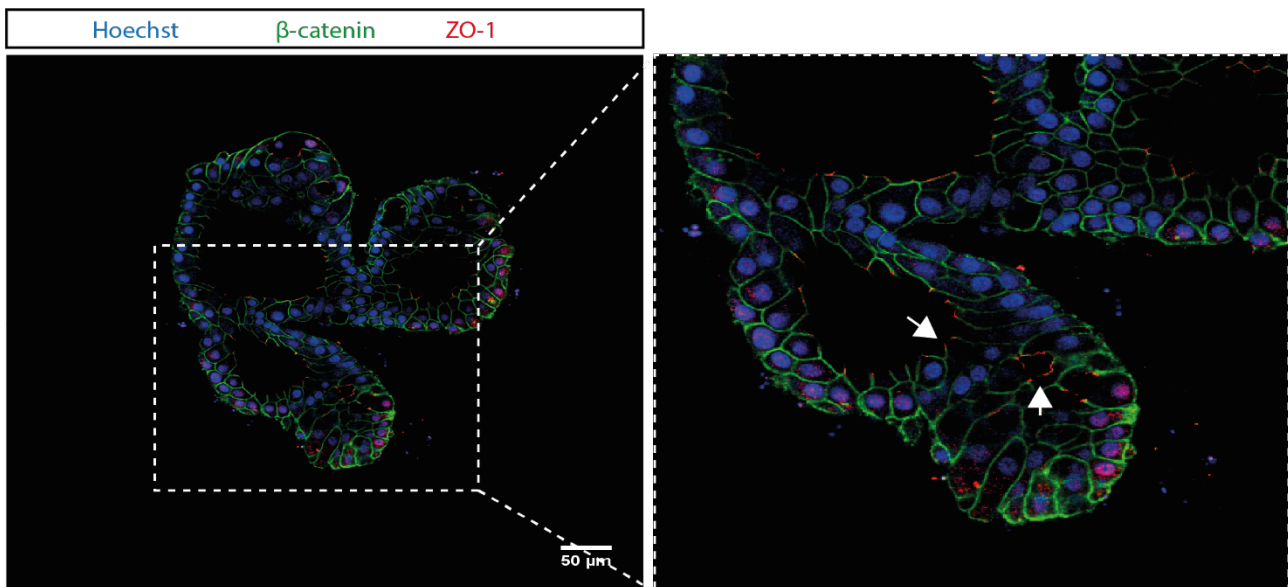


Figure 4.8 **ZO-1 and β-Catenin expression in DM+VP Orgs.** ZO-1(white arrow) is expressed between neighbouring cells and within the hollow structures. Scale bar: 50μm.

To further our understanding on the polarisation of our organoids, analysis performed with the TEM showed the formation of canalicular like structures between neighbouring cells in both DM+ and DM+VP Orgs (Figure 4.9). As expected, this was not observed in Chol. Orgs grown in EM. Of note, well rounded nuclear shape of DM+VP Orgs further demonstrated the change in cell fate from ductal cells to hepatocytes (Figure 4.9).

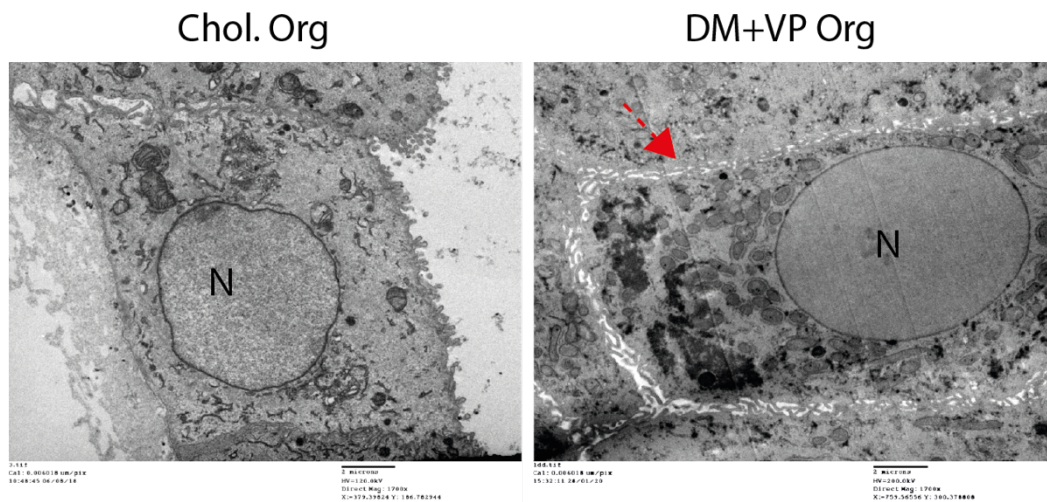


Figure 4.9 **DM+VP Orgs present formation of bile canalicular like structures.** Transmission electron microscopy images of Chol. Org and DM+VP Org. Red arrow shows canalicular like structure in DM+VP Org. Abbreviations: N=nucleus. Scale bar 2 μ m.

To further confirm the presence of bile canaliculi in DM+VP Orgs, I have targeted one of the apical proteins expressed in the bile canalicular compartment, DPPIV. *In vivo*, immunostaining analysis of DPPIV in human liver tissue showed expression of DPPIV with BSEP colocalization between neighbouring cells (Figure 4.10).

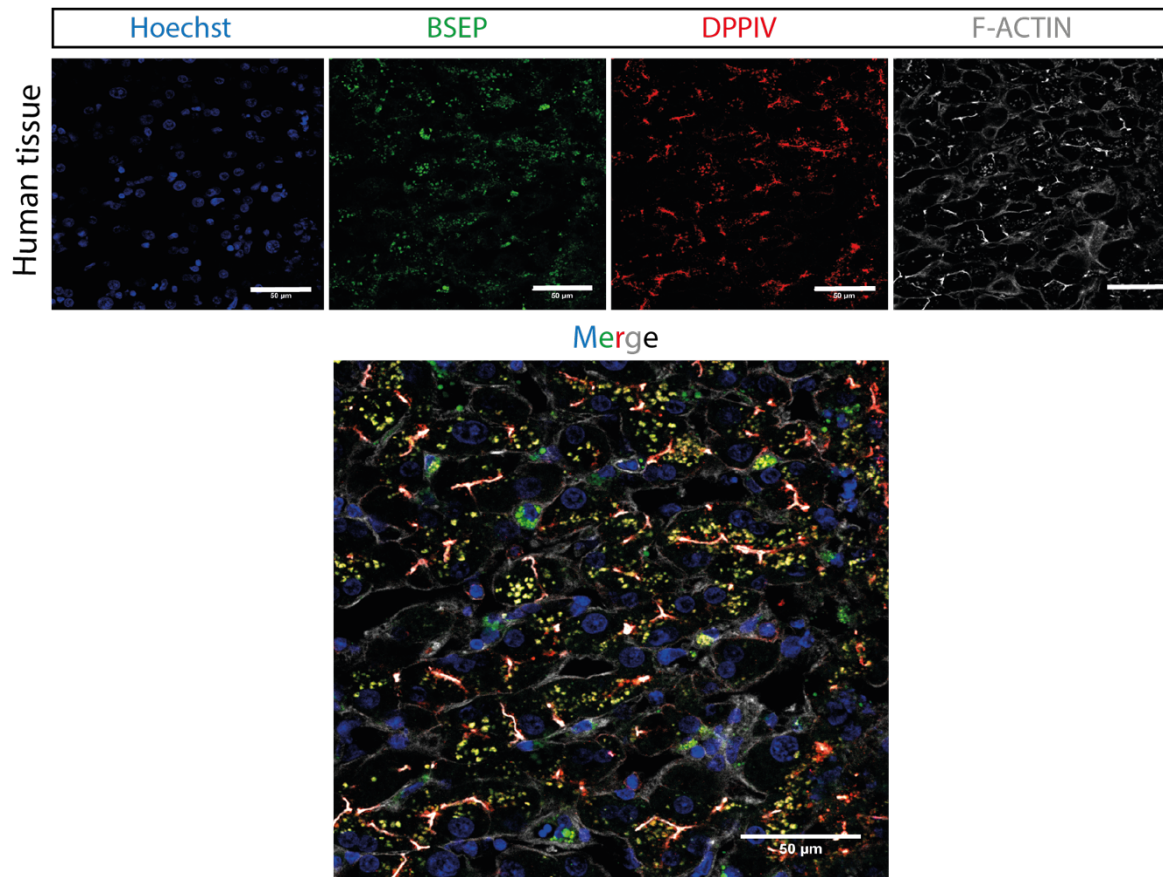


Figure 4.10 **DPPIV expression in human liver tissue.** DPPIV (yellow) and BSEP (green) are colocalised at the apical membrane of hepatocytes. Scale bar: 50 µm.

In vitro, analysis of DPPIV on DM+VP Orgs showed expression of the bile canalicular marker between neighbouring cells and within the hollow structures (Figure 4.11), but to a reduced extent compared to the *in vivo* human liver (Figure 4.10). The expression of DPPIV instead was not observed in DM Orgs (Figure 4.11), further outlining the difference between these two models.

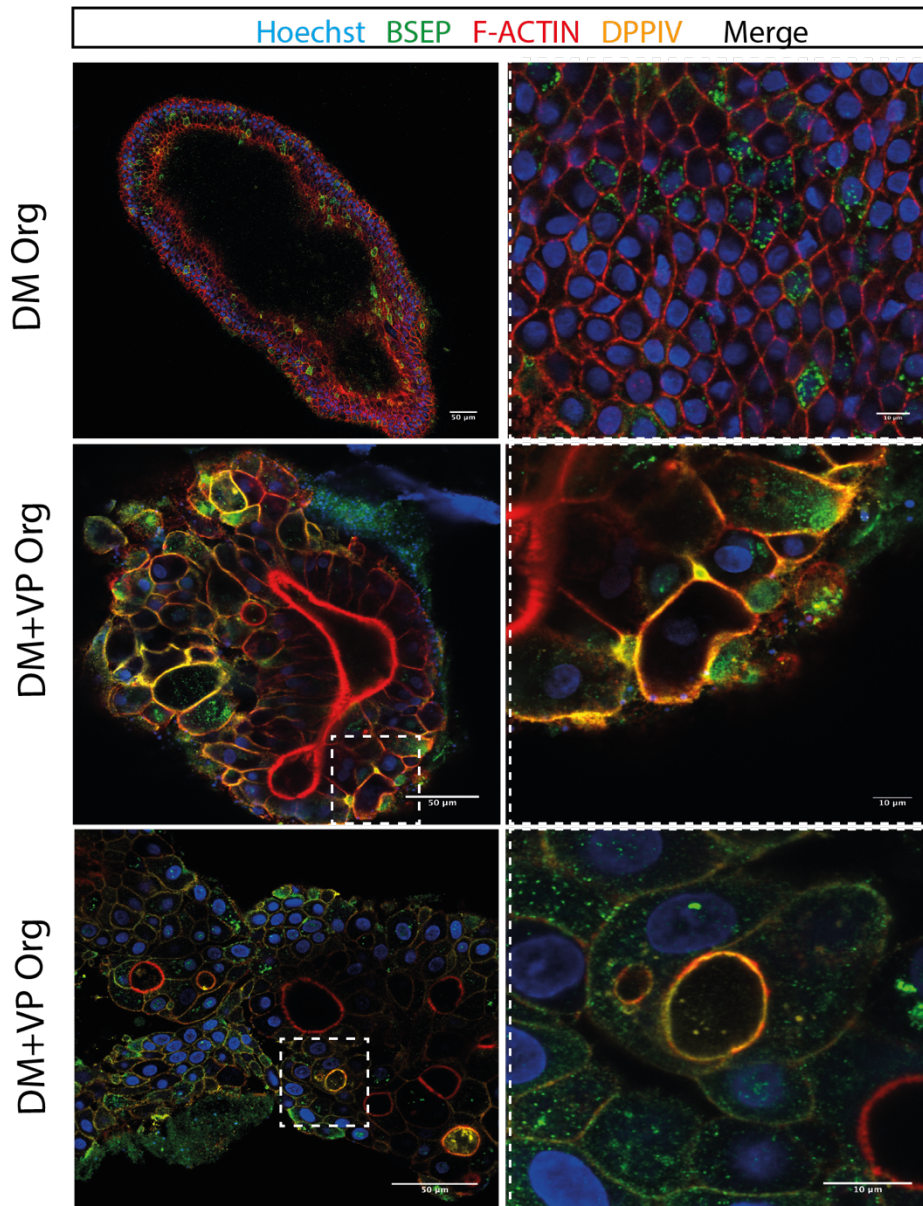


Figure 4.11 **DPPIV is expressed in DM+VP Orgs.** Immunostaining analysis of DPPIV in DM Orgs and DM+VP Orgs. DPPIV (yellow) is expressed between neighbouring cells and across the circular actin structures (red). BSEP (green) colocalise with DPPIV and F-actin. DM Orgs do not express DPPIV. Scale bar: 50 μm .

Overall, DM+VP Orgs displayed features of hepatocyte secretory system at the structural level marked by bile canalicular and apical membrane transporters expression. Next, I have assessed the functionality of this system. The most widely used screening

model to study drug-BSEP interaction is the kinetics of bile acid transport from the hepatocyte to the bile canaliculus.

For this purpose, I have used a substrate of BSEP called CMFDA which is cleared out from the hepatocyte via BSEP activity. This particular assay is widely used to assess the functionality of BSEP as a membrane transporter. Interestingly, the compound nicely showed accumulation between cells, hence suggesting that the hepatic secretory system in our organoid model is functional (Figure 4.12).

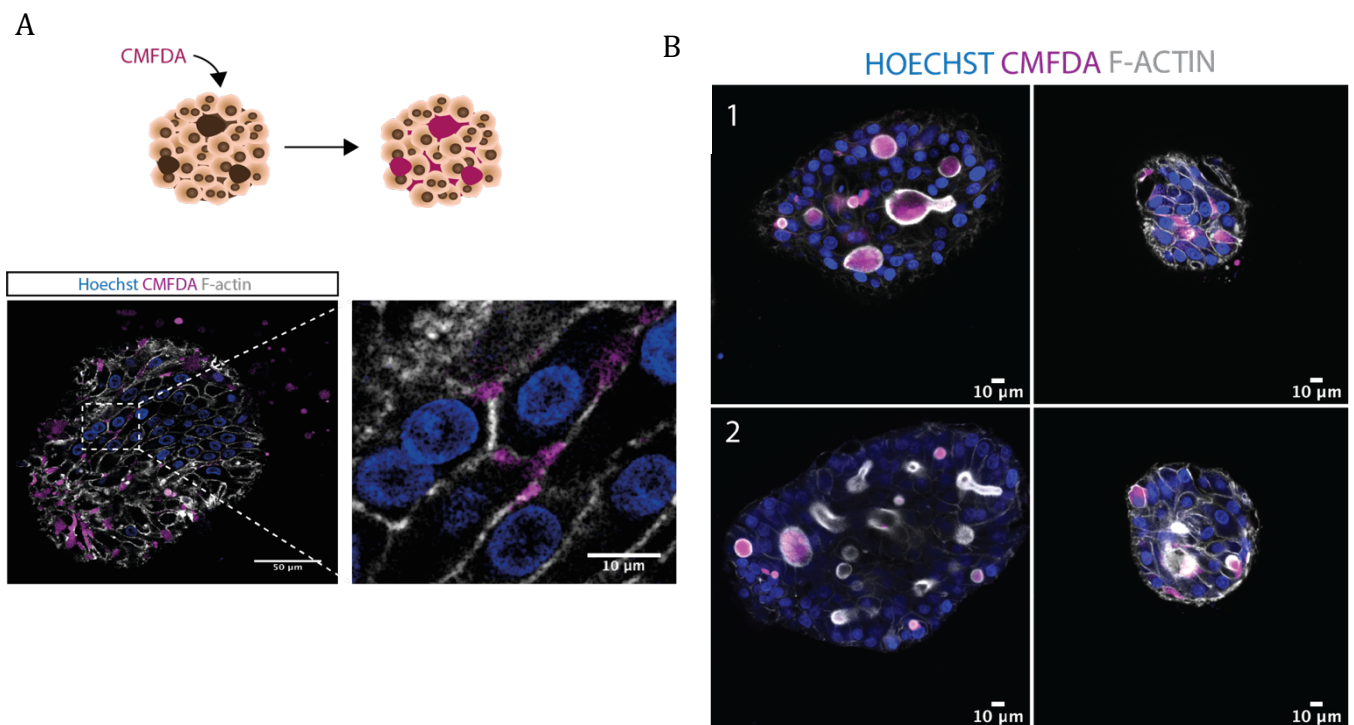


Figure 4.12 **Active secretion of CMFDA into the bile canaliculi.** **A)** Experimental scheme of CMFDA live staining. Live staining of CMFDA (purple) shows secretion of the fluorescent bile inside the bile canaliculi. Scale bar: 50 µm. Scale bar zoom: 10 µm. **B)** two different organoids at different planes in z: mid plane (1) and top plane (2) showing CMFDA clearance.

In addition, to further emphasise the efficiency of YAP inhibition and WNT signalling pathway modulation to enhance hepatocyte functionality, I have performed the CMFDA transport assay on them compared to the DM Orgs and 2D cells. In DM+VP Orgs, CMFDA is accumulated inside the bile canaliculi, whilst this is partially not the case for DM Orgs (Figure 4.13). Indeed, as already pointed out in the previous chapters, DM Orgs cultures presented an heterogenous population of organoids with the majority exhibiting a ductal phenotype and very few undergoing the differentiation process into hepatocyte organoids. This observation is further strengthened in Figure 4.13, with some organoids successfully recapitulating a functional hepatocyte secretory system and others failing (Figure 4.13). This supports the inefficiency of the DM to promote a homogenous differentiation of Chol. Orgs into a hepatocyte fate. However, when compared to a human cancer cell line as HepG2, DM orgs are better in recapitulating a functional polarisation (Figure 4.13).

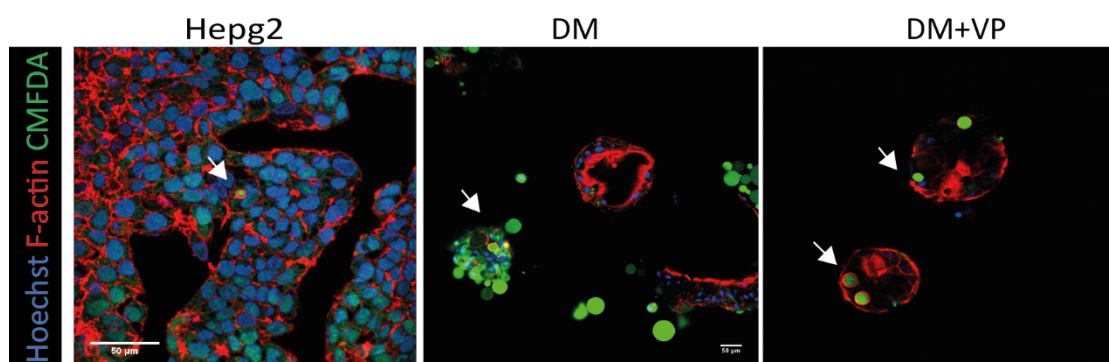


Figure 4.13 **Higher efficiency of DM+VP Orgs secretory system compared to HepG2 cells and DM Orgs.** Live staining of CMFDA (green) in HepG2 cells, DM Orgs and DM+VP Orgs. Low CMFDA secretion in HepG2 cells is observed while the DM Orgs presented an heterogenous pool of functional organoids with some presenting CMFDA secretion inside the bile canaliculi. While all the DM+VP Orgs exhibited a homogenous secretion of CMFDA. White arrows indicate CMFDA accumulation. Scale bar: 50 μ m.

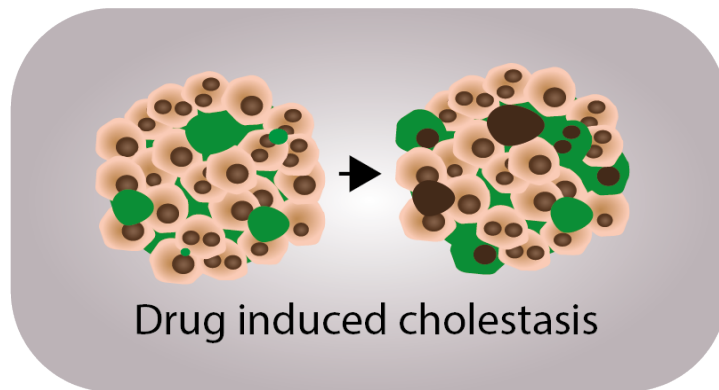
Overall, the data indicate the partial recapitulation *in vitro* of the structural and functional features of the *in vivo* hepatocyte secretory system. Therefore, this opens up

avenues to use the DM+VP Orgs as hepatic systems for the screening of hepatotoxins that specifically target the hepatocyte apical clearance activity.

Chapter 5

Results III:

Toxicology



5.1 Organoids recapitulate drug induced cholestasis *in vitro*

Drug induced cholestasis (DIC) is marked by the excessive intracellular accumulation of bile and metabolites which leads to hepatocellular damage. Very often DIC is the result of an impairment in BSEP activity due the inhibitory action of certain drugs, including CsA and Bosentan (Dragovic et al., 2016). For the purpose of this Thesis, CsA has been selected as a DIC candidate as its effects in the liver have been widely documented *in vivo* and *in vitro* (Román et al., 2003; Dragovic et al., 2016). Having evaluated the expression of BSEP and its functional activity in DM+VP Orgs, I have tested the ability of the organoid system to detect CsA induced cholestatic phenotypes. With this aim, CsA titration was performed in single cells of dissociated Chol. Orgs (Figure 5.1) to identify the toxic concentration at which CsA did not induce cell death. After 8 days, Chol. Orgs treated with CsA 100 nM and 1 μ M exhibited a lower organoid growth compared to the untreated sample (Figure 5.1). Whilst at concentration above 1 μ M, organoid degradation occurred (Figure 5.1).

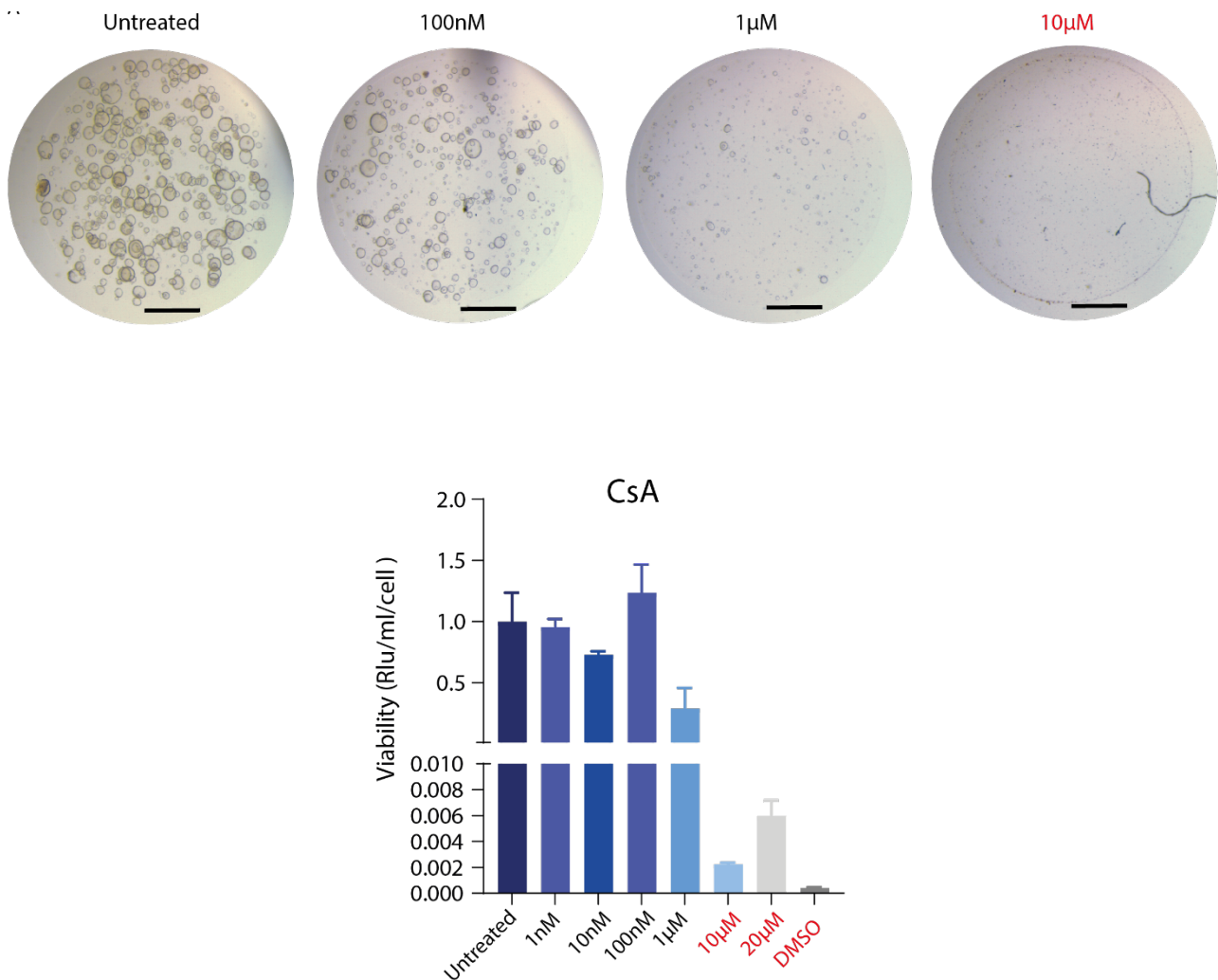


Figure 5.1 **Chol. Orgs treated with CsA exhibit cell death above 1µM.** Brightfield images and ATP measurement of single cells derived Chol. Orgs treated with a gradient of CsA: 1 nM, 10 nM, 100 nM, 1 µM, 10 µM, 20 µM. 20% DMSO was used as dead control. Above 1 µM cell death occurred. Scale bar: 2 mm.

Based on the above data, DM+VP Orgs were exposed to 100 nM and 1 uM CsA for 4 days (Figure 5.2). Specifically, a total of 4 days incubation regimen was chosen after the identification of DM+VP Orgs viability (Figure 4.1). Exposure to CsA resulted in the cytoplasmic accumulation of CMFDA compared to the control (untreated) (Figure 5.2). No significant difference was detected between 100 nM and 1 uM CsA treated DM+VP Orgs (Figure 5.2).

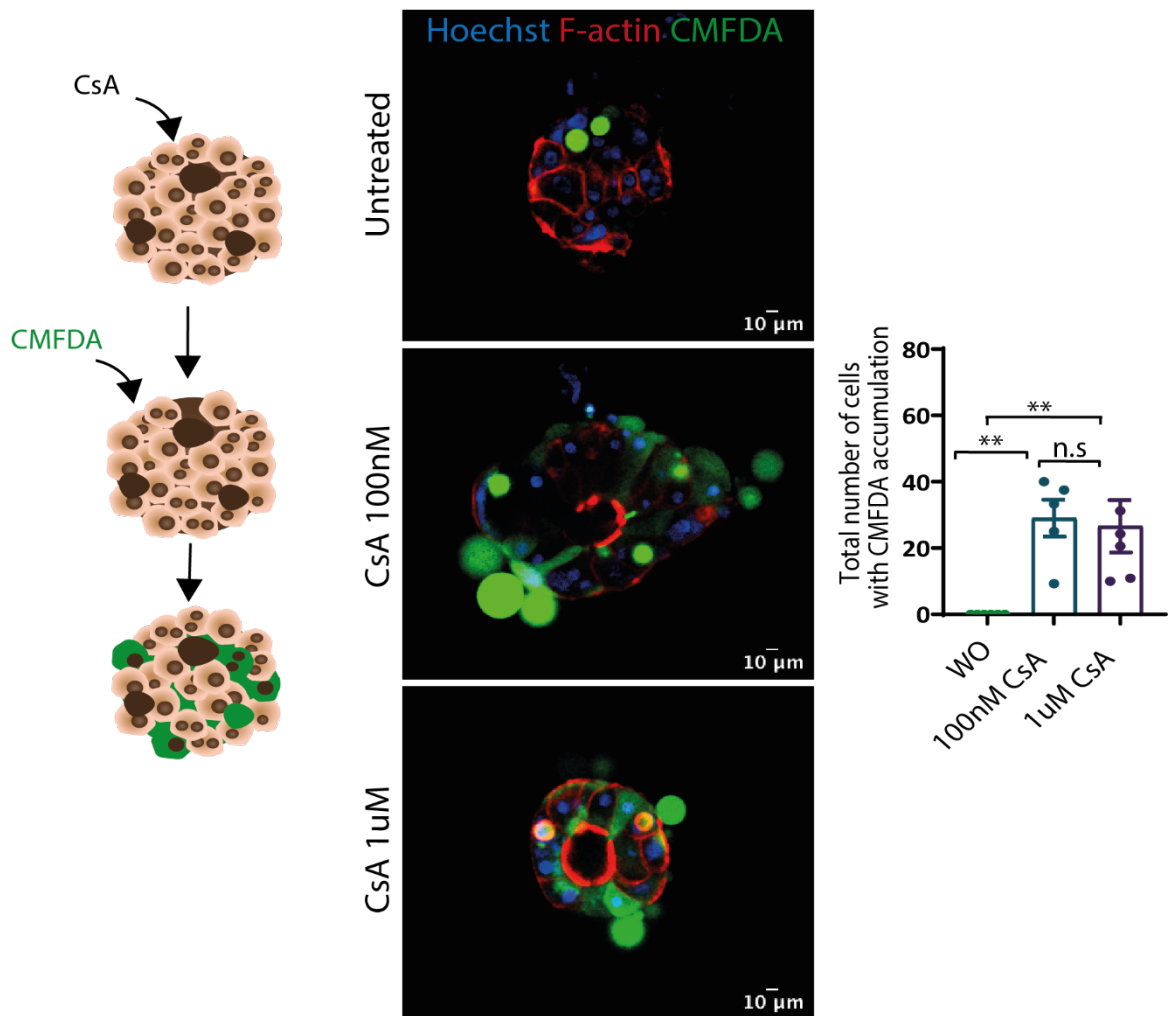
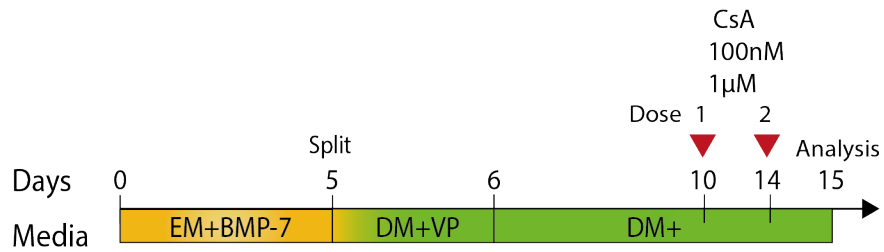


Figure 5.2 **CMFDA intracellular accumulation in DM+VP Orgs following CsA treatment.** CsA was dosed for two times on DM+VP Orgs on day 10 and day 14 for a total of 4 days. CMFDA (green) intracellular accumulation is observed in treated organoids compared to the control (WO). No statistical significance was observed between 100 nM and 1 µM treated DM+VP Orgs, N=2, P < 0.01 (**). Scale bar: 10 µm.

Additionally, intracellular accumulation of CMFDA coincided with a decrease in total bile secretion in the medium (Figure 5.3A); further confirming the impairment of hepatocyte secretory system upon CsA incubation.

CsA induced cholestasis has been further associated to be a potent competent inhibitor of BSEP activity (Dragovic et al., 2016). Consistently, CsA induced a downregulation of *ABCB11* (Figure 5.3B), but also at the protein level with lower expression of the encoding protein BSEP (Figure 5.3C). Interestingly, another apical membrane transporter *ABCC2* expression was downregulated following CsA treatment (Figure 5.3B).

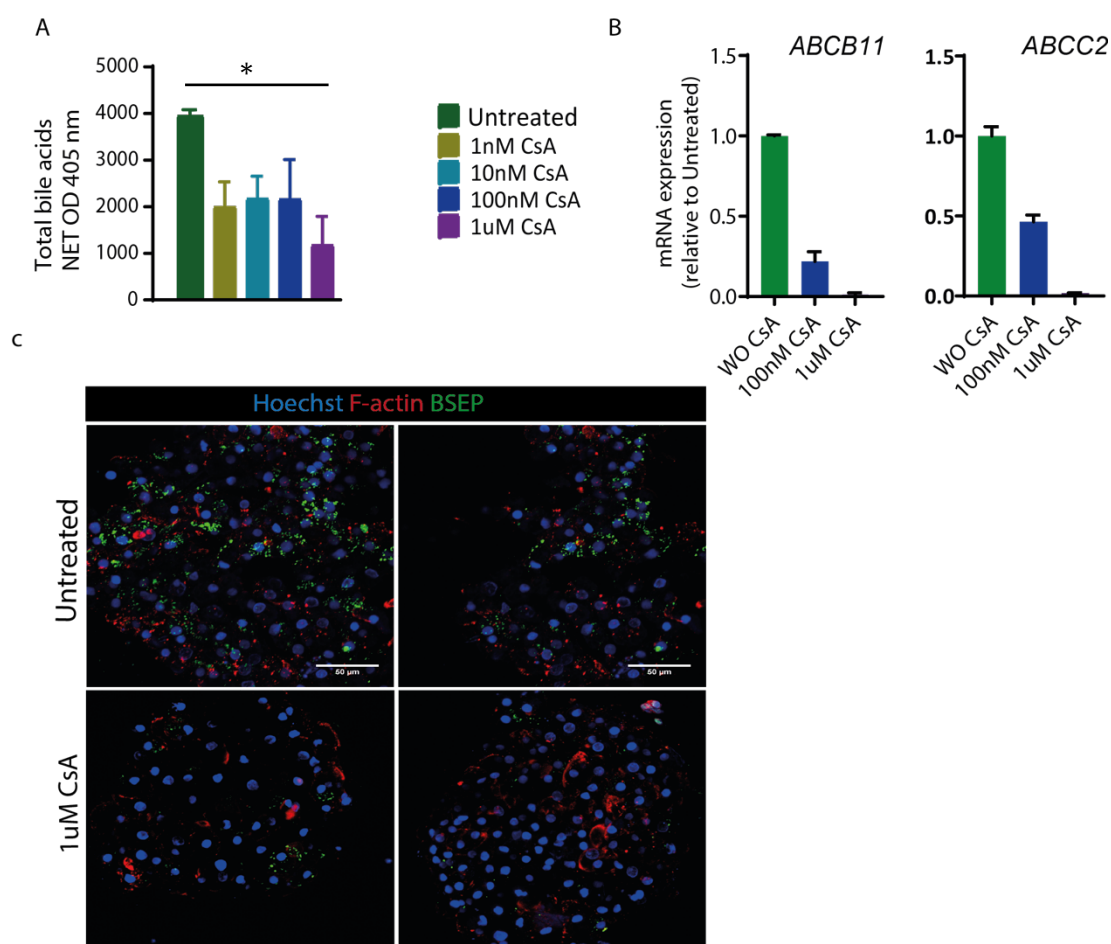
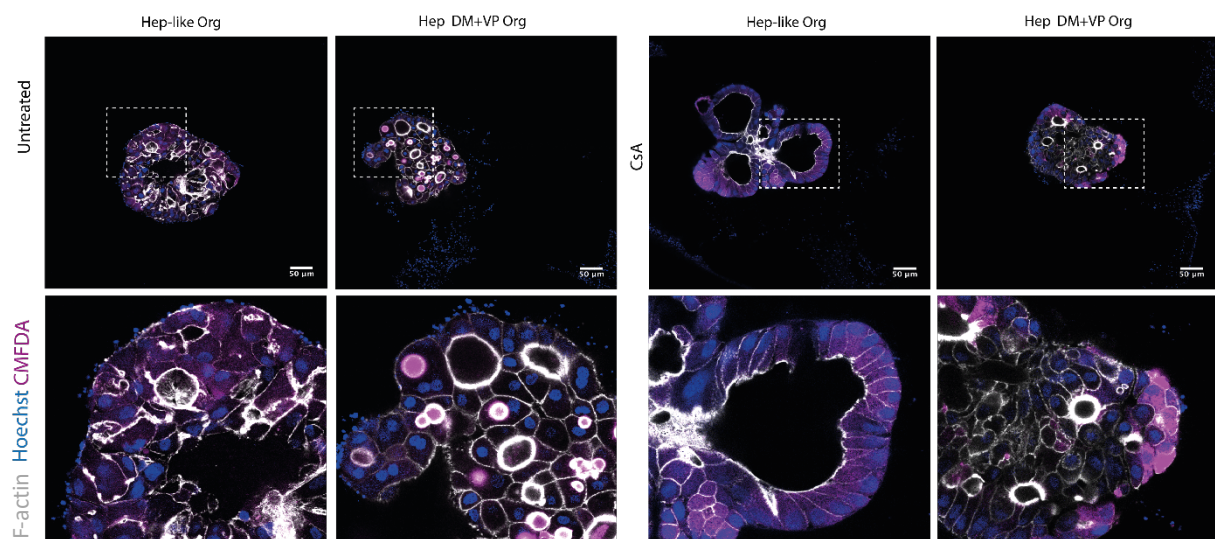


Figure 5.3 CsA treated DM+VP Orgs exhibited lower hepatocyte secretory activity. **A)** Total bile acids quantification in the medium in DM+VP Orgs showed lower bile secretion at CsA toxic concentration. Total bile acids values normalised to the total number of cells. N=2 Mann–Whitney non-parametric test $P < 0.05$ between untreated and $1\mu\text{M}$ CsA. **B)** qPCR analysis of treated DM+VP Orgs showed downregulation of *ABCB11* and *ABC22*, two apical membrane transporters. mRNA expression was normalised to the housekeeping gene *HPRT* and are represented as fold change relative to untreated. N=2, error bars denote \pm SEM. **C)** Immunostaining analysis of BSEP (green) showed downregulation of the protein following treatment with CsA. N=1. Scale bar: $50\ \mu\text{m}$.

As a proof of concept, features of CsA induced cholestasis were also observed in hepatocyte organoids derived from isolated hepatocytes (Hep DM+VP Orgs) (Figure 5.4). Interestingly, untreated Hep-like Orgs exhibited a cholestatic pattern, hence suggesting the immaturity of the hepatocyte-like cells comprised in this model. Conversely, Hep DM+VP Orgs showed accumulation of CMFDA inside the bile canalicular compartment when untreated (Figure 5.4). Following CsA treatment, Hep-like Orgs presented intracellular accumulation of CMFDA, although this observation could be the result of a pre-existing cholestatic condition in the Hep-like Orgs as shown in the untreated sample. On the other hand, treated Hep DM+VP Orgs displayed features of cholestasis (Figure 5.4) like the cholangiocyte-derived DM+VP Orgs (Figure 5.2). The results, further strengthens the role of targeting WNT and YAP inhibition in promoting functional hepatocyte fate specification.

Figure 5.4 Differentiated Hep-like Orgs presented featured of CsA induced cholestasis. Live staining of CMFDA (purple) in Hep-like Orgs and differentiated Hep-like Org (Hep DM+VP Orgs). Untreated and treated Hep-like Orgs presented cholestasis phenotype with intracellular accumulation of CMFDA. Treated Hep DM+VP Orgs showed cholestatic features compared to the untreated sample which instead showed no intracellular accumulation of the fluorescent bile acid. Scale bar: 50 μ m.

To confirm that the cholestatic phenotypes observed upon CsA treatment are not off target effects but are instead CsA specific, I have utilised DILI drugs that exerts liver toxicity via a non-cholestatic pathway such as acetaminophen and amiodarone. Acetaminophen has been previously reported to be a human hepatotoxin which early clinical toxic manifestation have been associated with the formation of reactive metabolites (NAPQI) in the hepatocytes (Dragovic et al., 2016). On the other hand, amiodarone has been previously described to be a DILI compound that specifically causes steatosis and phospholipidosis (Dragovic et al., 2016). Before using amiodarone and acetaminophen, I have initially identified their toxic concentrations. Consistently with CsA experimental procedure, I have repeatedly exposed DM+VP Orgs to the non-cholestatic DILI drugs for 4 days in total. Upon amiodarone and acetaminophen



treatment, CMFDA was actively cleared into the bile canaliculi (Figure 5.5), whilst DM+VP Orgs treated with CsA presented intracellular accumulation of CMFDA (Figure 5.5). Thus, the results indicate that CsA specifically induce cholestasis injury and that the organoid system is capable to specifically recapitulate cholestatic phenotypes of CsA-induced cholestasis.

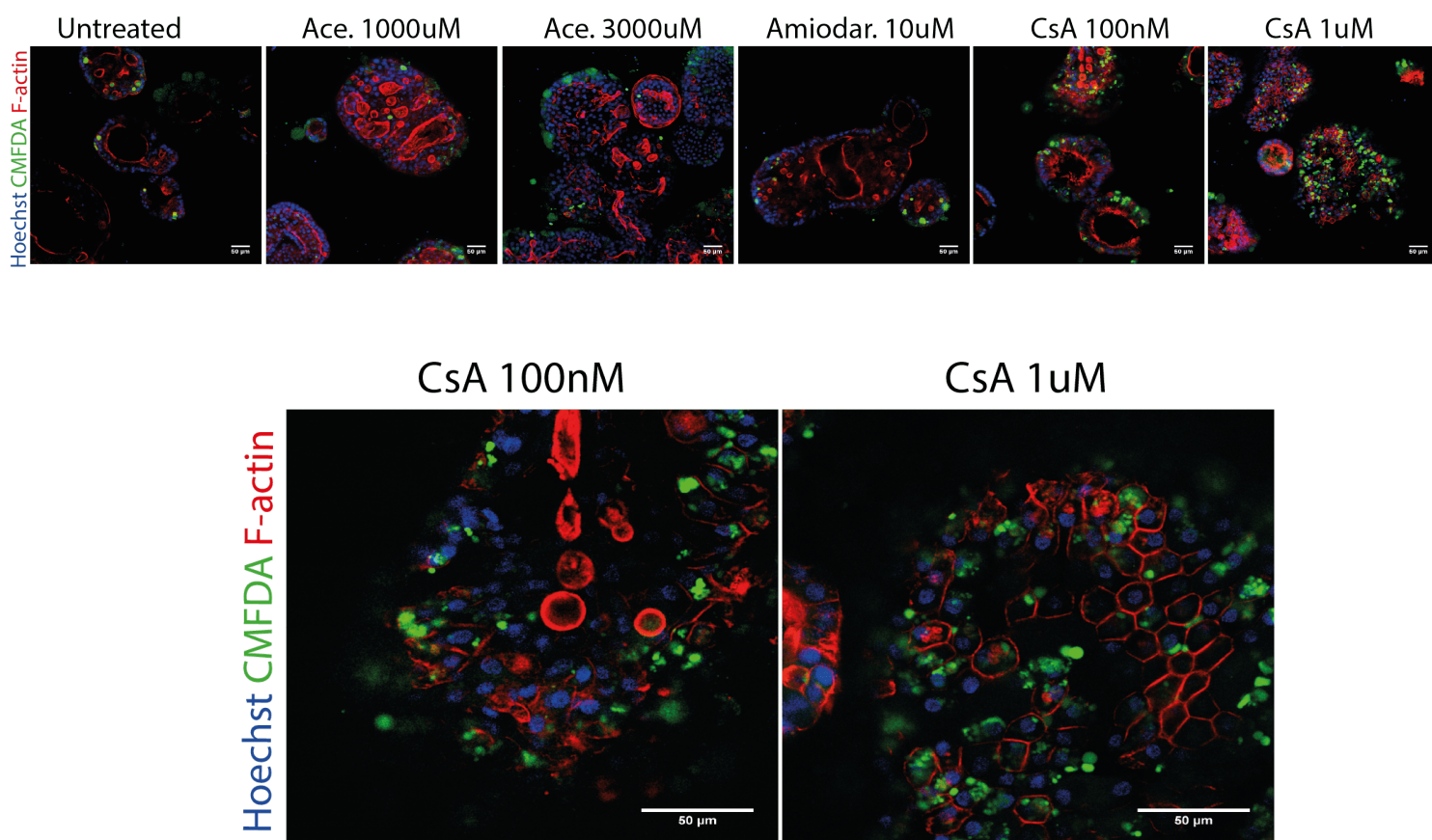


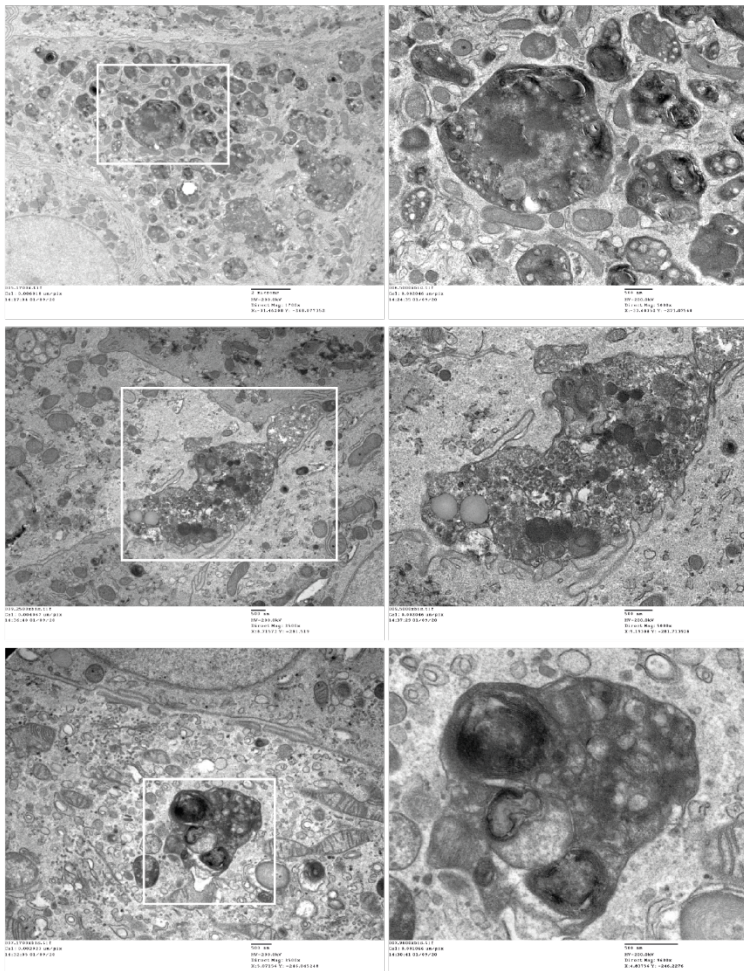
Figure 5.5 **CsA specifically induce cholestasis in the organoid system.** Immunofluorescence analysis of CMFDA (green) in DM+VP Orgs treated with CsA and non-cholestatic drugs (acetaminophen and amiodarone). Live staining of CMFDA showed intracellular accumulation in CsA treated organoids and not in organoids treated with acetaminophen and amiodarone. Scale bar: 50 μ m. Abbreviations: Ace: acetaminophen, Amiodar: amiodarone.

To gain a deeper insight on the effects of CsA induced cholestasis at the organelle level, transmission electron microscopy (TEM) evaluation was carried out (Figure 5.6A). Intracellular biliary pigments were observed (Figure 5.6A), hence confirming the cholestatic response upon CsA induction. Interestingly, lipid droplet accumulation is also observed in the cytoplasm (Figure 5.6B), suggesting that CsA might not only have cholestatic effects but also steatotic effects. Indeed, previous case studies have shown that CsA has been also associated to hepatic steatosis (Bell, Delilah F.G. Hendriks, *et al.*, 2016). Interestingly, although amiodarone has been reported to induce early steatosis

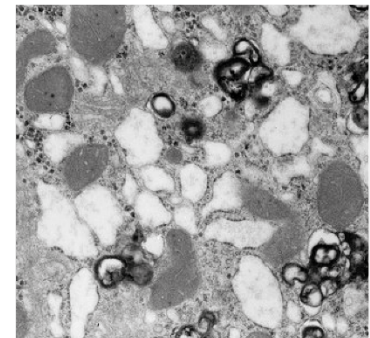
and phospholipidosis patterns in hepatocytes, I have instead mainly observed lamellar bodies formation in DM+VP Orgs (Figure 5.7), which is a clear sign of drug induced phospholipidosis and not steatosis. This suggests that CsA and amiodarone might induce fat accumulation in the hepatocytes via different mechanisms.

A

In vitro



In vivo



B

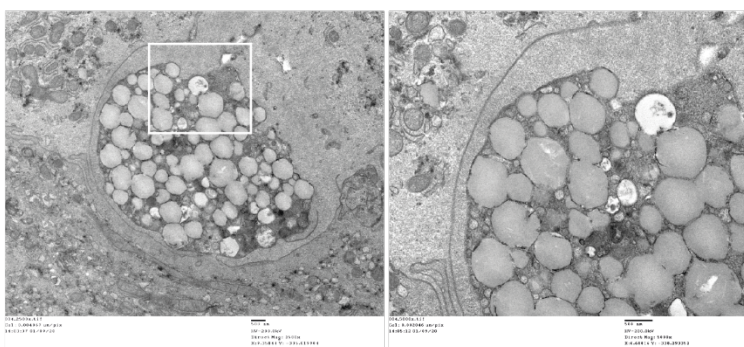


Figure 5.6 **Intracellular accumulation of biliary pigments and lipid droplets following CsA treatment.** **A)** TEM images of DM+VP Orgs treated with CsA showed similar bile accumulation structures as the *in vivo* condition. Zoomed images show representative images of biliary pigments. **B)** TEM images of lipid droplet formation. Scale bar: 2 μ m. Zoom-in image scale bar: 500 nm. *In vivo* image reference: (C. and Manov, 2011).

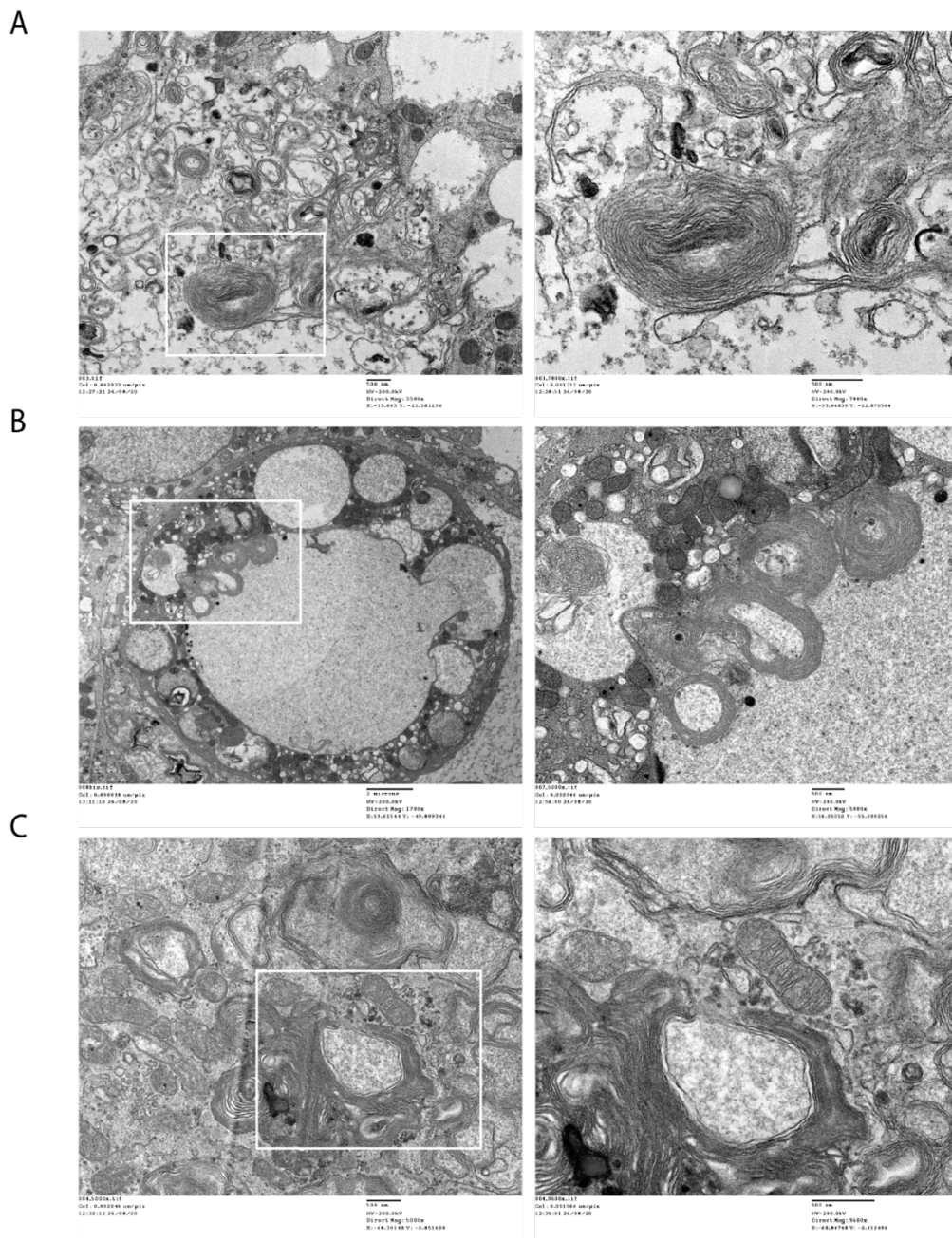


Figure 5.7 **Formation of lamellar bodies in amiodarone treated organoids A-B-C)** TEM images of DM+VP Orgs treated with amiodarone showed formation of lamellar bodies, a clear sign of phospholipidosis. Scale bar: 2 μ m. Zoom-in image scale bar: 500 nm.

5.2 Human differentiated liver organoids are susceptible to hepatotoxins

Sensitivity towards potential hepatotoxic compounds is very often assessed via the measurement of cellular viability in response to a dose dependent regimen. Based on the cellular response determined by the ATP levels, the IC50 value obtained is then compared to a defined IC50 threshold which discriminate DILI versus non-DILI compounds.

Based on the published data generated with other *in vitro* hepatic models, I have compared the organoid ability to detect DILI compounds. Specifically, in this Thesis I have tested three DILI compounds: bosentan, amiodarone, and acetaminophen (Table 5.1).

Table 5.1. Acetaminophen, amiodarone and bosentan DILI classification.

Compound	NEW FDA Descriptor 2018 (MOST, LESS, NO concern – FDA assignments only)	DILI mechanism of action	References
Acetaminophen	Most	Reactive metabolite	(Ju et al. 2015; Tujios and Fontana 2011)
Amiodarone	Most	Lipid droplet and phospholipids accumulation	(Bandyopadhyay et al. 1990; Begriche et al. 2011; Dake et al. 1985; Kia et al. 2015; Zahno et al. 2011)
Bosentan	Most	Transporter inhibition	(Eriksson et al. 2011; Fattinger et al. 2001; Lea et al. 2016)

DM+VP Org were exposed to a gradient of concentrations of the DILI compounds amiodarone, acetaminophen and bosentan (Figure 5.8). Similar to CsA, DM+VP Orgs treated with the cholestatic drug bosentan exhibited a reduced organoid growth which occurred at 100 μ M bosentan (Figure 5.8). On the other hand, organoids treated with amiodarone presented a dense phenotype which might be the result of the excessive intracellular fat accumulation induced by the drug (Figure 5.8). Conversely, treating DM+VP Orgs with acetaminophen did not show any morphological change compared to the control (untreated) (Figure 5.8).

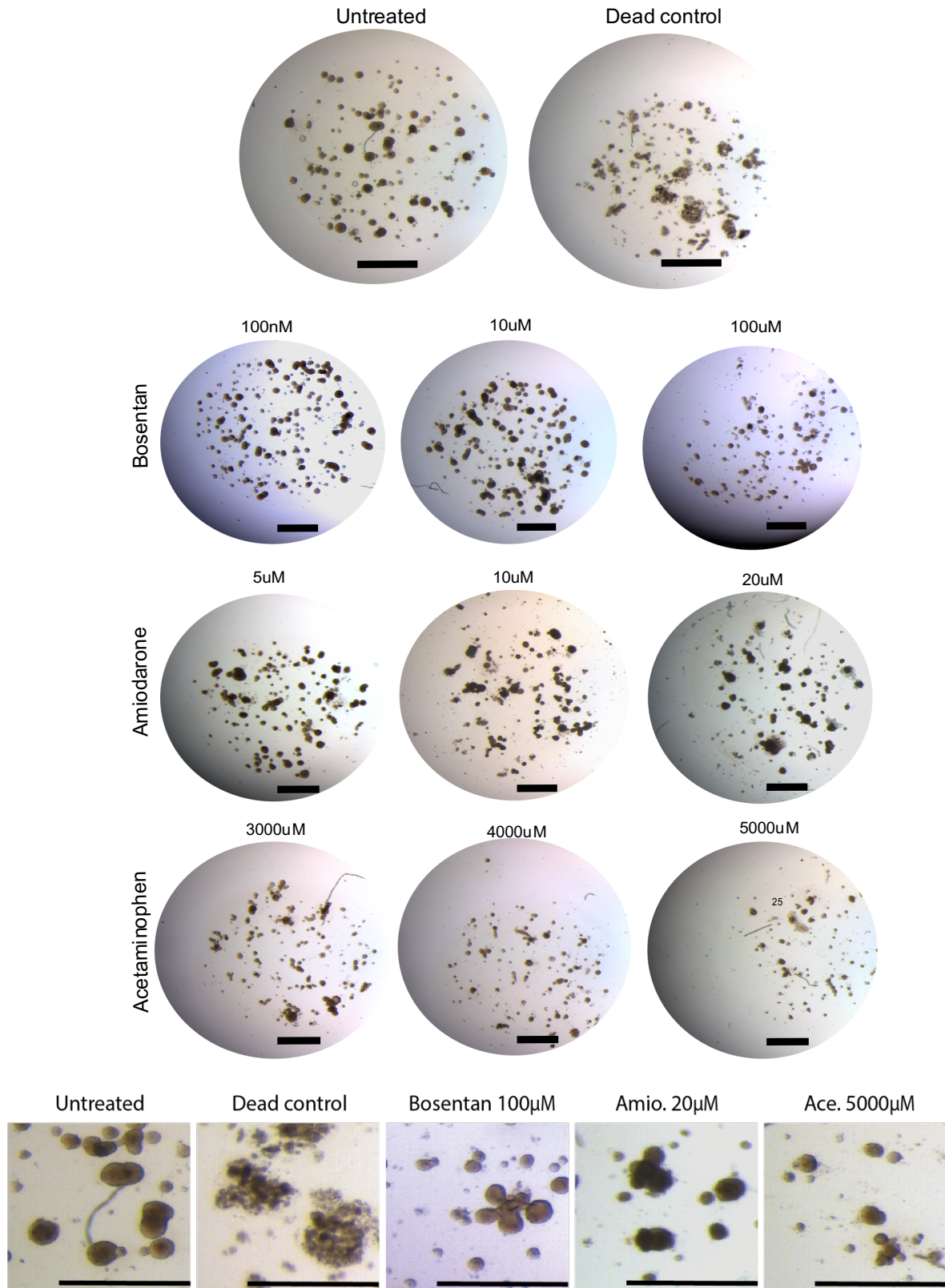
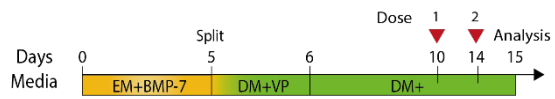
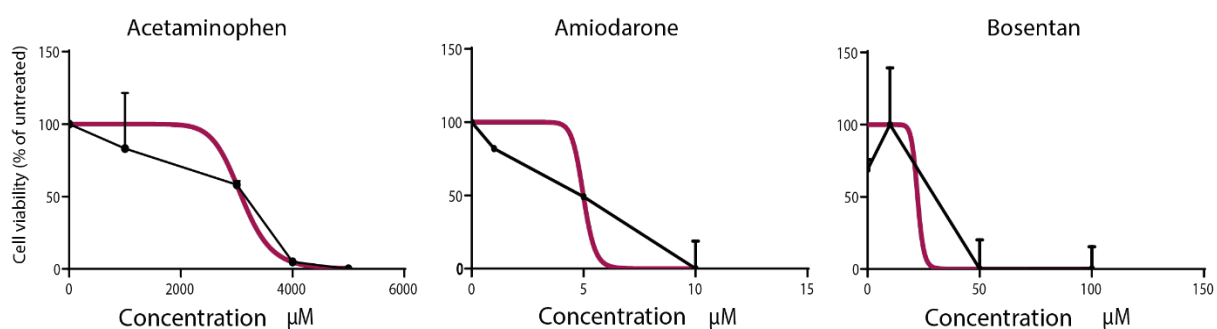


Figure 5.8 Titration of amiodarone, bosentan and acetaminophen in DM+VP Orgs. Brightfield images of DM+VP Orgs treated with bosentan, amiodarone and acetaminophen. Bosentan treated organoids exhibited a decrease in organoid growth at 100 μM . Amiodarone treated organoids displayed dense structures at 10 μM . No morphological differences compared to the untreated control were instead observed in acetaminophen treated organoids. Dead control is 20% DMSO. Scale bar: 2 mm. Zoom-in images show representative phenotypes for each DILI drug. Scale bar: 1 mm.

ATP levels were measured at the end of the 4-day compound dosing (Figure 5.9). A dose-dependent reduction in cell viability was observed in the organoids in response to all three hepatotoxins (Figure 5.9).

Based on the results, IC50 values were calculated. IC50 is the concentration at which a 50 % reduction in cell viability is observed. The values obtained were compared to IC50 values obtained from the literature for C3A spheroids (Figure 5.9) (Gaskell et al., 2016). C3A spheroids are generated from C3A hepatoma cell lines. Acetaminophen, bosentan and amiodarone were all more toxic to C3A spheroids indicated by lower IC50 values (Figure 5.9).



	Spheroids C3A (IC50 μM)	Organoids (IC50 μM)
Acetaminophen	7212	3087
Bosentan	373	22.3
Amiodarone	98	3.588

Figure 5.9 **DM+VP Orgs show a toxic response to DILI compounds.** DM+VP Orgs were treated with acetaminophen, bosentan and amiodarone for 4 days. A dose-dependent drop in cell viability is observed for all the three compounds. Cell viability was measured as a % of the untreated sample and normalised to the total number of cells. N= 2, error bars denote \pm SEM. IC50 values were calculated using the GraphPad Prism 8 and compared to the IC50 values of C3A spheroids taken from (Gaskell *et al*, 2016).

A method to describe the likelihood of a compounds to cause DILI is predicted via the measurement of the Safety Margin (SM), which is calculated as the ratio of IC10 and Cmax. IC10 is the concentration at which a 10 % reduction in cell viability is observed. Whereas Cmax is the highest concentration of a drug in the blood. Compounds with a SM value below 20 are determined as DILI positive. Based on the cell viability data obtained from Figure 5.9, IC10 values were also determined and compared to the IC10 values of C3A spheroids and PHH spheroids (InSphero) taken from the literature (Gaskell *et al*, 2016). When comparing to C3A spheroids, DM+VP Orgs were more sensitive towards acetaminophen and amiodarone (Table 5.2), whilst similar IC10 was observed towards bosentan (Table 5.2). On the other hand, comparison to PHH spheroids, DM+VP Orgs were more sensitive to bosentan and amiodarone, while similar values were observed towards acetaminophen. From the IC10 values and Cmax values obtained from the literature (Bell, Delilah F.G. Hendriks, *et al*, 2016; Gaskell *et al*, 2016), SM was calculated (Table 5.2). Organoids successfully classified all the compounds as risk to cause DILI. Strikingly, amiodarone was not detected as hepatotoxic in the other two hepatic models but was only detected in the organoid system.

	Spheroids C3A (IC10 μ M)	InSphero (IC10 μ M)	Organoids (IC10 μ M)
Acetaminophen	1463	300	343
Bosentan	2	100	2.48
Amiodarone	42	20	0.39

Safety Margin (SM) = IC10 / Cmax (SM<20 = DILI)				
	Cmax (μ M)	Spheroids C3A	InSphero	Organoids
Acetaminophen	139	10.53	2.16	2.47
Bosentan	7.39	0.27	13.53	0.34
Amiodarone	0.81	51.85	24.69	0.49

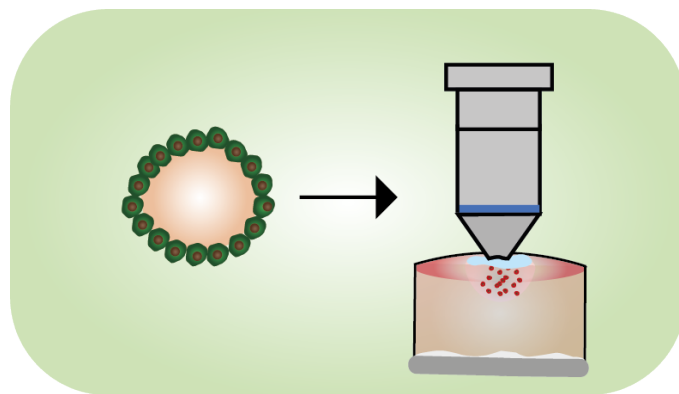
Table 5.2 **DM+VP Orgs can predict the risk of a compound to cause DILI.** DM+VP Orgs were treated with acetaminophen, bosentan and amiodarone for 4 days. Cell viability was analysed and IC10 values calculated. DILI risk was predicted by calculating the Cytotoxicity-based Safety Margin (SM) = IC10 / Cmax and compounds with a SM value below 20 were determined hepatotoxic. Organoids detected all the compounds as potential to cause DILI. InSphero and C3A spheroids failed to classify amiodarone as DILI compound with SM values above 20 (red), while organoids successfully detected amiodarone as DILI (green). Cmax values were obtained from literature. N= 2.

Overall, the results showed the susceptibility of the organoid system to detect a toxic compound which was not detected in other 3D hepatic system, yet its predisposition towards other human hepatotoxins remains to be formally investigated. Overall, the data suggests the potential use of DM+VP Orgs as complementary hepatic *in vitro* models to detect human hepatotoxins.

Chapter 6

Results IV:

Implementation of a time-lapse imaging system to study organoid proliferation



6.1 Establishment of an inverted imaging system for organoid proliferation

Assessment of DILI is very often based on endpoint measurements, while real-time studies of cell response towards compound is poorly investigated. As new complex *in vitro* models are developed, the need for new imaging tools to study the whole system both temporally and spatially is essential. Organoids are complex 3D structures embedded in extracellular matrix, thus it requires an imaging system that can offer deeper imaging inside the organoid culture with very limited light scattering. Current imaging system developed for such purpose are the multi-photon and light sheet microscopy. With the aim to establish a real time imaging system for liver organoid proliferation, in this Thesis I have approached the upright 2-photon excitation microscope (2P) available at the Cambridge Advance Imaging Centre. In addition, for optimisation purposes mouse Chol. Orgs with a nuclear fluorescent reporter were used. Thus, the organoids were dissociated into single cells and processed for live imaging (Figure 6.1A) (see Methods). Following 3 days of live imaging, I have observed cellular death (Figure 6.1B), and culture media evaporation.

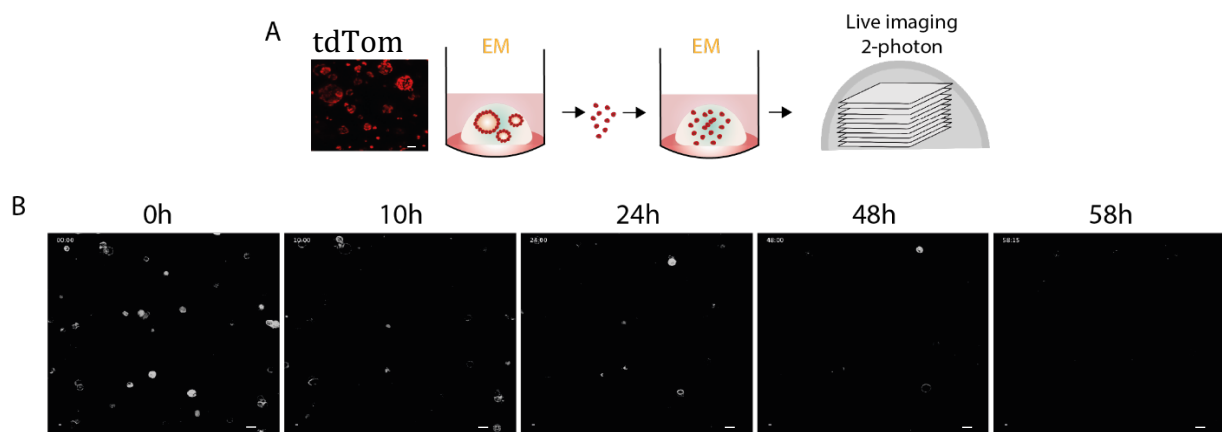


Figure 6.1 **Cellular degradation is observed after 3 days of live imaging.** **A)** Model of live imaging experimental procedure of mouse Chol. Orgs expressing an endogenous Td-Tomato nuclear reporter. Organoids were dissociated to single cells and processed for live imaging using the 2P. **B)** Time-course 2P images of single cells at 0h, 10h, 24h, 48h and 58h show a temporal degradation of single cells with no organoid formation. Scale bar: 10 μm .

To tackle the problem, the culture dish was fully filled with culture media and sealed with parafilm and dish lid to minimise media evaporation. Additionally, to adjust the sample to the working distance of the objectives, I have established an imaging system that takes inspiration from the setting of an inverted microscope but instead applied to an upright microscope ([Figure 6.2A](#)) (See Methods section). Essentially, the culture dish was rotated upside down with the Matrigel drop facing downward. As a result, organoid viability was maintained following three days of live imaging ([Figure 6.2B](#)).

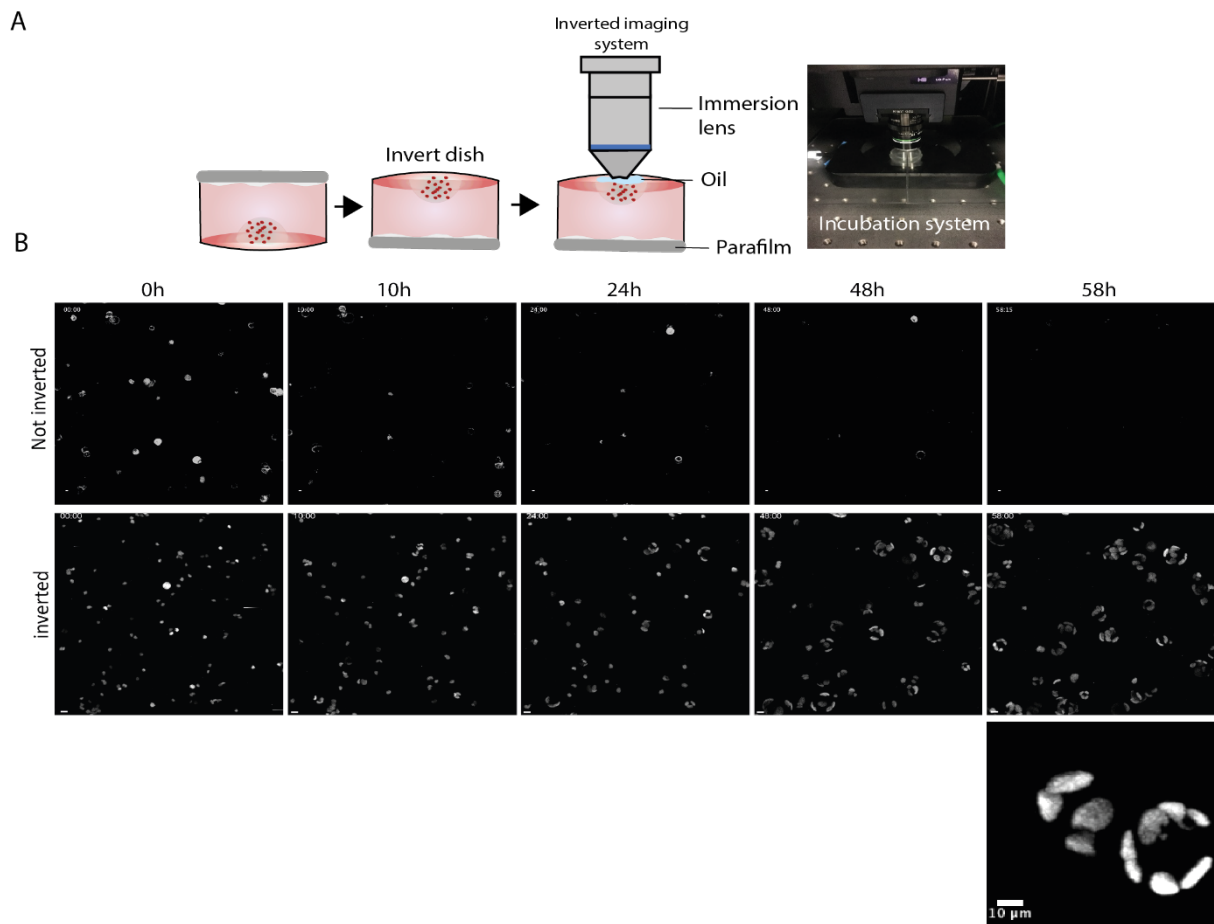


Figure 6.2 Establishment of an inverted imaging system enabled the real time imaging of single cells turning into organoids. A) Model of the inverted imaging system. **B)** 3 days' time-course 2P images of single cells when using the standard upright settings (Not inverted) and when using the inverted system. Organoid formation is only observed in the inverted condition. Zoom-in image show representative organoids expressing td-tomato in the nuclei. Scale bar: 10 μm .

Having obtained an imaging system that allows the maintenance of organoid viability, next I have optimised the culture conditions to obtain consistent readouts from the organoid proliferation. With this aim, initial optimisation of single cell densities was assessed. At higher cellular concentrations single cells are localised in close proximity (data not shown), which indicates the likelihood of organoids fusion incidence (Figure 6.3A). As a result, formation of organoids with larger area is observed at the expense of

multiple single clonal organoids (Figure 6.3A). Maintenance of single organoid clonality is important for cell tracking purposes. In fact, when performing live imaging I have observed that 1000 single cells embedded in a standard 50 μl Matrigel drop displayed long distances from each other (data not shown). Therefore, this provides sufficient space for the cells to expand in the form of organoids and highly prevents cellular fusion at least for one week. On the other hand, although a concentration of 1000 single cells yielded a higher organoid formation efficiency, downscaling considerations were taken to fit the 2P system. As a 50 μl Matrigel drop has an xyz dimensions greater than 1 mm^3 in size, it would require long period of time and massive local data storage to support the imaging acquisition. Therefore, with the aim to capture many single cells at one single view in the Matrigel, further investigation on Matrigel size and single cell densities were explored. By taking into consideration that the maximum field of view of the 2P in our hand was 400 μm (x) x 400 μm (y), to nearly capture 100 cells in a volume of 400x400x400 μm^3 (0.064 μl), an initial seeding density of approximately 60.000 cells in a Matrigel drop of 50 μl is needed. Additionally, I have further downscaled the Matrigel drop to 15 μl and embedded 18.000 single cells. To further confirm that the sample size chosen was optimal, I have performed live imaging of high and low cell densities (Figure 6.3B). After 3 days, I have observed higher organoid formation efficiency in the low-density condition and few organoids formation at high densities. This additionally suggest that cell-cell contact could be an important parameter for organoid development.

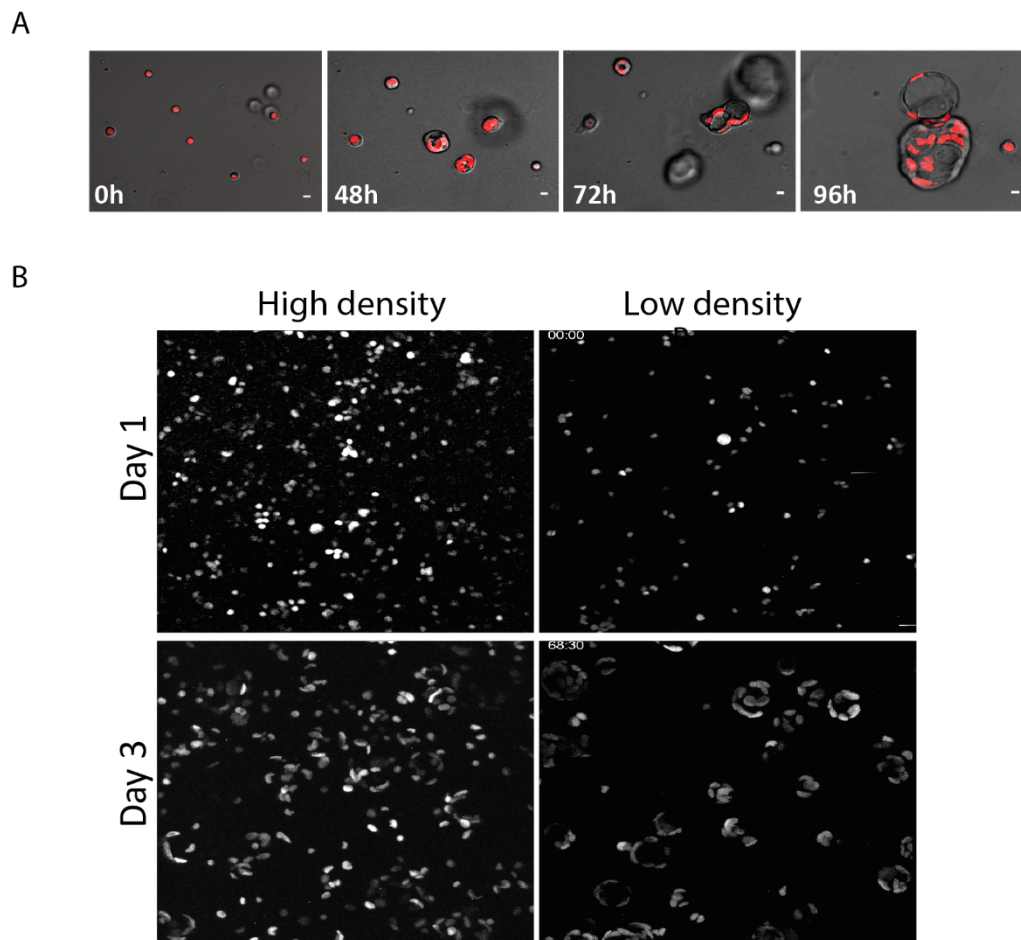


Figure 6.3 **Organoid formation efficiency is higher at low cellular concentration.** **A)** Confocal images of mouse Chol. Orgs expressing Td-Tomato in the nuclei. Representative images of organoid fusion overtime. Scale bar: 10 μ m **B)** 2P images of single cells 3-day live imaging. On day 3, at high seeding density condition less organoid formation is observed, while higher organoid formation efficiency is seen at low density.

Based on the data obtained from successful 3 days live imaging of single cells derived Chol. Orgs (Figure 6.2), I have tracked each single cell (Figure 6.4) and analysed the timepoint at which ductal cells enter the cell cycle and its duration (Figure 6.4C). As previously shown in Aloia et al (2019), the first cell cycle division occurred at approximately 40h (Figure 6.4C). No difference in cell cycle duration is observed when cells are in the form of single cells or aggregates (Figure 6.4D). After 40h from the first division of the parent cell, a shortening of the cell cycle duration of the daughter cells is observed, which seems to coincide with organoid formation (Figure 6.4C).

Taken together, I have optimised an imaging system that favours organoid proliferation for a period of 3 days. The system could be potentially extended to study the proliferation of DM+VP Orgs as an additional parameter in the study of DILI.

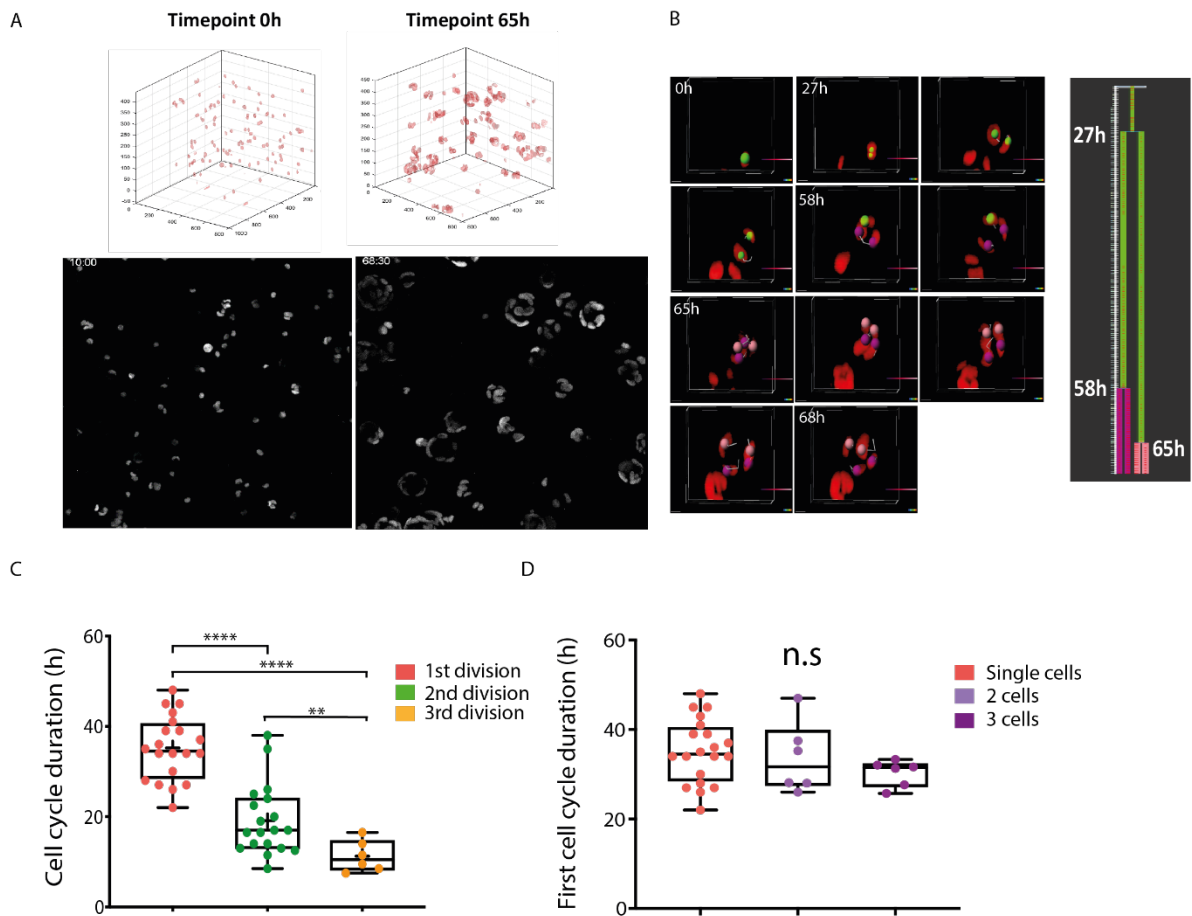


Figure 6.4 Single cells derived liver organoids shows approximately 40h cell cycle duration before forming organoids. **A)** Representative images of single cells at timepoint 0 and timepoint 65h used for tracking analysis. **B)** Representative images of one single cell tracking analysis using the IMARIS software and its cell division tree (see Methods). **C)** 3-day quantification of cell cycle duration (h) of single cells and their daughter cells. 80 single cells were counted. Box and Whiskers plot – Min to Max, each dot represent one single cell. Mann–Whitney non-parametric test $P < 0.01$ (*), $P < 0.0001$ (****), $P < 0.01$ (**). **D)** 3-day quantification of single cells and aggregate of cells with 2 and 3 cells. No significance is observed in the cell cycle duration. Box and Whiskers plot – Min to Max.

Chapter 7

Discussion

DILI is a huge threat for pharmaceutical companies as it impedes the bridge between clinical trials and market, and for the healthcare system due to the challenges derived to diagnose and treat DILI (Watkins, 2011). Despite the promising results, reports of adverse liver safety at the clinical trial step highlights the vast gap between preclinical safety liver prediction and clinical outcome. This suggests that the problem resides on the use of unsuitable preclinical drug discovery methods that are not capable to identify the adverse liver safety profiles observed in the clinics. Extensive studies using *in vitro* models and *in vivo* animal models are often not sufficient to mimic the biological response achieved by the human system. Therefore, the potential harmful nature of the medication to the liver is only revealed until it reaches clinical trials.

The challenges of studying DILI are linked with the poor knowledge of the mechanisms behind it. An *in vitro* hepatic system capable to reproduce the essential features of the human liver tissue *in vivo* is thus key to better understand DILI and to how it is triggered. The existence of inter-species difference between animals and human fail to faithfully mimic the correct biological effect in response to a drug observed in the human liver (Martignoni, Groothuis and de Kanter, 2006)– this has been supported with clinical cases of hepatotoxicity observed in patients after taking drugs that did not show any evidence of liver injury in the animal model, e.g. fialuridine (Olson *et al.*, 2000; Lai, Tse and Unadkat, 2004; Lee *et al.*, 2006; Xu *et al.*, 2014). Therefore, along with *in vivo* animal data, more focus is given to human *in vitro* hepatic systems to increase the chances to capture potential hepatotoxic compounds. Current state-of-the-art *in vitro* systems rely on a platform of 2D and 3D models, with PHH spheroids being the leading model after showing promising results for the detection of DILI drugs (Bell, Delilah F.G. Hendriks, *et al.*, 2016).

In parallel to PHH spheroids breakthrough in the liver safety field, novel 3D models – organoids – began to gain more attention due to their remarkable proliferative capacity *in vitro* while retaining several of the functional characteristics of the tissue of origin (Prior, Inacio and Huch, 2019; Kaluthantrige Don and Huch, 2021). Since the

advent of the very first liver organoid system, excitement in the use of such complex organotypic system has been growing in the toxicology field (Huch *et al.*, 2013, 2015). Very recently, a novel paper from Takebe's lab showed for the first time the use of PSC-derived liver organoids as a preclinical system to study DILI (Shinozawa *et al.*, 2021); However, one could argue that one limitation factor of iPSCs-derived organoids is their level of cellular maturation. Therefore, in this Thesis, I have showed instead the use of human adult stem cell derived liver organoids as a system to predict DILI *in vitro*.

7.1 Roadmap of hepatocyte maintenance *in vitro*

In vivo, the process of hepatocyte specification from hepatic progenitors is sustained by the simultaneous activity of cell-to-cell, cell-to-ECM interactions, and secreted growth factors from the surrounding niche.

A current unmet need in the drug toxicology field is the achievement of an *in vitro* hepatic system that maintains viable and functional hepatocytes overtime. Historically, isolated primary hepatocytes rapidly lose their maturation state and revert towards a dedifferentiated state once cultured *in vitro* (Elaut *et al.*, 2006). Additionally, differentiated cells appear to have a finite proliferative capacity, which renders their overtime culture highly challenging. Unlike the challenges derived from the culture of primary cells, stem cells have the intrinsic capacity to proliferate and differentiate *in vitro*. How to drive hepatocyte differentiation *in vitro* and how to sustain a balance between hepatocyte viability and functionality overtime?

To date, several different protocols achieved the propagation of hepatocytes *in vitro*. Hepatocytes have been generated from human induced pluripotent stem cells (hiPCs) and human embryonic stem cells (hESCs) with a multistep process involving definite endoderm (DE) specification, liver precursors induction and differentiation

towards an hepatocyte lineage (Hay *et al.*, 2008). However, the above axis from progenitor to differentiated cells can also be bypassed towards an alternative approach which instead used non-hepatic cell types as cells of origin to direct the differentiation into a hepatocyte fate. This was achieved via the induction of HNF4a and Foxa1-2-3 transcription factors (Sekiya and Suzuki, 2011).

Additionally, other studies favoured the use of small molecules to direct hepatocyte differentiation. Work conducted by (Katsuda *et al.*, 2017) showed that by solely using small molecules, it is possible to reprogram human mature hepatocytes into bipotent progenitor cells as previously shown *in vivo* (Tanimuzu *et al.*, 2014; Tarlow *et al.*, 2014, Yimlamai *et al.*, 2014). Indeed, with the use of A8301 (TGF- β inhibition), CHIR99201 (GSK-3 inhibitor) and the mitogen HGF, they were able to generate bipotent progenitors with retained capacity to differentiate either as functional hepatocytes or cholangiocytes upon transplantation in mice (Katsuda *et al.*, 2017). Nevertheless, the same study did not report an *in vitro* differentiation of these hepatic progenitors, therefore it is unclear which signalling pathways could direct hepatocyte and cholangiocyte fate. Another study instead, used a combination of growth factors, Wnt3a, A8301 and Rho-kinase inhibitor to expand hepatocytes for 1 month (Zhang *et al.*, 2018). The use of Wnt3a was essential to maintain hepatocyte proliferation; however how this is impacting the hepatocyte maturation compared to the *in vivo* human liver remains as an open question. Another landmark study used five chemicals to expand primary human hepatocyte *in vitro* – Forskolin, DAPT, IWP-2, SB431542 (TGF- β inhibitor) – for two months (Xiang *et al.*, 2019).

All the above studies lacked the three-dimensional cellular arrangement observed *in vivo*, which was instead achieved with the generation of hepatocyte organoids. Pioneering work conducted in 2015 (Huch *et al.*, 2015) established self-renewing human organoids (Chol. Orgs) that retained bipotential capacity to differentiate into cholangiocytes and hepatocytes. Similar to (Katsuda *et al.*, 2017), the differentiation of Chol. Orgs was achieved via the use of small molecules, in this case DAPT and A8301 (Huch *et al.*, 2015). Although the establishment of organoids added a new level of

complexity in the achievement of a hepatic system that can closely mimic the *in vivo* environment, yet the process of differentiation towards a hepatocyte fate lacked the efficiency to generate a homogenous population of hepatocyte organoids. In this Thesis I have enhanced the differentiation of Chol. Orgs to hepatocyte organoids through the modulation of WNT signalling and YAP inhibition.

In vitro, Chol. Orgs are a direct testimony of the importance of WNT signalling as a key factor to maintain the bipotentiality of hepatic progenitors and ductal proliferation upon liver injury *in vivo*. To enhance the differentiation of Chol. Orgs into a hepatocyte fate, I have showed that addition of WNT inhibitors – IWP2 and ICRT3 - to the DM enhanced the hepatocyte fate. Similar studies on PSCs-derived hepatic spheroids have shown improved hepatocyte formation via WNT inhibition through WIF-1, which binds to WNT proteins and DKK-1, which binds to LPR5-6/WNT/Frizzled complex (Pettinato *et al.*, 2016). I speculate that WNT inhibition primes the ductal/progenitor cells for differentiation.; however, the exact molecular mechanism remains to be elucidated. This is in agreement with a study that has demonstrated a role of WNT signalling in the maintenance of naïve pluripotency. By blocking porcupine via IWP-2, they observed the suppression of ESCs self-renewal, which was rescued by addition of Wnt3a protein (Berge *et al.*, 2011).

Paradoxically, despite the addition of WNT inhibitors, when I added a WNT agonist/GSK-3 inhibitor (CHIR), I still observed a transition into a hepatocyte fate. I speculate that inhibition of GSK-3 might lead to downstream effects other than the ones related to WNT signalling activation. Multiple studies have reported the contribution of GSK-3 inhibition to the maintenance of ESC self-renewal and differentiation (Ding *et al.*, 2003; Sato *et al.*, 2004; Doble *et al.*, 2007; Ying *et al.*, 2008; Bone *et al.*, 2009). Specifically, it was observed that GSK-3 inhibition on primed pluripotent stem cells stimulated differentiation, while pluripotency was maintained in naïve pluripotent stem cells (Greber *et al.*, 2010).

Nevertheless, WNT signalling is also important to direct hepatic zonation (Gebhardt, 1992). A gradient of WNT signalling directs the metabolic identity of the hepatocytes located across the portal-venous axis of the liver lobule. Near the central vein, high WNT signalling corresponds to hepatocytes with xenobiotic metabolism function (pericentral hepatocytes). I have observed that organoids in DM+ supplemented with CHIR had an increase of genes related to drug metabolism (*CYP2C8*, *CYP2C9* and *CYP3A4*). I speculate that WNT activation via GSK-3 inhibition could direct pericentral hepatocyte specification. This is in agreement with recent studies in which hepatic zonation *in vitro* was modulated by WNT signalling (Ahn *et al.*, 2019; Wahlicht *et al.*, 2020).

Taken together, these findings indicate that GSK-3 inhibition might not only direct differentiation but also stimulate a functional hepatocyte fate. In line with this, it was shown that β -catenin activation via GSK3 inhibition leads to an upregulation of definitive endoderm specification genes such as GATA4, FOXA2 and SOX17 (Huang *et al.*, 2017). Studies conducted on mouse ESCs showed that β -catenin and c-Myc activity upon GSK3 inhibition directly enhanced DE specification through inhibition of the transcription factor Tcf7l1 (Morrison *et al.*, 2016), which has led to the hypothesis that GSK3 inhibition is essential to drive endoderm lineage specification (Huang *et al.*, 2017). Work conducted on human embryonic stem cells and human induced pluripotent stem cells showed that GSK-3 inhibition leads to the formation of a population of cells with high DE specificity, which are prone to be chemically induced into functional hepatocytes (Siller *et al.*, 2015). This in agreement with another study, which observed a higher differentiation efficiency of human ESCs by first priming the cells towards a DE fate using CHIR. In the same study they also argue the effectiveness of the differentiation was even higher when the cells were primed only with CHIR and not with other WNT signalling activators (Bone *et al.*, 2009). Therefore, I speculate a role of GSK-3 inhibition to direct the differentiation of progenitor/ductal cells in our Chol. Orgs into a population of cells with hepatic progenitors.

I have also shown that mechanical dissociation of organoids in combination with the DM+ enhances hepatocyte differentiation. When I investigated the activity of a mechanical transducer, YAP, upon dissociation I observed an increase of YAP nuclear translocation which coincides with its activation. Based on the studies conducted by (Yimlamai *et al.*, 2014), YAP activity differs along the hepatic epithelium, with ductal/progenitor cells having high and hepatocytes low YAP activity. This suggest that mechanical dissociation of organoids might trigger a change in cell fate into a more ductal/progenitor state, which goes in line with the activation of a ductal reaction upon liver regeneration. Supplementation of Verteporfin (VP) to the DM+ (DM+VP) enhanced the transition into functional hepatocyte organoids. I speculate that YAP activity inhibition at the point of mechanical dissociation, inhibits the ductal fate to direct the differentiation towards a hepatocyte fate along with Notch inhibition and TGF- β inhibition.

Overall, I speculate that the enhancement of differentiation is achieved when more progenitor cells are present or primed for differentiation. Despite the DM+VP enhanced the differentiation into a hepatocyte fate, I also observed comparable levels of ductal fate gene expression as non-differentiate Chol. Orgs, though no Chol. Org structures were observed in the DM+VP. This indicates that only a sub-population of cells in the Chol. Orgs respond to the differentiation signal of the DM+VP, therefore suggesting the chimeric nature of DM+VP Orgs comprising both hepatocytes and ductal cells. Further investigation at the single cell level using the single cell RNA sequencing (scRNAseq) technique will help to identify the subpopulations that coexist within our DM+VP Orgs and the level of cellular maturation of both hepatocytes and cholangiocytes compared to DM Orgs and Chol. Orgs. Nevertheless, compared to DM Orgs and Chol. Orgs, our DM+VP Orgs still exhibited higher hepatic functionality despite the presence of ductal cells.

Based on these observations, I propose the following mechanistic model of our differentiation media ([Figure 7.1](#)). First, ductal/progenitor cells are primed for differentiation via WNT inhibition; GSK-3 inhibition allows the Chol. Orgs to differentiate; addition of A8301, DAPT and VP instead directs the transition into a hepatocyte

functional state. However, inhibition of these three pathways is not sufficient to suppress the ductal fate since I have observed mRNA expression of ductal markers comparable to Chol. Orgs expression, which indicates that further investigation on the signalling molecules involved in hepatic cell lineage specification is needed; or simply these cells do not respond to the differentiation signals. This further suggests that the efficiency of the DM+ Orgs to enhance hepatocyte differentiation might lie on the ability to differentiate more cells and not on the generation of more mature hepatocyte cells compared to DM Orgs. By performing scRNAseq will be able to answer the above question.

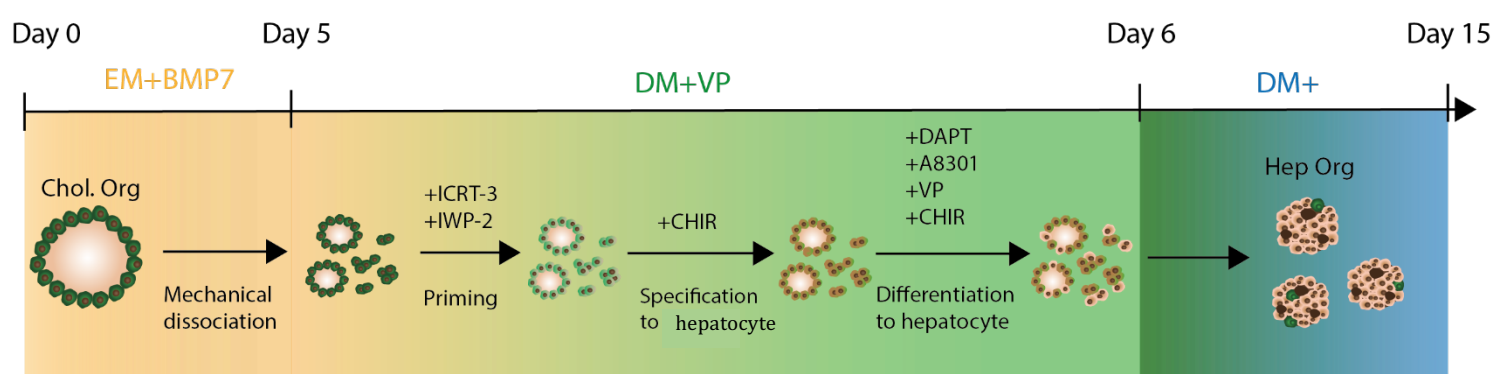


Figure 7.1 Working model for the differentiation of Chol. Org into DM+VP Org. As a working hypothesis I propose a stepwise *in vitro* differentiation protocol from ductal/progenitor organoids to hepatocyte organoids. Chol. Orgs are grown in EM+BMP-7 for 5 days. On day 5, mechanical dissociation of Chol. Orgs promotes the activation of progenitor/ductal cells identity, confirmed with an upregulation of YAP activity. I suggest that addition of WNT inhibitors (IWP-2 and ICRT-3) on these cells primes the progenitor/ductal cells for differentiation. I speculate that GSK-3 inhibition through CHIR specifies the primed cells towards an endodermal fate. To direct the differentiation towards the hepatocyte lineage, ductal fate is suppressed through TGF- β and Notch signalling inhibition respectively with A8301 and DAPT. I suggest that continuous addition of CHIR promotes hepatic specification towards perivenous hepatocytes which are involved in drug metabolism. Additionally, for the first 24h post dissociation, when YAP activity is high, VP is supplemented to the media. I suggest that inhibition of YAP activity promotes an enhancement towards functional hepatocytes. On day 6, VP is removed, and organoids are only supplemented with the DM+ media that contains the WNT inhibitors, ductal fate suppressors and CHIR for a total of 10 days.

Overall, the cholangiocyte-derived DM+VP Orgs hold the great advantage in the drug toxicology field to have an unlimited cell source for generation of functional

hepatocytes through the directed stepwise differentiation *in vitro* using chemically defined culture conditions.

Recently, two studies have successfully reported the long-term expansion of hepatocyte organoids directly from isolated hepatocytes, a long-standing problem in the field. In the work conducted by Hu *et al.*, (2018) they were able to expand isolated mouse primary hepatocytes and foetal human hepatocytes *in vitro* for almost three months through the activation of WNT signalling via RSPO-1 and the use of a cocktail of growth factors and inhibitors - CHIR, A8301, DAPT. Peng *et al.*, (2018) has shown that supplementation of tumour necrosis factor- α , an inflammatory cytokine, promoted the long-term expansion of mouse primary hepatocytes for approximately 6 months. Both studies, contributed with insights for overcoming the finite proliferative capacity of primary cells, however at the expense of hepatocyte maturation. Indeed, I showed that in comparison with our DM+VP Orgs, the hepatocytes generated in the Hu Orgs had lower expression of hepatocyte functional genes. Despite I observed a decrease of ductal cell specific genes, long term culture of Hu Orgs generated Chol. Orgs-like organoids, indicating that overtime the culture conditions favour ductal cell growth over the hepatocyte proliferation. Further studies are needed to elucidate the mechanisms of this cellular “competition” between ductal cells and hepatocyte. Alternatively, trans-differentiation of Hu Orgs into Chol. Orgs could be another possible explanation.

To counteract the formation of Chol. Orgs in organoids generated from hepatocytes, I have also shown that differentiation with DM+VP enhances an increase of hepatocyte functionality over Hep Orgs generated from hepatocyte. It would be interesting to compare the degree of differentiation between ductal derived DM+VP Orgs and hepatocyte derived DM+VP Orgs.

7.2 Hepatocyte organoids as complementary systems to study drug induced cholestasis.

For the organoid system to be implemented in drug studies, the acquisition of an *in vivo* like hepatocyte physiology must be validated. First, I have validated key biological features needed to study DILI *in vitro*. Preservation of a functional bile canalicular network is essential for both detoxification and transportation of metabolites and bile to the digestive system. Our DM+VP Orgs showed formation of canalicular-like structure at the protein level and ultra-structural level. Expression at the mRNA level of key hepatocyte markers involved in drug metabolism and clearance were also observed. Liver functionality showed the ability of the model to produce and secrete bile and albumin. Transport assays showed accumulation of fluorescent bile within the bile canalicular-like structures, indicating the existence of a functional secretory systems in our DM+VP Orgs. The data was further reinforced when compared to DM Orgs, which showed intracellular accumulation of fluorescent bile, indicating a failure to properly differentiate into a hepatocyte fate. When compared to monolayer HepG2 cells instead, the latter showed an improper polarisation suggested by the failure to form bile canaliculi, which further emphasise the importance of a 3D cellular cultivation over a two-dimensional culture (Bell *et al.*, 2018).

Another crucial parameter to consider is the viability of the hepatocytes overtime in culture. In this work I have adopted a 4-day dosing regimen, with 2 repeated dosing based on the viability profile of our DM+VP Org in time. Despite the short dosing, I observed comparable IC50 levels as in the 14-day dosed spheroid system. This indicates that short exposure to DILI compounds was sufficient to classify these compounds as DILI positive in our DM+VP Org. However, this might not hold true for other compounds. Indeed, many hepatotoxins require longer period of incubation before these reveal any

sign of toxicity in the hepatic system. Since our organoids displayed a viability of 18 days in culture, this would highly hamper the use of our system for long-term DILI effects.

I went on studying the potential of the organoid system as a model for liver disease, focusing on cholestasis. Specifically, I looked at the effects of CsA-induced liver cholestasis. The organoid system reproduced intracellular bile accumulation which is a hallmark of cholestasis after exposure to CsA. CsA is shown to be a competitive inhibitor of BSEP (Román *et al.*, 2003). I have observed downregulation of mRNA levels of *ABCB11* and its encoding protein BSEP. This data goes in line with what has been observed *in vitro* and *in vivo* (Román *et al.*, 2003; Dragovic *et al.*, 2016). Of note, I have also observed formation of lipid droplets using the TEM, which indicated additional toxic mechanism derived by CsA exposure. This is in line with studies conducted *in vivo* and also *in vitro* using PHH spheroids (Fuhrmann *et al.*, 2014; Bell, Delilah F. G. Hendriks, *et al.*, 2016). In this line, treatment with amiodarone, known to induce both steatosis and phospholipidosis, showed phospholipidosis-like features in our DM+VP Orgs indicated by the formation of lamellar bodies in the cytoplasm, which are derived by an impairment of phospholipids metabolism within the lysosomes. However, no evidence of steatosis similar to CsA induced lipid droplet accumulation was observed. In line with this observation, a study conducted in HepaRG cells showed steatosis-like features only after a prolonged exposure with amiodarone, specifically after 14 days. While, induction of phospholipidosis was seen after only 24h treatment with amiodarone (Anthérieu *et al.*, 2011). Overall, the data demonstrate that our organoids would be an invaluable resource for the modelling of drug-induced cholestasis, yet further optimisations are needed to maintain cellular viability to perform long term drug screening and therefore capture other types of DILI. This leads to an open question: how to maintain proliferative capacity and differentiated cellular identity in the same hepatic system? Perhaps the closest system to address the question will be the use of the Hu Orgs since these retain the hepatocyte proliferative capacity. It is tempting to speculate that by giving shots of DM+VP to the Hu Orgs, this could enhance the hepatocyte functionality and possibly be adopted in the study of chronic DILI.

While the organoid culture system employed in this thesis could be attractive for drug development, yet many challenges still need to be surmounted. Organoids recapitulate only some aspects of the *in vivo* cellular complexity and physical environment. Oxygenation levels can induce toxic artifacts in cells, which renders the prediction of DILI even more challenging. On this direction, multiple approaches are currently investigated in the hope to achieve a more physiologically relevant organoid system, from coculture systems (Cordero-Espinoza *et al.*, 2020) to microfluidic devices (Wang *et al.*, 2018). In that respect, integration of organoids into microfluidic chips would enable a more realistic regulation of the microenvironment and a better recapitulation of cellular interaction with other organs.

Another target to reach in the advancement of the organoid technology is the formation of reproducible and scalable organoid cultures. For the organoids to be implemented in the drug development field, production of a huge number of identical organoids at once is crucial to perform high throughput screening of novel compounds. In that respect, the use of micro-engineered cell culture devices has enabled the generation of a large number of highly reproducible gastrointestinal organoids (Brandenberg *et al.*, 2020). Additionally, the use of 3D bioprinters enabled the manufacture of kidney organoids at a large scale (Lawlor *et al.*, 2021). It would be interesting to apply these engineered devices to our 2-photon live imaging system and track multiple organoids at once.

Conclusion

In this Thesis I have identified a novel hepatic organoid system that comprise functional hepatocytes. By taking advantage of other hepatic model it could be complementarily used to study multiple drugs and get a better understanding of the whole drug metabolic pathway. Therefore, this work presented a novel human liver system that holds potential to bridge preclinical liver safety field and clinical trials.

References

Ahn, J. *et al.* (2019) 'Human three-dimensional in vitro model of hepatic zonation to predict zonal hepatotoxicity', *Journal of Biological Engineering*. doi: 10.1186/s13036-019-0148-5.

Amadi, C. N. and Orisakwe, O. E. (2018) 'Herb-Induced Liver Injuries in Developing Nations: An Update.', *Toxics*, 6(2). doi: 10.3390/toxics6020024.

Ananthanarayanan, M. *et al.* (2001) 'Human Bile Salt Export Pump Promoter Is Transactivated by the Farnesoid X Receptor/Bile Acid Receptor', *Journal of Biological Chemistry*. doi: 10.1074/jbc.M011610200.

Anthérieu, S. *et al.* (2011) 'Induction of vesicular steatosis by amiodarone and tetracycline is associated with up-regulation of lipogenic genes in heparg cells', *Hepatology*. doi: 10.1002/hep.24290.

Anthérieu, S. *et al.* (2013) 'Oxidative stress plays a major role in chlorpromazine-induced cholestasis in human HepaRG cells', *Hepatology*. doi: 10.1002/hep.26160.

Antoniu, A. *et al.* (2009) 'Intrahepatic Bile Ducts Develop According to a New Mode of Tubulogenesis Regulated by the Transcription Factor SOX9', *Gastroenterology*. doi: 10.1053/j.gastro.2009.02.051.

Atienzar, F. A. *et al.* (2014) 'Predictivity of dog co-culture model, primary human hepatocytes and HepG2 cells for the detection of hepatotoxic drugs in humans', *Toxicology and Applied Pharmacology*. doi: 10.1016/j.taap.2013.11.022.

Azzolin, L. *et al.* (2014) 'YAP/TAZ incorporation in the β -catenin destruction complex orchestrates the Wnt response', *Cell*. doi: 10.1016/j.cell.2014.06.013.

Barker, N. *et al.* (2007) 'Identification of stem cells in small intestine and colon by marker gene Lgr5', *Nature*. doi: 10.1038/nature06196.

Bedogni, G. *et al.* (2005) 'Prevalence of and risk factors for nonalcoholic fatty liver

disease: The dionysos nutrition and liver study', *Hepatology*. doi: 10.1002/hep.20734.

Begrache, K. *et al.* (2011) 'Drug-induced toxicity on mitochondria and lipid metabolism: Mechanistic diversity and deleterious consequences for the liver', *Journal of Hepatology*. doi: 10.1016/j.jhep.2010.11.006.

Bell, C. C., Hendriks, Delilah F.G., *et al.* (2016) 'Characterization of primary human hepatocyte spheroids as a model system for drug-induced liver injury, liver function and disease', *Scientific Reports*. doi: 10.1038/srep25187.

Bell, C. C., Hendriks, Delilah F. G., *et al.* (2016) 'Characterization of primary human hepatocyte spheroids as a model system for drug-induced liver injury, liver function and disease', *Scientific Reports*, 6(1), p. 25187. doi: 10.1038/srep25187.

Bell, C. C. *et al.* (2018) 'Comparison of hepatic 2D sandwich cultures and 3D spheroids for long-term toxicity applications: A multicenter study', *Toxicological Sciences*. doi: 10.1093/toxsci/kfx289.

Berg, T. *et al.* (2007) 'Fibroblast growth factor 10 is critical for liver growth during embryogenesis and controls hepatoblast survival via β -catenin activation', *Hepatology*. doi: 10.1002/hep.21814.

Berge, D. Ten *et al.* (2011) 'Embryonic stem cells require Wnt proteins to prevent differentiation to epiblast stem cells', *Nature Cell Biology*. doi: 10.1038/ncb2314.

Bessone, F. *et al.* (2018) 'Review article: drug-induced liver injury in the context of nonalcoholic fatty liver disease – a physiopathological and clinical integrated view', *Alimentary Pharmacology and Therapeutics*. doi: 10.1111/apt.14952.

Bi, Y. A., Kazolias, D. and Duignan, D. B. (2006) 'Use of cryopreserved human hepatocytes in sandwich culture to measure hepatobiliary transport', *Drug Metabolism and Disposition*. doi: 10.1124/dmd.105.009118.

Blau, B. J. and Miki, T. (2019) 'The role of cellular interactions in the induction of hepatocyte polarity and functional maturation in stem cell-derived hepatic cells', *Differentiation*. doi: 10.1016/j.diff.2019.02.006.

Blouin, A., Bolender, R. P. and Weibel, E. R. (1977) 'Distribution of organelles and membranes between hepatocytes and nonhepatocytes in the rat liver parenchyma. A stereological study', *Journal of Cell Biology*. doi: 10.1083/jcb.72.2.441.

Böhme, M. *et al.* (1994) 'Cholestasis caused by inhibition of the adenosine triphosphate-dependent bile salt transport in rat liver', *Gastroenterology*. doi: 10.1016/0016-5085(94)90084-1.

Bone, H. K. *et al.* (2009) 'Involvement of GSK-3 in Regulation of Murine Embryonic Stem Cell Self-Renewal Revealed by a Series of Bisindolylmaleimides', *Chemistry and Biology*. doi: 10.1016/j.chembiol.2008.11.003.

Bort, R. *et al.* (2006) 'Hex homeobox gene controls the transition of the endoderm to a pseudostratified, cell emergent epithelium for liver bud development', *Developmental Biology*. doi: 10.1016/j.ydbio.2005.11.006.

Boyer, J. L. (2013) 'Bile formation and secretion', *Comprehensive Physiology*. doi: 10.1002/cphy.c120027.

Brandenberg, N. *et al.* (2020) 'High-throughput automated organoid culture via stem-cell aggregation in microcavity arrays', *Nature Biomedical Engineering*. doi: 10.1038/s41551-020-0565-2.

Broutier, L. *et al.* (2016) 'Culture and establishment of self-renewing human and mouse adult liver and pancreas 3D organoids and their genetic manipulation.', *Nature protocols*, 11(9), pp. 1724–43. doi: 10.1038/nprot.2016.097.

De Bruyn, T. *et al.* (2013) 'Sandwich-cultured hepatocytes: Utility for in vitro exploration of hepatobiliary drug disposition and drug-induced hepatotoxicity', *Expert Opinion on Drug Metabolism and Toxicology*. doi: 10.1517/17425255.2013.773973.

C., T. and Manov, I. (2011) 'Electron Microscopy of Liver Biopsies', in *Liver Biopsy*. doi: 10.5772/20385.

Camargo, F. D. *et al.* (2007) 'YAP1 Increases Organ Size and Expands Undifferentiated Progenitor Cells', *Current Biology*. doi: 10.1016/j.cub.2007.10.039.

Carpentier, R. *et al.* (2011) 'Embryonic ductal plate cells give rise to cholangiocytes, periportal hepatocytes, and adult liver progenitor cells', *Gastroenterology*. doi: 10.1053/j.gastro.2011.06.049.

Centonze, V. E. and White, J. G. (1998) 'Multiphoton excitation provides optical sections from deeper within scattering specimens than confocal imaging', *Biophysical Journal*. doi: 10.1016/S0006-3495(98)77643-X.

Chang, T. T. and Hughes-Fulford, M. (2009) 'Monolayer and spheroid culture of human liver hepatocellular carcinoma cell line cells demonstrate distinct global gene expression patterns and functional phenotypes', *Tissue Engineering - Part A*. doi: 10.1089/ten.tea.2007.0434.

Cheng, W. *et al.* (2006) 'HNF factors form a network to regulate liver-enriched genes in zebrafish', *Developmental Biology*. doi: 10.1016/j.ydbio.2006.03.018.

Childs, S. *et al.* (1998) 'Taxol resistance mediated by transfection of the liver-specific sister gene of P-glycoprotein', *Cancer Research*.

Chung, W. S., Shin, C. H. and Stainier, D. Y. R. (2008) 'Bmp2 Signaling Regulates the Hepatic versus Pancreatic Fate Decision', *Developmental Cell*. doi: 10.1016/j.devcel.2008.08.019.

Clotman, F. *et al.* (2002) 'The onecut transcription factor HNF6 is required for normal development of the biliary tract', *Development*.

Clotman, F. *et al.* (2005) 'Control of liver cell fate decision by a gradient of TGF β signaling modulated by Onecut transcription factors', *Genes and Development*. doi: 10.1101/gad.340305.

Clotman, F. and Lemaigre, F. P. (2006) 'Control of hepatic differentiation by activin/TGF β signaling', *Cell Cycle*. doi: 10.4161/cc.5.2.2341.

Coffinier, C. *et al.* (2002) 'Bile system morphogenesis defects and liver dysfunction upon targeted deletion of HNF1 β ', *Development*.

Conchello, J. A. and Lichtman, J. W. (2005) 'Optical sectioning microscopy', *Nature Methods*. doi: 10.1038/nmeth815.

Cordero-Espinoza, L. *et al.* (2020) 'The proportion of periportal mesenchyme to ductal epithelial cells acts as a proliferative rheostat in liver regeneration', *bioRxiv*.

Dash, A. *et al.* (2013) 'Hemodynamic flow improves rat hepatocyte morphology, function, and metabolic activity in vitro', *American Journal of Physiology - Cell Physiology*. doi: 10.1152/ajpcell.00331.2012.

Dawson, S. *et al.* (2012) 'In vitro inhibition of the bile salt export pump correlates with risk of cholestatic drug-induced liver injury in humans', *Drug Metabolism and Disposition*. doi: 10.1124/dmd.111.040758.

Decaens, T. *et al.* (2008) 'Stabilization of β -catenin affects mouse embryonic liver growth and hepatoblast fate', *Hepatology*. doi: 10.1002/hep.21952.

Defrances, M. C. *et al.* (1992) 'The presence of hepatocyte growth factor in the developing rat', *Development*.

Deng, X. *et al.* (2018) 'Chronic Liver Injury Induces Conversion of Biliary Epithelial Cells into Hepatocytes', *Cell Stem Cell*. doi: 10.1016/j.stem.2018.05.022.

Denk, W. *et al.* (1994) 'Anatomical and functional imaging of neurons using 2-photon laser scanning microscopy', *Journal of Neuroscience Methods*. doi: 10.1016/0165-0270(94)90189-9.

Denk, W., Strickler, J. H. and Webb, W. W. (1990) 'Two-photon laser scanning fluorescence microscopy', *Science*. doi: 10.1126/science.2321027.

Ding, S. *et al.* (2003) 'Synthetic small molecules that control stem cell fate', *Proceedings of the National Academy of Sciences of the United States of America*. doi: 10.1073/pnas.0732087100.

Doble, B. W. *et al.* (2007) 'Functional Redundancy of GSK-3 α and GSK-3 β in Wnt/ β -Catenin Signaling Shown by Using an Allelic Series of Embryonic Stem Cell Lines', *Developmental Cell*. doi: 10.1016/j.devcel.2007.04.001.

Dodge, M. E. *et al.* (2012) 'Diverse chemical scaffolds support direct inhibition of the membrane-bound O-acyltransferase porcupine', *Journal of Biological Chemistry*. doi: 10.1074/jbc.M112.372029.

Dong, J. *et al.* (2007) 'Elucidation of a Universal Size-Control Mechanism in Drosophila and Mammals', *Cell*. doi: 10.1016/j.cell.2007.07.019.

Donnelly, K. L. *et al.* (2005) 'Sources of fatty acids stored in liver and secreted via lipoproteins in patients with nonalcoholic fatty liver disease', *Journal of Clinical Investigation*. doi: 10.1172/JCI23621.

Dragovic, S. *et al.* (2016) 'Evidence-based selection of training compounds for use in the mechanism-based integrated prediction of drug-induced liver injury in man', *Archives of Toxicology*. doi: 10.1007/s00204-016-1845-1.

Duane, W. C. and Javitt, N. B. (1999) '27-Hydroxycholesterol: Production rates in normal human subjects', *Journal of Lipid Research*. doi: 10.1016/s0022-2275(20)33481-

7.

Duncan, A. W., Dorrell, C. and Grompe, M. (2009) 'Stem Cells and Liver Regeneration', *Gastroenterology*. doi: 10.1053/j.gastro.2009.05.044.

Eiraku, M. *et al.* (2008) 'Self-Organized Formation of Polarized Cortical Tissues from ESCs and Its Active Manipulation by Extrinsic Signals', *Cell Stem Cell*. doi: 10.1016/j.stem.2008.09.002.

Elaut, G. *et al.* (2006) 'Molecular Mechanisms Underlying the Dedifferentiation Process of Isolated Hepatocytes and Their Cultures', *Current Drug Metabolism*. doi: 10.2174/138920006778017759.

Ewart, L. *et al.* (2018) 'Application of Microphysiological Systems to Enhance Safety Assessment in Drug Discovery', *Annual Review of Pharmacology and Toxicology*. doi: 10.1146/annurev-pharmtox-010617-052722.

Farber, E. (1956) 'Similarities in the Sequence of Early Histological Changes Induced in the Liver of the Rat by Ethionine, 2-Acetylaminofluorene, and 3'-Methyl-4-dimethylaminoazobenzene', *Cancer Research*.

Farrell, G. C. and Larter, C. Z. (2006) 'Nonalcoholic fatty liver disease: From steatosis to cirrhosis', *Hepatology*. doi: 10.1002/hep.20973.

Fattinger, K. *et al.* (2001) 'The endothelin antagonist bosentan inhibits the canalicular bile salt export pump: A potential mechanism for hepatic adverse reactions', *Clinical Pharmacology and Therapeutics*. doi: 10.1067/mcp.2001.114667.

Faubion, W. A. *et al.* (1999) 'Toxic bile salts induce rodent hepatocyte apoptosis via direct activation of Fas', *Journal of Clinical Investigation*. doi: 10.1172/JCI4765.

Feng, D. *et al.* (2014) 'Acute and Chronic Effects of IL-22 on Acetaminophen-Induced Liver Injury', *The Journal of Immunology*, 193(5), pp. 2512 LP - 2518. doi: 10.4049/jimmunol.1400588.

Font-Burgada, J. *et al.* (2015) 'Hybrid Periportal Hepatocytes Regenerate the Injured Liver without Giving Rise to Cancer', *Cell*. doi: 10.1016/j.cell.2015.07.026.

Fromenty, B. (2017) 'Role of nonalcoholic fatty liver disease as risk factor for drug-induced hepatotoxicity', *Journal of Clinical and Translational Research*. doi: 10.18053/jctres.03.2017s1.006.

Fuhrmann, A. *et al.* (2014) 'Molecular mechanisms underlying the effects of cyclosporin A and sirolimus on glucose and lipid metabolism in liver, skeletal muscle and adipose tissue in an in vivo rat model', *Biochemical Pharmacology*. doi: 10.1016/j.bcp.2014.01.020.

Funk, C., Ponelle, C., *et al.* (2001) 'Cholestatic potential of troglitazone as a possible factor contributing to troglitazone-induced hepatotoxicity: In vivo and in vitro interaction at the canalicular bile salt export pump (Bsep) in the rat', *Molecular Pharmacology*. doi: 10.1124/mol.59.3.627.

Funk, C., Pantze, M., *et al.* (2001) 'Troglitazone-induced intrahepatic cholestasis by an interference with the hepatobiliary export of bile acids in male and female rats. Correlation with the gender difference in troglitazone sulfate formation and the inhibition of the canalicular bile salt', *Toxicology*. doi: 10.1016/S0300-483X(01)00460-7.

Furuyama, K. *et al.* (2011) 'Continuous cell supply from a Sox9-expressing progenitor zone in adult liver, exocrine pancreas and intestine', *Nature Genetics*. doi: 10.1038/ng.722.

Gao, X. and Liu, Y. (2017) 'A transcriptomic study suggesting human iPSC-derived hepatocytes potentially offer a better in vitro model of hepatotoxicity than most hepatoma cell lines', *Cell Biology and Toxicology*. doi: 10.1007/s10565-017-9383-z.

Gaskell, H. *et al.* (2016) 'Characterization of a functional C3A liver spheroid model', *Toxicology Research*. doi: 10.1039/c6tx00101g.

Gebhardt, R. (1992) 'Metabolic zonation of the liver: Regulation and implications for liver function', *Pharmacology and Therapeutics*. doi: 10.1016/0163-7258(92)90055-5.

George K. Michalopoulos* and Marie C. DeFrances (1997) 'Liver regeneration1. George K. Michalopoulos* and Marie C. DeFrances (1997) Liver regeneration. *Science* (80-.). 276, 60–66', *Science*.

Gerloff, T. *et al.* (1998) 'The sister of P-glycoprotein represents the canalicular bile salt export pump of mammalian liver', *Journal of Biological Chemistry*. doi: 10.1074/jbc.273.16.10046.

Giacomini, K. M. *et al.* (2010) 'Membrane transporters in drug development', *Nature Reviews Drug Discovery*. doi: 10.1038/nrd3028.

Giuliano, K. A. *et al.* (2010) 'Early safety assessment using cellular systems biology yields insights into mechanisms of action.', *Journal of biomolecular screening*, 15(7), pp. 783–797. doi: 10.1177/1087057110376413.

Godoy, P. *et al.* (2013) 'Recent advances in 2D and 3D in vitro systems using primary hepatocytes, alternative hepatocyte sources and non-parenchymal liver cells and their use in investigating mechanisms of hepatotoxicity, cell signaling and ADME', *Archives of Toxicology*. doi: 10.1007/s00204-013-1078-5.

Gomez-Lechon, M. *et al.* (2005) 'Human Hepatocytes in Primary Culture: The Choice to Investigate Drug Metabolism in Man', *Current Drug Metabolism*. doi: 10.2174/1389200043335414.

Gonsalves, F. C. *et al.* (2011) 'An RNAi-based chemical genetic screen identifies three small-molecule inhibitors of the Wnt/wingless signaling pathway', *Proceedings of the National Academy of Sciences of the United States of America*. doi: 10.1073/pnas.1017496108.

Goss, A. M. *et al.* (2009) 'Wnt2/2b and beta-catenin signaling are necessary and sufficient to specify lung progenitors in the foregut.', *Developmental cell*, 17(2), pp. 290–298. doi: 10.1016/j.devcel.2009.06.005.

Greber, B. *et al.* (2010) 'Conserved and Divergent Roles of FGF Signaling in Mouse Epiblast Stem Cells and Human Embryonic Stem Cells', *Cell Stem Cell*. doi: 10.1016/j.stem.2010.01.003.

Gualdi, R. *et al.* (1996) 'Hepatic specification of the gut endoderm in vitro: Cell signaling and transcriptional control', *Genes and Development*. doi: 10.1101/gad.10.13.1670.

Gudbrandsen, O. A., Rost, T. H. and Berge, R. K. (2006) 'Causes and prevention of tamoxifen-induced accumulation of triacylglycerol in rat liver', *Journal of Lipid Research*. doi: 10.1194/jlr.M600148-JLR200.

Hay, D. C. *et al.* (2008) 'Highly efficient differentiation of hESCs to functional hepatic endoderm requires ActivinA and Wnt3a signaling', *Proceedings of the National*

Academy of Sciences of the United States of America. doi: 10.1073/pnas.0806522105.

Hayashi, H. *et al.* (2005) 'Two common PFIC2 mutations are associated with the impaired membrane trafficking of BSEP/ABCB11', *Hepatology*. doi: 10.1002/hep.20627.

He, L. *et al.* (2021) 'Proliferation tracing reveals regional hepatocyte generation in liver homeostasis and repair', *Science*. doi: 10.1126/science.abc4346.

He, X. *et al.* (1995) 'Glycogen synthase kinase-3 and dorsoventral patterning in *Xenopus* embryos', *Nature*. doi: 10.1038/374617a0.

Higgins, G. M. (1931) 'Experimental pathology of the liver. Restoration of the liver of the white rat following partial surgical removal', *Archives of Pathology*.

Ho, R. H. *et al.* (2010) 'Polymorphic variants in the human bile salt export pump (BSEP; ABCB11): Functional characterization and interindividual variability', *Pharmacogenetics and Genomics*. doi: 10.1097/FPC.0b013e3283349eb0.

Hofmann, A. F. (2004) 'Detoxification of lithocholic acid, a toxic bile-acid: Relevance to drug hepatotoxicity', *Drug Metabolism Reviews*. doi: 10.1081/DMR-200033475.

Hofmann, K. (2000) 'A superfamily of membrane-bound O-acyltransferases with implications for Wnt signaling', *Trends in Biochemical Sciences*. doi: 10.1016/S0968-0004(99)01539-X.

Hoshiba, T. *et al.* (2016) 'Decellularized Extracellular Matrix as an In Vitro Model to Study the Comprehensive Roles of the ECM in Stem Cell Differentiation', *Stem cells international*. 2015/12/06, 2016, p. 6397820. doi: 10.1155/2016/6397820.

Houssaint, E. (1980) 'Differentiation of the mouse hepatic primordium. I. An analysis of tissue interactions in hepatocyte differentiation', *Cell Differentiation*. doi: 10.1016/0045-6039(80)90026-3.

Hu, H. *et al.* (2018) 'Long-Term Expansion of Functional Mouse and Human Hepatocytes as 3D Organoids', *Cell*. doi: 10.1016/j.cell.2018.11.013.

Huang, J. *et al.* (2005) 'The Hippo signaling pathway coordinately regulates cell proliferation and apoptosis by inactivating Yorkie, the *Drosophila* homolog of YAP', *Cell*. doi: 10.1016/j.cell.2005.06.007.

Huang, J. *et al.* (2017) 'Activation of Wnt/ β -catenin signalling via GSK3 inhibitors

direct differentiation of human adipose stem cells into functional hepatocytes', *Scientific Reports*. doi: 10.1038/srep40716.

Huch, M. *et al.* (2013) 'In vitro expansion of single Lgr5 + liver stem cells induced by Wnt-driven regeneration', *Nature*. doi: 10.1038/nature11826.

Huch, M. *et al.* (2015) 'Long-term culture of genome-stable bipotent stem cells from adult human liver', *Cell*. doi: 10.1016/j.cell.2014.11.050.

Hughes, B. (2008) 'Industry concern over EU hepatotoxicity guidance', *Nature Reviews Drug Discovery*. doi: 10.1038/nrd2677.

Hussain, S. Z. *et al.* (2004) 'Wnt impacts growth and differentiation in ex vivo liver development', *Experimental Cell Research*. doi: 10.1016/j.yexcr.2003.08.020.

Iyer, K. R. and Sinz, M. W. (1999) 'Characterization of Phase I and Phase II hepatic drug metabolism activities in a panel of human liver preparations', *Chemico-Biological Interactions*. doi: 10.1016/S0009-2797(99)00007-1.

James, L. P., Mayeux, P. R. and Hinson, J. A. (2003) 'Acetaminophen-induced hepatotoxicity', *Drug Metabolism and Disposition*. doi: 10.1124/dmd.31.12.1499.

Jamieson, P. R. *et al.* (2017) 'Derivation of a robust mouse mammary organoid system for studying tissue dynamics', *Development (Cambridge)*. doi: 10.1242/dev.145045.

Jones, D. E. J. (2016) 'Obeticholic acid for the treatment of primary biliary cirrhosis', *Expert Review of Gastroenterology and Hepatology*. doi: 10.1080/17474124.2016.1216784.

Jung, J. *et al.* (1999) 'Initiation of mammalian liver development from endoderm by fibroblast growth factors', *Science*. doi: 10.1126/science.284.5422.1998.

Jungermann, K. and Kietzmann, T. (1996) 'Zonation of parenchymal and nonparenchymal metabolism in liver', *Annual Review of Nutrition*. doi: 10.1146/annurev.nu.16.070196.001143.

Kaluthantrige Don, F. and Huch, M. (2021) 'Organoids, Where We Stand and Where We Go', *Trends in Molecular Medicine*. Elsevier Ltd. doi: 10.1016/j.molmed.2021.03.001.

Kamiya, A. *et al.* (1999) 'Fetal liver development requires a paracrine action of oncostatin M through the gp130 signal transducer', *EMBO Journal*. doi:

10.1093/emboj/18.8.2127.

Kamiya, A., Kinoshita, T. and Miyajima, A. (2001) 'Oncostatin M and hepatocyte growth factor induce hepatic maturation via distinct signaling pathways', *FEBS Letters*. doi: 10.1016/S0014-5793(01)02140-8.

Kanwar, P. and Kowdley, K. V. (2016) 'The Metabolic Syndrome and Its Influence on Nonalcoholic Steatohepatitis', *Clinics in Liver Disease*. doi: 10.1016/j.cld.2015.10.002.

Katsuda, T. *et al.* (2017) 'Conversion of Terminally Committed Hepatocytes to Culturable Bipotent Progenitor Cells with Regenerative Capacity', *Cell Stem Cell*. doi: 10.1016/j.stem.2016.10.007.

Kennedy, S. *et al.* (1995) 'Experiments in transgenic mice show that hepatocytes are the source for postnatal liver growth and do not stream', *Hepatology*. doi: 10.1016/0270-9139(95)90369-0.

Kietzmann, T. (2017) 'Metabolic zonation of the liver: The oxygen gradient revisited', *Redox Biology*. doi: 10.1016/j.redox.2017.01.012.

Kipp, H. and Arias, I. M. (2000) 'Newly synthesized canalicular ABC transporters are directly targeted from the Golgi to the hepatocyte apical domain in rat liver', *Journal of Biological Chemistry*. doi: 10.1074/jbc.M909875199.

Kipp, H., Pichetshote, N. and Arias, I. M. (2001) 'Transporters on demand. Intrahepatic pools of canalicular ATP binding cassette transporters in rat liver', *Journal of Biological Chemistry*. doi: 10.1074/jbc.M007794200.

Knobeloch, D. *et al.* (2012) 'Human hepatocytes: Isolation, culture, and quality procedures', *Methods in Molecular Biology*. doi: 10.1007/978-1-61779-367-7_8.

Kyrmizi, I. *et al.* (2006) 'Plasticity and expanding complexity of the hepatic transcription factor network during liver development', *Genes and Development*. doi: 10.1101/gad.390906.

Lafite, P. *et al.* (2007) 'Selective, competitive and mechanism-based inhibitors of human cytochrome P450 2J2', *Archives of Biochemistry and Biophysics*. doi: 10.1016/j.abb.2007.03.028.

Lai, Y., Tse, C. M. and Unadkat, J. D. (2004) 'Mitochondrial Expression of the Human Equilibrative Nucleoside Transporter 1 (hENT1) Results in Enhanced Mitochondrial

Toxicity of Antiviral Drugs', *Journal of Biological Chemistry*. doi: 10.1074/jbc.M307938200.

Landry, J. *et al.* (1985) 'Spheroidal aggregate culture of rat liver cells: Histotypic reorganization, biomatrix deposition, and maintenance of functional activities', *Journal of Cell Biology*. doi: 10.1083/jcb.101.3.914.

Lasser, K. E. *et al.* (2002) 'Timing of new black box warnings and withdrawals for prescription medications', *Journal of the American Medical Association*. doi: 10.1001/jama.287.17.2215.

Lauschke, V. M. *et al.* (2016) 'Novel 3D Culture Systems for Studies of Human Liver Function and Assessments of the Hepatotoxicity of Drugs and Drug Candidates', *Chemical Research in Toxicology*. doi: 10.1021/acs.chemrestox.6b00150.

Lautt, W. W. (2009) *Hepatic Circulation Physiology and Pathophysiology, Colloquium Series on Integrated Systems Physiology: From Molecule to Function*.

Lawlor, K. T. *et al.* (2021) 'Cellular extrusion bioprinting improves kidney organoid reproducibility and conformation', *Nature Materials*. doi: 10.1038/s41563-020-00853-9.

Lazarou, J., Pomeranz, B. H. and Corey, P. N. (1998) 'Incidence of adverse drug reactions in hospitalized patients: A meta- analysis of prospective studies', *Journal of the American Medical Association*. doi: 10.1001/jama.279.15.1200.

LeCluyse, E. L. *et al.* (2012) 'Organotypic liver culture models: Meeting current challenges in toxicity testing', *Critical Reviews in Toxicology*. doi: 10.3109/10408444.2012.682115.

Lee-Montiel, F. T. *et al.* (2017) 'Control of oxygen tension recapitulates zone-specific functions in human liver microphysiology systems', *Experimental Biology and Medicine*. doi: 10.1177/1535370217703978.

Lee, E. W. *et al.* (2006) 'Identification of the mitochondrial targeting signal of the human equilibrative nucleoside transporter 1 (hENT1): Implications for interspecies differences in mitochondrial toxicity of fialuridine', *Journal of Biological Chemistry*. doi: 10.1074/jbc.M513825200.

Lemaigre, F. P. (2003) 'Development of the biliary tract', *Mechanisms of*

Development. doi: 10.1016/S0925-4773(02)00334-9.

Lewis, J. H. *et al.* (1990) 'Histopathologic analysis of suspected amiodarone hepatotoxicity', *Human Pathology*. doi: 10.1016/0046-8177(90)90076-H.

Li, L. *et al.* (1997) 'Alagille syndrome is caused by mutations in human Jagged1, which encodes a ligand for notch1', *Nature Genetics*. doi: 10.1038/ng0797-243.

Li, Y. *et al.* (2008) 'Sfrp5 coordinates foregut specification and morphogenesis by antagonizing both canonical and noncanonical Wnt11 signaling', *Genes and Development*. doi: 10.1101/gad.1687308.

Lin, S. *et al.* (2018) 'Distributed hepatocytes expressing telomerase repopulate the liver in homeostasis and injury', *Nature*. doi: 10.1038/s41586-018-0004-7.

Loneker, A. E. *et al.* (2016) 'Solubilized liver extracellular matrix maintains primary rat hepatocyte phenotype in-vitro.', *Journal of biomedical materials research. Part A*, 104(4), pp. 957–965. doi: 10.1002/jbm.a.35636.

Looney, M. R. *et al.* (2011) 'Stabilized imaging of immune surveillance in the mouse lung', *Nature Methods*. doi: 10.1038/nmeth.1543.

Lu, W.-Y. *et al.* (2015) 'Hepatic progenitor cells of biliary origin with liver repopulation capacity.', *Nature cell biology*, 17(8), pp. 971–983. doi: 10.1038/ncb3203.

Lübberstedt, M. *et al.* (2015) 'Serum-free culture of primary human hepatocytes in a miniaturized hollow-fibre membrane bioreactor for pharmacological in vitro studies', *Journal of Tissue Engineering and Regenerative Medicine*. doi: 10.1002/term.1652.

Magami, Y. *et al.* (2002) 'Cell proliferation and renewal of normal hepatocytes and bile duct cells in adult mouse liver', *Liver*. doi: 10.1034/j.1600-0676.2002.01702.x.

Malato, Y. *et al.* (2011) 'Fate tracing of mature hepatocytes in mouse liver homeostasis and regeneration', *Journal of Clinical Investigation*. doi: 10.1172/JCI59261.

Marcinak, J. F. *et al.* (2018) 'Liver Safety of Fasiglifam (TAK-875) in Patients with Type 2 Diabetes: Review of the Global Clinical Trial Experience', *Drug Safety*. doi: 10.1007/s40264-018-0642-6.

Margagliotti, S. *et al.* (2008) 'Role of metalloproteinases at the onset of liver development', *Development Growth and Differentiation*. doi: 10.1111/j.1440-

169X.2008.01031.x.

Martignoni, M., Groothuis, G. M. M. and de Kanter, R. (2006) 'Species differences between mouse, rat, dog, monkey and human CYP-mediated drug metabolism, inhibition and induction', *Expert Opinion on Drug Metabolism and Toxicology*. doi: 10.1517/17425255.2.6.875.

Matsumoto, T. *et al.* (1979) 'A Study on the normal Structure of the human Liver, with special Reference to its Angioarchitecture', *Kanzo*. doi: 10.2957/kanzo.20.223.

Matsuzawa, A., Matsusaki, M. and Akashi, M. (2015) 'Construction of three-dimensional liver tissue models by cell accumulation technique and maintaining their metabolic functions for long-term culture without medium change', *Journal of Biomedical Materials Research - Part A*. doi: 10.1002/jbm.a.35292.

McLin, V. A., Rankin, S. A. and Zorn, A. M. (2007) 'Repression of Wnt/ β -catenin signaling in the anterior endoderm is essential for liver and pancreas development', *Development*. doi: 10.1242/dev.001230.

Michalopoulos, G. K. *et al.* (2002) 'Hepatocytes undergo phenotypic transformation to biliary epithelium in organoid cultures', *Hepatology*. doi: 10.1053/jhep.2002.34858.

Michalopoulos, G. K. *et al.* (2003) 'HGF-, EGF-, and dexamethasone-induced gene expression patterns during formation of tissue in hepatic organoid cultures', *Gene Expression*. doi: 10.3727/000000003108748964.

Michalopoulos, G. K. (2007) 'Liver regeneration', *Journal of Cellular Physiology*. doi: 10.1002/jcp.21172.

Monga, Satdarshan P S *et al.* (2003) 'Beta-catenin antisense studies in embryonic liver cultures: role in proliferation, apoptosis, and lineage specification.', *Gastroenterology*, 124(1), pp. 202–216. doi: 10.1053/gast.2003.50000.

Monga, Satdarshan P.S. *et al.* (2003) ' β -catenin antisense studies in embryonic liver cultures: Role in proliferation, apoptosis, and lineage specification', *Gastroenterology*. doi: 10.1053/gast.2003.50000.

Morgan, R. E. *et al.* (2010) 'Interference with bile salt export pump function is a susceptibility factor for human liver injury in drug development', *Toxicological Sciences*.

doi: 10.1093/toxsci/kfq269.

Morrison, G. *et al.* (2016) 'Convergence of cMyc and β -catenin on Tcf7l1 enables endoderm specification', *The EMBO Journal*. doi: 10.15252/embj.201592116.

Müller, M. *et al.* (2002) 'Farnesoid X receptor and bile salts are involved in transcriptional regulation of the gene encoding the human bile salt export pump', *Hepatology*. doi: 10.1053/jhep.2002.31724.

Navarro, V. J. and Senior, J. R. (2006) 'Drug-Related Hepatotoxicity', *New England Journal of Medicine*. doi: 10.1056/nejmra052270.

Nichols, W. G. *et al.* (2008) 'Hepatotoxicity observed in clinical trials of aplaviroc (GW873140)', *Antimicrobial Agents and Chemotherapy*. doi: 10.1128/AAC.00821-07.

Nishikawa, A. *et al.* (1987) 'ALAGILLE'S SYNDROME: A Case with a Hamartomatous Nodule of the Liver', *Pathology International*. doi: 10.1111/j.1440-1827.1987.tb00464.x.

Noé, J., Stieger, B. and Meier, P. J. (2002) 'Functional expression of the canalicular bile salt export pump of human liver', *Gastroenterology*. doi: 10.1053/gast.2002.36587.

Ober, E. A. *et al.* (2006) 'Mesodermal Wnt2b signalling positively regulates liver specification', *Nature*. doi: 10.1038/nature04888.

Oda, T. *et al.* (1997) 'Mutations in the human Jagged1 gene are responsible for Alagille syndrome', *Nature Genetics*. doi: 10.1038/ng0797-235.

Okabe, H. *et al.* (2016) 'Wnt signaling regulates hepatobiliary repair following cholestatic liver injury in mice', *Hepatology*. doi: 10.1002/hep.28774.

Olivier, N. *et al.* (2010) 'Cell lineage reconstruction of early zebrafish embryos using label-free nonlinear microscopy', *Science*. doi: 10.1126/science.1189428.

Olson, H. *et al.* (2000) 'Concordance of the toxicity of pharmaceuticals in humans and in animals', *Regulatory Toxicology and Pharmacology*. doi: 10.1006/rtph.2000.1399.

Parlow, M. H. *et al.* (1991) 'Localization of bFGF-like proteins as punctate inclusions in the preseptation myocardium of the chicken embryo', *Developmental Biology*. doi: 10.1016/0012-1606(91)90454-B.

'Pathology of the liver: Edited by R.N.M. MacSween, P.P. Anthony, and P.J. Scheuer, Foreward by H. Popper. 458 pp., \$67.50. Churchill Livingstone, New York, 1979' (1980)

Gastroenterology. doi: 10.5555/uri:pii:0016508580902681.

Pawley, J. B. (1996) '*Handbook of Biological Confocal Microscopy, Second Edition*', *Optical Engineering*. doi: 10.1117/1.600871.

Peifer, M., Pai, L. M. and Casey, M. (1994) 'Phosphorylation of the drosophila adherens junction protein armadillo: Roles for wingless signal and zeste-white 3 kinase', *Developmental Biology*. doi: 10.1006/dbio.1994.1336.

Peng, W. C. *et al.* (2018) 'Inflammatory Cytokine TNF α Promotes the Long-Term Expansion of Primary Hepatocytes in 3D Culture', *Cell*. doi: 10.1016/j.cell.2018.11.012.

Pepe-Mooney, B. J. *et al.* (2019) 'Single-Cell Analysis of the Liver Epithelium Reveals Dynamic Heterogeneity and an Essential Role for YAP in Homeostasis and Regeneration', *Cell Stem Cell*. doi: 10.1016/j.stem.2019.04.004.

Perez, M. J. and Britz, O. (2009) 'Bile-acid-induced cell injury and protection', *World Journal of Gastroenterology*. doi: 10.3748/wjg.15.1677.

Pettinato, G. *et al.* (2016) 'Scalable Differentiation of Human iPSCs in a Multicellular Spheroid-based 3D Culture into Hepatocyte-like Cells through Direct Wnt/ β -catenin Pathway Inhibition', *Scientific Reports*. doi: 10.1038/srep32888.

Planas-Paz, L. *et al.* (2016) 'The RSPO-LGR4/5-ZNRF3/RNF43 module controls liver zonation and size', *Nature Cell Biology*. doi: 10.1038/ncb3337.

Pontoglio, M. *et al.* (1996) 'Hepatocyte nuclear factor 1 inactivation results in hepatic dysfunction, phenylketonuria, and renal Fanconi syndrome', *Cell*. doi: 10.1016/S0092-8674(00)81033-8.

Prior, N. *et al.* (2019) 'Lgr5+ stem and progenitor cells reside at the apex of a heterogeneous embryonic hepatoblast pool', *Development (Cambridge)*. doi: 10.1242/dev.174557.

Prior, N., Inacio, P. and Huch, M. (2019) 'Liver organoids: From basic research to therapeutic applications', *Gut*. doi: 10.1136/gutjnl-2019-319256.

Prot, J. M. *et al.* (2012) 'Predictive toxicology using systemic biology and liver microfluidic "on chip" approaches: Application to acetaminophen injury', *Toxicology and Applied Pharmacology*. doi: 10.1016/j.taap.2011.12.017.

Raju, R. *et al.* (2018) 'In vitro pluripotent stem cell differentiation to hepatocyte

ceases further maturation at an equivalent stage of e15 in mouse embryonic liver development', *Stem Cells and Development*. doi: 10.1089/scd.2017.0270.

Raven, A. *et al.* (2017) 'Cholangiocytes act as facultative liver stem cells during impaired hepatocyte regeneration', *Nature*. doi: 10.1038/nature23015.

Reuben, A., Koch, D. G. and Lee, W. M. (2010) 'Drug-induced acute liver failure: Results of a U.S. multicenter, prospective study', *Hepatology*. doi: 10.1002/hep.23937.

Rogers, A. B. and Dintzis, R. Z. (2012) 'Liver and Gallbladder', in *Comparative Anatomy and Histology*. doi: 10.1016/B978-0-12-381361-9.00013-5.

Roman, I. D. *et al.* (1990) 'Inhibition of hepatocytary vesicular transport by cyclosporin a in the rat: Relationship with cholestasis and hyperbilirubinemia', *Hepatology*. doi: 10.1002/hep.1840120114.

Román, I. D. *et al.* (2003) 'Cyclosporin A induced internalization of the bile salt export pump in isolated rat hepatocyte couplets', *Toxicological Sciences*. doi: 10.1093/toxsci/71.2.276.

Rossi, J. M. *et al.* (2001) 'Distinct mesodermal signals, including BMPs from the septum, transversum mesenchyme, are required in combination for hepatogenesis from the endoderm', *Genes and Development*. doi: 10.1101/gad.904601.

Ruebner, B. H. *et al.* (1990) 'Development and transformation of the ductal plate in the developing human liver', *Fetal and Pediatric Pathology*. doi: 10.3109/15513819009067096.

Sampaziotis, F. *et al.* (2015) 'Cholangiocytes derived from human induced pluripotent stem cells for disease modeling and drug validation', *Nature Biotechnology*. doi: 10.1038/nbt.3275.

Sato, N. *et al.* (2004) 'Maintenance of pluripotency in human and mouse embryonic stem cells through activation of Wnt signaling by a pharmacological GSK-3-specific inhibitor', *Nature Medicine*. doi: 10.1038/nm979.

Sato, T. *et al.* (2009) 'Single Lgr5 stem cells build crypt-villus structures in vitro without a mesenchymal niche', *Nature*. doi: 10.1038/nature07935.

Sato, T. and Clevers, H. (2013) 'Growing self-organizing mini-guts from a single intestinal stem cell: Mechanism and applications', *Science*. doi:

10.1126/science.1234852.

Sayiner, M. *et al.* (2016) 'Epidemiology of Nonalcoholic Fatty Liver Disease and Nonalcoholic Steatohepatitis in the United States and the Rest of the World', *Clinics in Liver Disease*. doi: 10.1016/j.cld.2015.10.001.

Schaub, J. R. *et al.* (2018) 'De novo formation of the biliary system by TGF β -mediated hepatocyte transdifferentiation', *Nature*. doi: 10.1038/s41586-018-0075-5.

Scherer, M. *et al.* (2009) 'Rapid quantification of bile acids and their conjugates in serum by liquid chromatography-tandem mass spectrometry', *Journal of Chromatography B: Analytical Technologies in the Biomedical and Life Sciences*. doi: 10.1016/j.jchromb.2009.09.038.

Schummers, J., Yu, H. and Sur, M. (2008) 'Tuned responses of astrocytes and their influence on hemodynamic signals in the visual cortex', *Science*. doi: 10.1126/science.1156120.

Scott, D. A. *et al.* (1991) 'Incidental Microvesicular Steatosis Due to Valproic Acid Anticonvulsant Therapy', *The American Journal of Gastroenterology*. doi: 10.1111/j.1572-0241.1991.tb07045.x.

Sekiya, S. and Suzuki, A. (2011) 'Direct conversion of mouse fibroblasts to hepatocyte-like cells by defined factors', *Nature*. doi: 10.1038/nature10263.

Shinozawa, T. *et al.* (2021) 'High-Fidelity Drug-Induced Liver Injury Screen Using Human Pluripotent Stem Cell-Derived Organoids', *Gastroenterology*. doi: 10.1053/j.gastro.2020.10.002.

Siller, R. *et al.* (2015) 'Small-molecule-driven hepatocyte differentiation of human pluripotent stem cells', *Stem Cell Reports*. doi: 10.1016/j.stemcr.2015.04.001.

SMITH, E. and COCHRANE, W. J. (1946) 'Cystic organoid teratoma; report of a case', *Canadian Medical Association journal*.

Soroka, C. J. and Boyer, J. L. (2014) 'Biosynthesis and trafficking of the bile salt export pump, BSEP: Therapeutic implications of BSEP mutations', *Molecular Aspects of Medicine*. doi: 10.1016/j.mam.2013.05.001.

Stieger, B. *et al.* (2000) 'Drug- and estrogen-induced cholestasis through inhibition of the hepatocellular bile salt export pump (Bsep) of rat liver', *Gastroenterology*. doi:

10.1016/S0016-5085(00)70224-1.

Strautnieks, S. S. *et al.* (1998) 'A gene encoding a liver-specific ABC transporter is mutated in progressive familial intrahepatic cholestasis', *Nature Genetics*. doi: 10.1038/3034.

Strazzabosco, M. and Fabris, L. (2008) 'Functional anatomy of normal bile ducts', *Anatomical Record*. doi: 10.1002/ar.20664.

Sugimoto, H. *et al.* (2007) 'BMP-7 functions as a novel hormone to facilitate liver regeneration', *The FASEB Journal*. doi: 10.1096/fj.06-6837com.

Takahashi, K. *et al.* (2007) 'Induction of Pluripotent Stem Cells from Adult Human Fibroblasts by Defined Factors', *Cell*. doi: 10.1016/j.cell.2007.11.019.

Takahashi, K. and Yamanaka, S. (2006) 'Induction of Pluripotent Stem Cells from Mouse Embryonic and Adult Fibroblast Cultures by Defined Factors', *Cell*. doi: 10.1016/j.cell.2006.07.024.

Takahashi, Y. *et al.* (2015) '3D spheroid cultures improve the metabolic gene expression profiles of HepaRG cells', *Bioscience Reports*. doi: 10.1042/BSR20150034.

Takebe, T. *et al.* (2013) 'Vascularized and functional human liver from an iPSC-derived organ bud transplant', *Nature*. doi: 10.1038/nature12271.

Takebe, T. *et al.* (2015) 'Vascularized and complex organ buds from diverse tissues via mesenchymal cell-driven condensation', *Cell Stem Cell*. doi: 10.1016/j.stem.2015.03.004.

Tan, X. *et al.* (2008) ' β -catenin deletion in hepatoblasts disrupts hepatic morphogenesis and survival during mouse development', *Hepatology*. doi: 10.1002/hep.22225.

Tandra, S. *et al.* (2011) 'Presence and significance of microvesicular steatosis in nonalcoholic fatty liver disease', *Journal of Hepatology*. doi: 10.1016/j.jhep.2010.11.021.

Tapia, N. and Schöler, H. R. (2016) 'Molecular Obstacles to Clinical Translation of iPSCs', *Cell Stem Cell*. doi: 10.1016/j.stem.2016.06.017.

Tarantino, G. *et al.* (2007) 'A prospective study of acute drug-induced liver injury in patients suffering from non-alcoholic fatty liver disease', *Hepatology Research*. doi: 10.1111/j.1872-034X.2007.00072.x.

Tarlow, B. D. *et al.* (2014) 'Bipotential adult liver progenitors are derived from chronically injured mature hepatocytes', *Cell Stem Cell*. doi: 10.1016/j.stem.2014.09.008.

Thomson, J. A. (1998) 'Embryonic stem cell lines derived from human blastocysts', *Science*. doi: 10.1126/science.282.5391.1145.

Tong, J. Z. *et al.* (1992) 'Long-term culture of adult rat hepatocyte spheroids', *Experimental Cell Research*. doi: 10.1016/0014-4827(92)90179-C.

Tribe, R. M. *et al.* (2010) 'Longitudinal profiles of 15 serum bile acids in patients with intrahepatic cholestasis of pregnancy', *American Journal of Gastroenterology*. doi: 10.1038/ajg.2009.633.

Twersky, V. (1964) 'Rayleigh Scattering', *Applied Optics*. doi: 10.1364/ao.3.001150.

Vivares, A. *et al.* (2015) 'Morphological behaviour and metabolic capacity of cryopreserved human primary hepatocytes cultivated in a perfused multiwell device', *Xenobiotica*. doi: 10.3109/00498254.2014.944612.

Vorrink, S. U. *et al.* (2018) 'Prediction of drug-induced hepatotoxicity using long-term stable primary hepatic 3D spheroid cultures in chemically defined conditions', *Toxicological Sciences*. doi: 10.1093/toxsci/kfy058.

Wahlicht, T. *et al.* (2020) 'Controlled Functional Zonation of Hepatocytes in Vitro by Engineering of Wnt Signaling', *ACS Synthetic Biology*. doi: 10.1021/acssynbio.9b00435.

Wang, B. *et al.* (2015) 'Self-renewing diploid Axin2 + cells fuel homeostatic renewal of the liver', *Nature*. doi: 10.1038/nature14863.

Wang, C. *et al.* (2016) 'Verteporfin inhibits YAP function through up-regulating 14-3-3 σ sequestering YAP in the cytoplasm', *American Journal of Cancer Research*.

Wang, N. D. *et al.* (1995) 'Impaired energy homeostasis in C/EBP α knockout mice', *Science*. doi: 10.1126/science.7652557.

Wang, Y. *et al.* (2018) 'Engineering stem cell-derived 3D brain organoids in a perfusable organ-on-a-chip system', *RSC Advances*. doi: 10.1039/c7ra11714k.

Watkins, P. B. (2005) 'Idiosyncratic Liver Injury: Challenges and Approaches', *Toxicologic Pathology*. doi: 10.1080/01926230590888306.

Watkins, P. B. (2011) 'Drug safety sciences and the bottleneck in drug development', *Clinical Pharmacology and Therapeutics*. doi: 10.1038/clpt.2011.63.

Wei, Y. *et al.* (2021) 'Liver homeostasis is maintained by midlobular zone 2 hepatocytes', *Science*. doi: 10.1126/science.abb1625.

Xiang, C. *et al.* (2019) 'Long-term functional maintenance of primary human hepatocytes in vitro', *Science*. doi: 10.1126/science.aau7307.

Xu, D. *et al.* (2014) 'Fialuridine Induces Acute Liver Failure in Chimeric TK-NOG Mice: A Model for Detecting Hepatic Drug Toxicity Prior to Human Testing', *PLoS Medicine*. doi: 10.1371/journal.pmed.1001628.

Xu, J. J., Diaz, D. and O'Brien, P. J. (2004) 'Applications of cytotoxicity assays and pre-lethal mechanistic assays for assessment of human hepatotoxicity potential', *Chemico-Biological Interactions*. doi: 10.1016/j.cbi.2004.09.011.

Yang, L. *et al.* (2017) 'A single-cell transcriptomic analysis reveals precise pathways and regulatory mechanisms underlying hepatoblast differentiation', *Hepatology*. doi: 10.1002/hep.29353.

Yanger, K. *et al.* (2013) 'Robust cellular reprogramming occurs spontaneously during liver regeneration', *Genes and Development*. doi: 10.1101/gad.207803.112.

Yimlamai, D. *et al.* (2014) 'Hippo pathway activity influences liver cell fate', *Cell*. doi: 10.1016/j.cell.2014.03.060.

Ying, Q. L. *et al.* (2008) 'The ground state of embryonic stem cell self-renewal', *Nature*. doi: 10.1038/nature06968.

ZAJICEK, G., OREN, R. and WEINREB, M. (1985) 'The streaming liver', *Liver*. doi: 10.1111/j.1600-0676.1985.tb00252.x.

Zanger, U. M. and Schwab, M. (2013) 'Cytochrome P450 enzymes in drug metabolism: Regulation of gene expression, enzyme activities, and impact of genetic variation', *Pharmacology and Therapeutics*. doi: 10.1016/j.pharmthera.2012.12.007.

Zhang, K. *et al.* (2018) 'In Vitro Expansion of Primary Human Hepatocytes with Efficient Liver Repopulation Capacity', *Cell Stem Cell*. doi: 10.1016/j.stem.2018.10.018.

Zhang, X., Ouyang, J. and Thung, S. N. (2013) 'Histopathologic manifestations of drug-induced hepatotoxicity', *Clinics in Liver Disease*. doi: 10.1016/j.cld.2013.07.004.

Zipfel, W. R., Williams, R. M. and Webb, W. W. (2003) 'Nonlinear magic: Multiphoton microscopy in the biosciences', *Nature Biotechnology*. doi: 10.1038/nbt899.

Zollner, G. and Trauner, M. (2008) 'Mechanisms of Cholestasis', *Clinics in Liver Disease*. doi: 10.1016/j.cld.2007.11.010.

Zorn (2008) 'Liver Development', *StemBook*. doi: 10.3824/stembook.1.25.1.

Zorn, A. M. and Wells, J. M. (2009) 'Vertebrate endoderm development and organ formation', *Annual Review of Cell and Developmental Biology*. doi: 10.1146/annurev.cellbio.042308.113344.

Zweers, S. J. L. B. *et al.* (2012) 'The human gallbladder secretes fibroblast growth factor 19 into bile: Towards defining the role of fibroblast growth factor 19 in the enterobiliary tract', *Hepatology*. doi: 10.1002/hep.24702.